NASA Technical Memorandum 82645

Surface Films and Metallurgy Related to Lubrication and Wear

Donald H. Buckley
Lewis Research Center
Cleveland, Ohio

July 1981

NASA

CONTENTS

SURFACE FILMS AND METALLURGY RELATED TO LUBRICATION AND WEAR

Donald H. Buckley

National Aeronautics and Space Administration
Lewis Research Center
Cleveland, Ohio U.S.A.

INTRODUCTION

Considerable amounts of data exist in the literature on the nature of liquid and gaseous interactions with solid surfaces in different fields (e.g., catalysis, surface chemistry, corrosion, etc.). The amount of fundamental information available on solid to solid interactions is, however, much more limited.

In tribological applications, two solid surfaces are in solid to solid contact whether the solids are bearings, gears, seals, or other mechanical components. Thus, in tribology, the solid surface and the interaction of two such surfaces are extremely important.

Metals and alloys are the most widely used solids in lubrication systems. Therefore, studies of metal and alloy surfaces are important. The nature of the surface, its interaction with the environment and constituents therein, lubricants, and the physics, chemistry, and metallurgy of the surface of metals and alloys must be understood in their relationships to adhesion, friction, wear, and lubrication of two solids in contact.

The objective of this thesis is to apply a number of analytical tools to study and characterize the tribological surface and the interactions of solid surfaces. Many of the studies involve in situ analysis of the adhesion, friction, wear, and lubrication behavior of solid surfaces in contact with surface analytical tools. The specific subjects to be addressed include the following: (1) nature of the tribological surface, (2) characterization of that tribological surface, (3) environmental effects, (4) solid to solid interactions in adhesion, friction, wear, and lubrication for various classes of

material combinations, and (5) the surface metallurgical properties related to tribological performance.

With respect to the identification of the surface, the ideal, real, and tribological surfaces will be distinguished. The tribological surface will be characterized physically, mechanically, chemically, and metallurgically. The adhesion, friction, wear, and lubrication of metals in contact with other metals, semiconductors, ceramics, carbons, and polymers will be addressed. Metallurgical surface characteristics to be related to tribology will include surface energy, crystallinity, grain boundary effects, orientation, texturing, crystal structure, order-disorder transformations, recrystallization, the degree of metallic nature, fracture and ideal shear strength, surface segregation, and alloying effects. The interaction of the environmental constituents with the surface of metals and alloys will also be discussed.

NATURE OF SURFACES AS THEY RELATE TO TRIBOLOGY

When a solid surface is examined either microscopically with the scanning electron microscope or mechanically with a surface profilometer, it is found to contain irregularities; that is, the surface is not flat and smooth. A depiction of a surface displaying these irregularities, or asperities as they are commonly called, is presented in figure 1(a).

Nearly all real surfaces contain the asperities except for brittle, single-crystal materials that have been cleaved along natural cleavage planes and metallic pin tips that have been field evaporated in the field ion microscope. Even with brittle materials, the cleavage process results in the generation of surfaces that contain cleavage steps, and it is only the terraces between these steps that are atomically smooth.

The actual shape and distribution of surface asperities has been the object of considerable research. An excellent review of the subject can be found in reference 1.

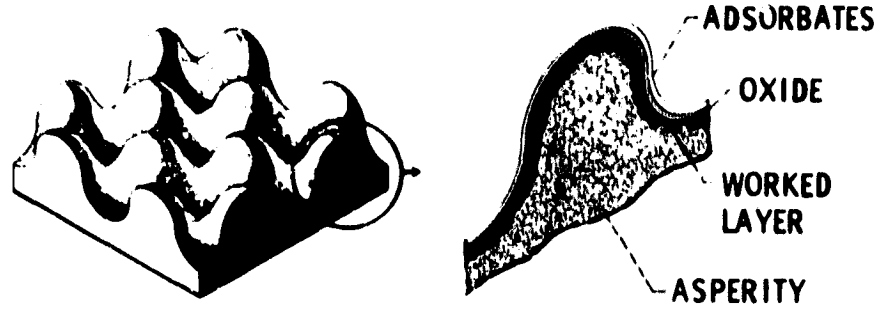

Figure 1. - Surface topography.

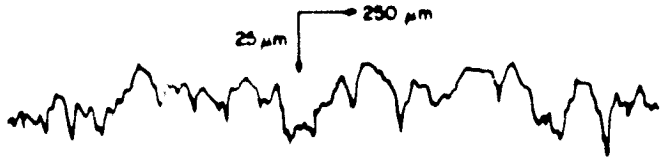

(a) Brushed.

(b) Ground.

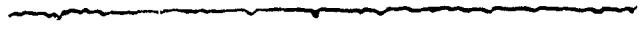

(c) Lapped.

Figure 2. - Profiles of steel surfaces finished by three different methods.

The surfaces of the asperities are not atomically clean but contain surface films (fig. 1(b)). For metals and alloys these films generally consist of oxides and adsorbed gases, usually water vapor, carbon monoxide, and carbon dioxide. With many nonmetals the surface films may simply consist of adsorbates. All the reacted and adsorbed film materials can exert a strong effect on the mechanical and metallurgical behavior of the solids to which they adhere, as indicated by the collection of papers in reference 2.

In addition to the films present on the surface of a solid, the surficial (near-surface) layers of the solid itself may vary considerably in structure from the bulk of the solid. With crystalline solids these layers may consist of recrystallized material, strain-hardened regions, and/or textured regions. These surficial layers develop when any type of finishing or polishing of the surface is done, particularly when that surface is a metal. These layers can also be a region rich in bulk impurities (ref. 3). In amorphous solids, these layers may contain voids and microcracks.

SURFACE PROFILE

A careful examination of industrially prepared metal and alloy surfaces with surface profilometers (devices capable of revealing the surface topography) indicates the true microroughness of these surfaces. They are, on a microscale, rough as indicated by the surface profile traces shown in figure 2. The surface represented by figure 2(a), steel finished by mechanical wire brushing, is extremely rough and contains many large irregularities. The surface of figure 2(b) is for steel prepared by conventional industrial grinding and is much smoother, but there still exist many microirregularities.

When a steel surface is very carefully lapped, smaller and fewer asperities are produced. This is demonstrated in the surface profile trace shown in figure 2(c), the smoothest of the three traces presented. Even the lapping, however, leaves some surface roughness.

Extremely smooth, asperity-free surfaces are shown in the profile traces of figures 3(a) and (b) for mica and quartz surfaces. Both

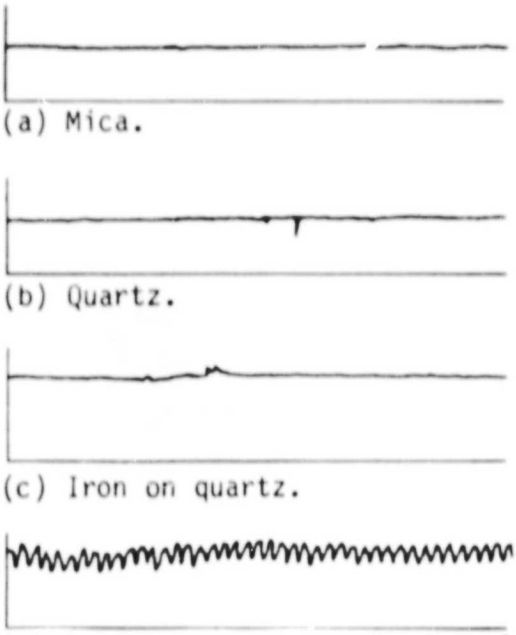

(a) Mica.

(b) Quartz.

(c) Iron on quartz.

(d) 1.0-Micrometer standard surface roughness.

Figure 3. - Surface profiles of various materials.

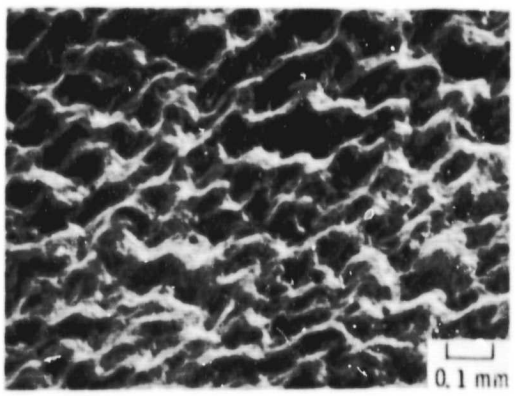

Figure 4. - Photomicrograph of a glass bead blasted aluminum surface.

surfaces were generated by cleavage. A crack that developed during the cleavage process is visible in the profile trace on the mica surface.

Normally, metal surfaces cannot be generated with the smoothness reflected in the profiles shown in figures 3(a) and (b). Such surfaces can be generated in the field ion microscope, but this only provides an atomically smooth surface over an area reflected by the pin tip radius of 500 to 1000 Å. Deposition of metal films on quartz surfaces such as that in figure 3(b) can be used to obtain an asperity-free metal surface. The results of such an approach are shown in the surface profile trace of figure 3(c) for iron vapor deposited in vacuum onto quartz. The surface is smooth compared with those surfaces shown in figure 2.

Very frequently it is desirable not to have extremely smooth surfaces - for example, when a greater surface area would promote such things as adhesion. A host of different methods, mechanical, chemical, and physical, can be used to increase surface area.

One of the most commonly used mechanical methods is to sand or bead blast the surface, thereby removing material through erosive wear. An example of such a surface is shown by the photomicrograph in figure 4. The surface looks like waves of water. This kind of surface topography may be very useful in certain bonding applications, catalysis, and chemical processes.

Among the chemical surface roughening methods, chemical etching is used. The particular reagents must be selected on the basis of the surface to be etched.

A very good technique for roughening surfaces involves using inert gas ions, which are made to bombard a surface and generate a surface texture. Ion etching, as it is called, is particularly versatile in that both bombarding species and ion energies can be selected to vary the surface topography. In addition, the incident angle of the ion beam can also be varied. The different surface textures that can be developed by this technique are indicated by the photomicrographs of silver surfaces in figure 5. In the upper portion of the figure the various surface orientations are depicted on the

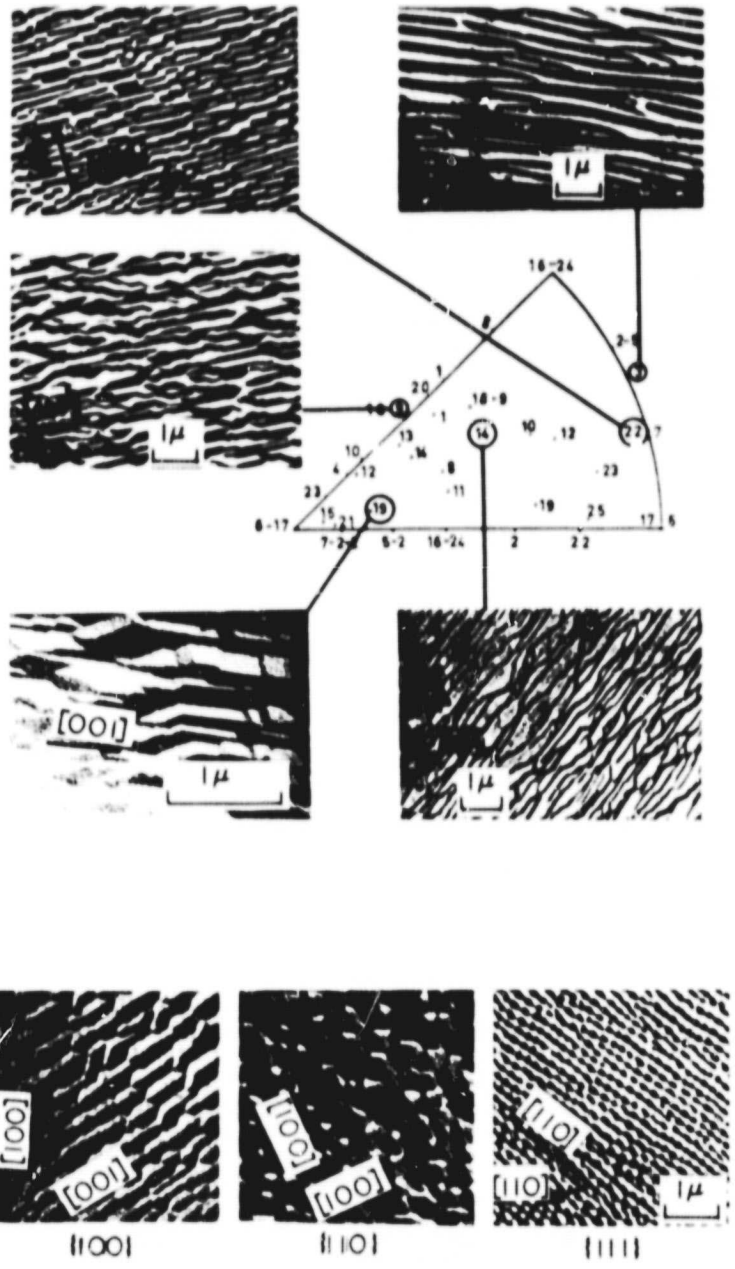

Figure 5. - Ion beam etched silver crystal surfaces with normal incident Ar^+ at 8 kiloelectron volts and dose of 7×10^{18} ions.

unit triangle. In the three micrographs in the lower portion of the figure, the ion etching effect on three principal planes of silver, namely, the (100), (110), and (111) surfaces, are shown. The photomicrographs in figure 5 indicate that considerable variation in surface texture can be developed with ion beam etching.

CRYSTALLINE STRUCTURE

The crystal structure of ideal surfaces for most practically used materials is generally one of three major types: body centered cubic, face centered cubic, or close packed hexagonal. All engineering surfaces vary from these ideal structures. Most real surfaces have grain boundaries which develop during the solidification of crystalline solids. These grain boundaries are, in a strict sense, defects which exist in the bulk solid and extend to the surface. They are atomic bridges linking the crystal structure of the two adjacent grains. Because of their role, they do not possess a regular structure, they are highly active, and they are very energetic. Grain boundaries are large defects that are readily observable on real surfaces. In addition to these, there are many lesser defects that may exist. These include subboundaries, twins, dislocations, interstitials, and vacancies.

Subboundaries are low-angle grain boundaries where only a slight mismatch in the orientation of adajcent grains occurs. When the crystal lattices of the adjacent grains are not parallel but are slightly tilted one toward the other, the defect is referred to as a tilt boundary. When the lattices are parallel, but one is rotated about a simple crystallographic axis relative to the other with the boundary being normal to this axis, the defect is a twist boundary.

The twin boundary occurs where there is only a degree or two of mismatch between the twins with the twins being mirror images of each other. They are frequently seen on the basal planes of hexagonal metals with deformation.

Dislocations are atomic line defects existing in crystalline solids. They may actually be in the subsurface and terminate with one

end at the surface or they may be in the surface. There are those dislocations that are entirely along a line where an extra half plane of atoms exists; these are called edge dislocations. In addition, there are screw dislocations that form along a spiral dislocation line. The screw dislocation can be seen on the surface as a wedge of atoms which is the terminus of the spiral. The small angle boundaries or subboundaries referred to earlier are generally composed of edge dislocations. It is the presence of these defects which causes crystalline solids to deviate so markedly from theoretical strength.

Some of the crystalline defects that may be found on a solid surface are presented schematically in figure 6. The vacant lattice site (fig. 6(a)) is simply the absence of one atom from a crystal lattice site. The interstitial (also shown in fig. 6(a)) is an extra atom crowded into the crystal lattice. Edge and screw dislocations are shown in figure 6(b), and the small angle boundary in figure 6(c).

Mechanically finished surfaces generally have undergone a high degree of strain and thus contain a large amount of lattice distortion and a high concentration of dislocations. While the initial presence of dislocations causes a reduction in strength, their multiplication and interaction during deformation produces an increase in surficial strength.

With plastic deformation of real surfaces, the strain produces a reduction, generally of the recrystallization temperature of the material at the surface. In many materials the combination of strain and temperature can bring about surface recrystallization, which has an annealing effect. Annealing relieves the lattice strain and the stored energy, and a sharp reduction in the concentration of surface defects results. In a dynamic, nonequilibrium system such as that encountered in mechanical activity on surfaces, the surface layers may be strained many times, recrystallized, and then strained again.

The application of surface forces such as may be associated with the techniques used to develop a desired surface topography can, in the absence of sufficient energy to produce recrystallization, result in a lattice strain such as that indicated in figure 7. The application of a surface force normal to the surface, that is, a

(a) Vacancy and interstitial crystal defects.

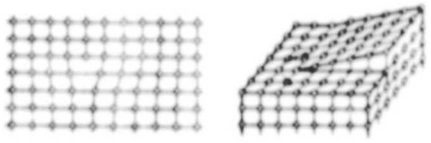

(b) Edge and screw dislocations.

(c) Small angle boundary composed of edge dislocations.

Figure 6. - Crystalline defects in solids.

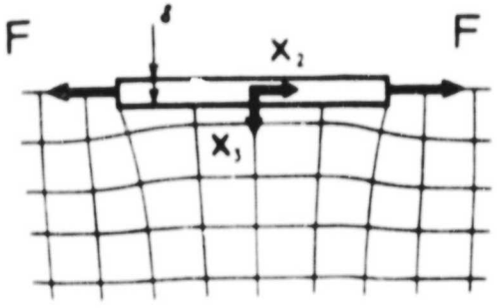

Figure 7. - Lattice distortion under compressed surface stress.

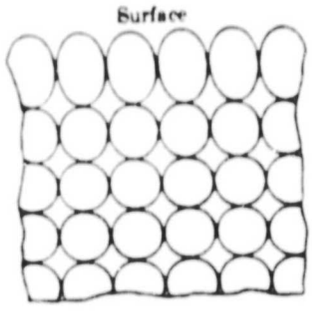

Figure 8. - Surface atoms (schematic). Since these atoms are not entirely surrounded by others, they possess more energy than internal atoms.

compressive force, causes forces X_2 and X_3 to develop. The resultant force normal to the surface, X_2, causes distortion in the crystal lattice.

CHEMISTRY OF SURFACES

Clean surfaces of solids are extremely chemically active. With an elemental metal, for example, the surface atoms are highly energetic. They are bound by like atoms everywhere but at the free surface. This boundary is depicted schematically in figure 8. A copper atom, for example, which lies in a (111) plane in the bulk of the solid has a coordination number of 12; that is, it is bonded to its 12 nearest neighbors. That same copper atom at the surface, however, has a coordination number of only 9. It has only nine nearest neighbors, three less than when it is in the bulk solid. Thus, the energy that normally would be associated with bonding to three additional like atoms is now available at the surface. This energy, expressed over an area consisting of many atoms in the surface lattice, is referred to as the surface energy.

Another way of looking at surface energy is to understand it as being the energy necessary to generate a new solid surface. This can be accomplished by separating adjacent planes in the solid. The energy required for separation is a function of atomic packing. For example, with copper, the atomic packing density is greatest in (111) planes (greatest number of nearest neighbors within the plane). As a result, the bonding forces between adjacent (111) planes is least and, therefore, the surface energy of new (111) surfaces generated, say by cleavage, is less than it is for other planes, such as the (110) and (100) planes. This lesser binding strength is also reflected in the distance between adjacent planes; the distance is greater between adjacent (111) planes than between other planes such as the (110) and (100) planes.

Because the atoms at the surface have this unused energy, they can interact with each other, with other atoms from the bulk, and with species from the environment. One of the things these surface atoms

can do, because they are not bound as rigidly as atoms in the bulk, is alter their lattice spacing at the surface (fig. 9). This is commonly called reconstruction. LEED (low-energy electron diffraction) studies have revealed reconstructed surfaces in some crystalline solids but not in others.

Another event that can occur in solids containing more than a single element (e.g., alloys) is for atoms from the bulk to diffuse to the surface and segregate there. In a simple binary alloy, for example, the solute atom can diffuse from the near-surface regions to the surface and completely cover the surface of the solvent. This has been observed for many binary alloy systems including aluminum in copper, tin in copper, indium in copper, aluminum in iron, and silicon in iron. The process of surface segregation is depicted schematically in figure 9.

The segregation mechanism is not really understood. One hypothesis is that the solute segregates on the surface because it reduces the surface energy. A second theory is that the solute produces a strain in the crystal lattice of the solvent and because of this unnatural lattice state, there is a necessary driving force to eject the solute atoms from the bulk. The result of this is segregation at the surface.

With ionic crystalline solids, surface charging can occur because of unequal vacancy energies. Near surface vacancies in these solids may be either positively or negatively charged. The energy associated with the formation of these vacancies varies and produces an excess of one or the other type of vacancy which causes a voltage between the surface and the interior of the solid. The overall energy of the system is decreased where there is an excess of positively charged ion vacancies in the solid, and these ions migrate toward the surface. When in the bulk (fig. 10(a)), they cause an internal rearrangement of vacancy charges (fig. 10(b)) such that the positive charge exists near the surface, and the Debye charged layer forms. This layer has no effect on the behavior of the solid surface, as, for example, in its interaction with adhesive.

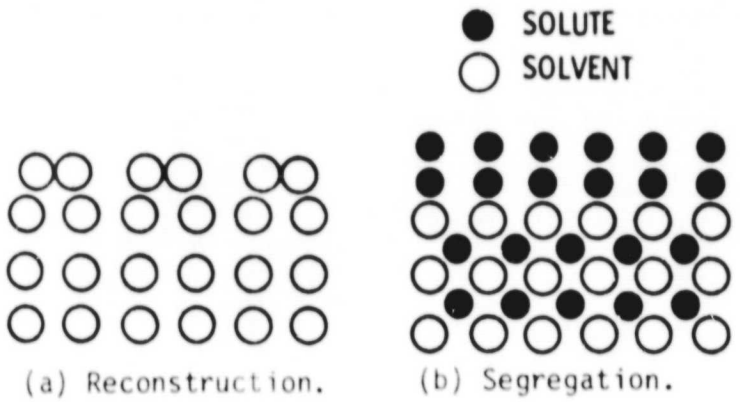

Figure 9. - Possible chemical surface events.

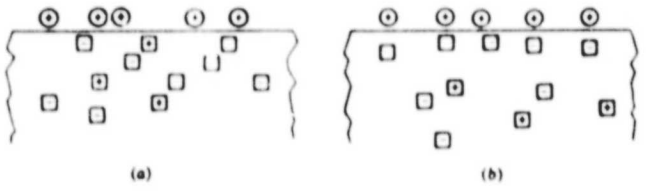

Figure 10. - Formation of Debye layers in ionic crystals due to unequal vacancy-formation energies with $E^- E^+$. Positive-ion vacancies are represented by - because of their effective negative charge and negative ion vacancies by +. (a) Uniform distribution of positive- and negative-ion vacancies which are present in different amounts because of different energies of vacancy formation. Voltage formed between the surface and the interior of the crystal. (b) Overall energy of crystal is decreased when the excess positive-ion vacancies migrate toward the surface to form a Debye space-charge layer. Interior of crystal below Debye layer now possesses equal numbers of positive-ion and negative-ion vacancies.

A great deal of concern must be given to the surface of polymer materials just as to metals and ionic solids. There are many variables in the preparation process that can alter the chemistry of a polymer surface as well as the chemistry of the metal surface - for example, topography resulting from the mode of preparation. With polymers, not only is the physical mode of surface preparation important but the environment in which the surface is prepared can also affect pronouncedly polymer surface chemistry.

The effect of the environment in which polymers are prepared has been carefully studied with ESCA (electron spectroscopy for chemical analysis). ECSA, or X-ray photoemission spectroscopy (XPS), as it is currently called, permits chemical analysis of surfaces by measuring the energies associated with electron levels in atoms and molecules and shifts in electron energies accompanying various chemical reactions. It is a surface-sensitive tool.

Films of high density polyethylene were prepared from powders by hand pressing the powder between sheets of clean aluminum foil at the minimum temperature of 200° C to insure plastic flow. The samples from the identical powders were prepared in three different environments: in air, in nitrogen, and, after being pumped down to 10^{-14} torr, in pure nitrogen or argon. The surfaces were examined with XPS for both oxygen (O_{1s}) and carbon (C_{1s}).

The O_{1s} and C_{1s} spectra corresponding to samples from the three modes of preparation are striking (fig. 11(a), (b), and (c)). ATR and TIR experiments did not reveal the presence of any oxygen function (-OH, $\geq$C=O, C-O-C, etc.), and, in fact, the spectra were virtually identical. This demonstrates the great power of XPS to distinguish minute differences in samples when such differences are localized at or near the surface. Comparison with the data for low-density polyethylene and with model monomer systems shows that the O_{1s} signal arises from $\geq$C=O environments. The three methods of preparation clearly indicate that "unoxidized" surfaces may be prepared most readily by excluding all traces of oxygen during the pressing stage. On leaving samples exposed to the atmosphere for some time, hydrogen bonds to the surface $\geq$C=O groups from extraneous

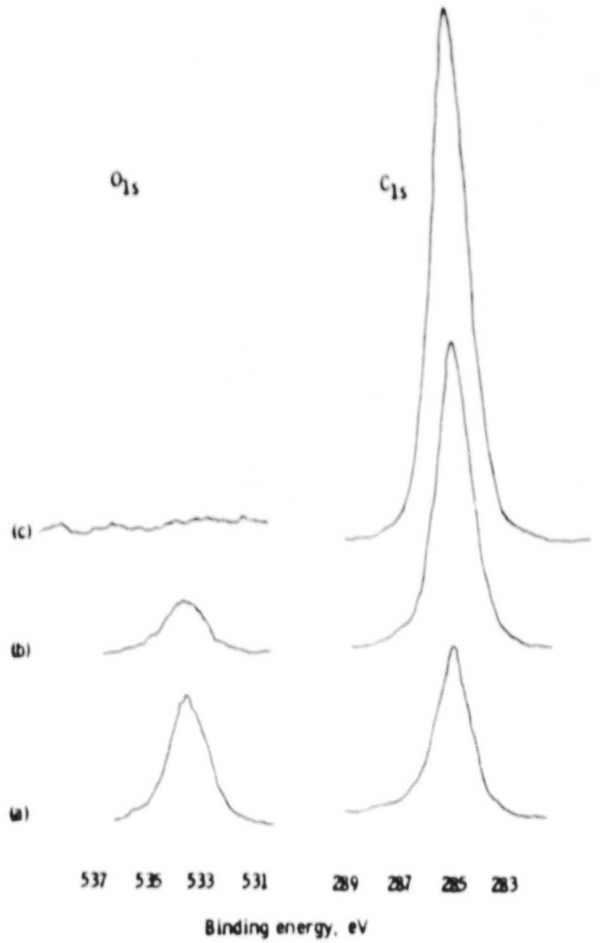

Figure 11. - XPS analysis of C_{15} and O_{15} levels of high-density polyethylene films pressed (a) in air, (b) in nitrogen, and (c) after gassification in a 10-torr vacuum (pure nitrogen or argon).

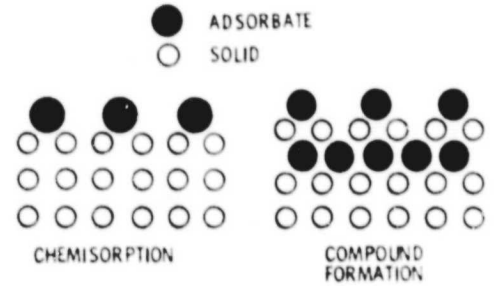

Figure 12. - Chemisorption and compound formation on solid surfaces.

water in the atmosphere, and the O_{1s} peak then acquires the characteristic doublet nature. Again, ATR and TIR do not reveal any changes since the hydrogen bonding is localized at the surface (ref. 4).

Chemisorption

In addition to the characteristic of the solid surface itself, the surface can interact with the environment. This interaction is extremely important because it alters the surface chemistry, physics, metallurgy, and mechanical behavior. If a metal surface is very carefully cleaned in a vacuum system and then a gas such as oxygen is admitted to the system, the gas adsorbs on the metal surface. This interaction results in strong bonds being formed between the metal and the adsorbing species. With the exception of inert gases, this adsorption results in bonding which is chemical in nature, and the process is referred to as chemisorption. The process is indicated schematically in figure 12. Once adsorbed, these films are generally difficult to remove.

Where the species adsorbing on a clean surface is elemental, the adsorption is direct. The atoms in the surface of the solid retain their individual identity as do the atoms of the adsorbate; yet each is chemically bonded to the other. When the adsorbing species is molecular, chemisorption may be a two-step process: first, dissociation of the molecule on contact with the energetic clean surface, and then adsorption of the dissociated constituents.

Chemisorption is a monolayer process. Furthermore, the bond strengths that exist between the adsorbing species and the solid surface are a function of chemical activity of the solid surface (surface energy), the degree of surface coverage of that adsorbate or another adsorbate, the reactivity of the adsorbing species, and its structure.

The surface energy of the solid surface is important because the more energetic the surface, the stronger the tendency to chemisorb. The effect of surface energy can be demonstrated by examining various

crystallographic planes of a single metal. In general, the high energy, low atomic density planes chemisorb environmental species much more rapidly than the high density, low surface energy planes. This has been demonstrated experimentally. Hydrogen sulfide adsorbs more readily on (110) and (100) surfaces of copper than on (111) surfaces.

When different solid surface materials are considered, adsorption differences are also observed. For example, copper, silver, and gold are the noble metals, and many of their properties are considered to be very similar. Yet with respect to chemisorption of a gas, such as oxygen, considerable differences are observed. Oxygen chemisorbs strongly to copper, weakly to silver, and not at all to gold.

The reactivity of the adsorbing species is also very important. Examination of the halogen family indicates that fluorine adsorbs more strongly than chlorine, chlorine more strongly than bromine, and bromine more strongly than iodine.

The structure of the adsorbing species is also very significant in surface bonding and chemisorption. This can be demonstrated with the adsorption of simple hydrocarbons. Something as simple as the degree of bond saturation in the molecule makes a difference. If ethane, ethylene, and acetylene are adsorbed on an iron surface, the tenacity of the resulting chemisorbed films is in direct relation to the degree of bond unsaturation. Acetylene is much more strongly bound to the surface than is ethylene, which, in turn, is more strongly bound than is ethane. The simple explanation for this is that the unsaturated carbon to carbon bonds break on adsorption and bond to the iron. The greater the number of carbon to carbon bonds, the greater the number from the hydrocarbon molecule to iron.

Compound Formation

Compound formation on the surface of solids is extremely important. The naturally occurring oxides present on metal surfaces prevent their destruction when in contact with other solids. Furthermore, their presence can alter deformation behavior. Solids

and liquids can readily react with clean solid surfaces to form compounds, the presence of which can alter surface properties.

Chemisorbed films can often interact with a surface to form chemical compounds. When this occurs the surface material and the adsorbate lose their individual identities and form an entirely new substance with its own properties. Unlike chemisorption, which is simply a monolayer process, constituents from the environment can react with the solid surface by diffusion of the solid surface material into the compound and diffusion of the environmental species into the film. The compound can continue to thicken on the surface if the film is porous and allows for the two-way diffusion to occur (fig. 12).

An example of the formation of a porous compound on a surface is the rust, or iron oxide, produced in the oxidation of iron in a moist air environment. The oxidation process continues to consume the iron. In contrast, the oxidation of aluminum to form aluminum oxide results in the formation of a thin, dense oxide which, because of the film's density, retards diffusion and further growth.

Metallurgical Effects

Surface behavior is altered by the presence of grain boundaries on the surface of crystalline solids as well as other surface defects. For example, grain boundaries, in addition to having a chemical effect because of their high energy, also influence mechanical properties. The microhardness is generally higher in grain boundaries than it is in the grains (ref. 5). This hardness effect is shown by the data in figure 13 for iron; as the grain boundary is approached, the hardness increases. The hardness is at a maximum directly in the boundary. The increase is marked and not marginal.

The increase in hardness seen in the grain boundary (fig. 13) can be explained on the basis of what has already been discussed relative to grain boundaries. They are regions of high dislocation concentration and lattice strain. Strained metal has a higher dislocation concentration than the annealed or strain-free material,

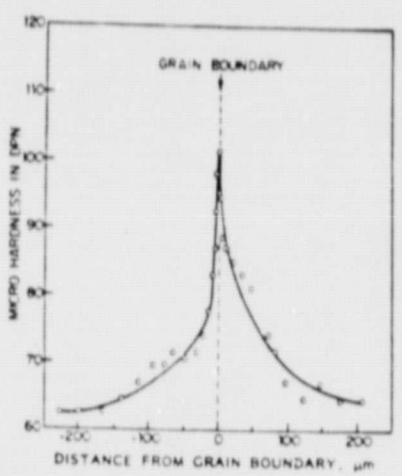

Figure 13. - Microhardness traverse across a grain boundary in iron containing 0.02-percent oxygen.

and the concentration generally increases with increased deformation until such time as recrystallization occurs.

Dislocations, like grain boundaries, are higher energy sites on a surface than nondislocation areas. It is for this reason that strained metal surfaces are chemically more active than are annealed or strain-free surfaces. This chemical activity of dislocation sites can be demonstrated by a technique called etch pitting. Certain chemical agents react on the surface of a material, and, because of the more energetic nature (i.e., greater reaction rates) of the dislocations, these sites are preferentially etched. The result is that pits are left on the surface at each dislocation site. From these pits it is possible to identify the location and concentration of the dislocations. The necessary reagents required for etch pitting various materials can be found in the metallurigical literature.

SURFACE FILM EFFECTS

The properties of solid surfaces are markedly altered by the presence of foreign substances. An atomically clean metal surface has certain characteristic chemical, physical, and metallurgical properties. As soon as something interacts chemically with that surface, those properties are changed. This is extremely important to understand because most real surfaces are not found in the atomically clean state but rather with film(s) present on their surfaces, as has already been discussed in reference to figure 1.

The wide variations found in the literature for the surface properties of materials can be directly attributed to the effect of these films. Some surfaces are more strongly influenced by these films than others, and the specific film composition produces varying effects.

The presence of oxides on metal surfaces has been observed to produce surface hardening. Roscoe, in some very fine experiments conducted in the 1930's, demonstrated this effect with cadmium oxide on a cadmium surface (ref. 6). Since then it has been demonstrated by

other investigators who have observed dislocations emerging at the surface with the oxide impeding their mobility.

While oxides and some films produce surface hardening, other surface films increase ductility. For example, water on alkali halide crystals allows an otherwise brittle solid to deform plastically. Water has the same effect on ceramics.

Magnesium oxide (MgO) is normally a very brittle material with a surface hardness in the clean state of about 750 kilograms per square millimeter. When MgO is cleaved under a hydrocarbon such as toluene to exclude moisture, a hardness value of this magnitude is measured for the MgO surface. If, however, the MgO is cleaved in moist air where the freshly generated clean surface can interact with the moisture in the air, a different result is obtained as indicated by the data in figure 14 (ref. 7).

Figure 14 presents the hardness of MgO as a function of identation time in the two environments, dry toluene and moist air. The increased surface ductility in the presence of water is striking. Not only is there an appreciable difference in hardness, but that difference increases with increasing indentation time. The hardness in moist air decreases with increasing identation time; in dry toluene, the hardness is unchanged. It is this change with time that makes the film effect a true surface property and not simply a lubricating effect produced by the water.

In the late 1920's the Russian researcher Rehbinder found that the presence of certain organic molecules on the surface of solids produced a softening effect (ref. 8). Mechanical behavior was altered by these films. Such substances as oleic acid in Vaseline oil are examples of the materials examined. This effect is important because many of the materials studied are commonly found substances. The surface softening can be very beneficial in certain instances such as in stopping the formation of fatigue cracks.

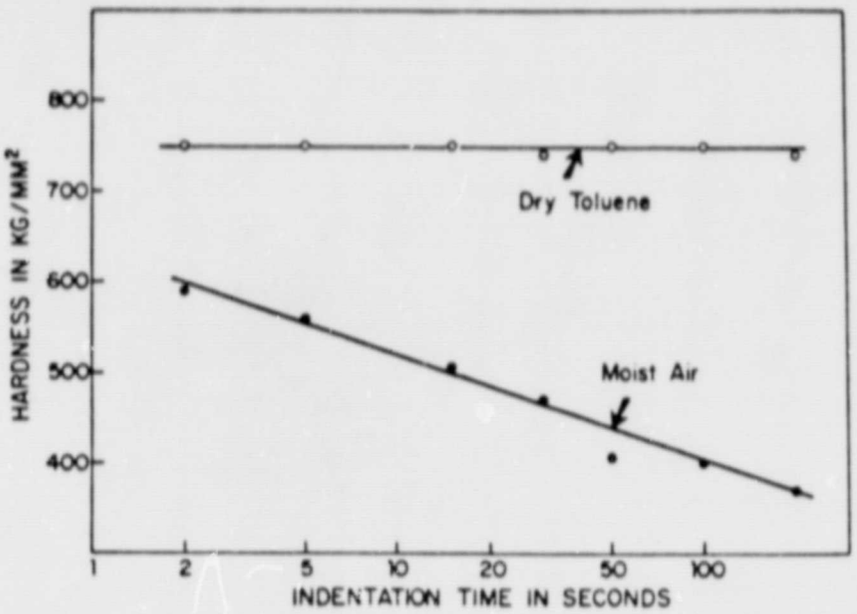

Figure 14. - Illustration of time dependence of microhardness of cleaned MgO in moist air.

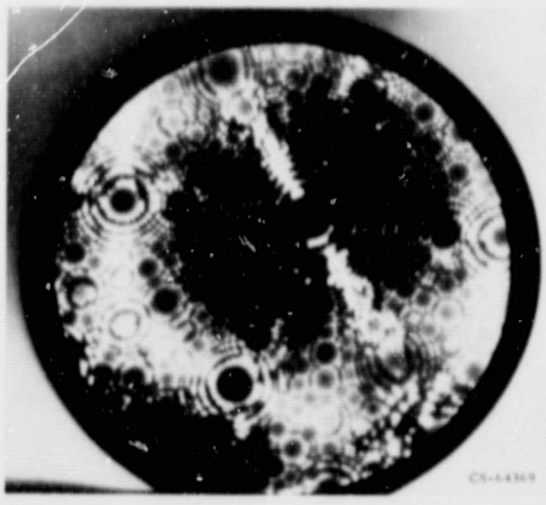

Figure 15. - FIM of tungsten surface prior to contact (16.0 kV).

CHARACTERIZATION OF TRIBOLOGICAL SURFACES

MICROSCOPY

The nature and character of the surface is extremely important to understanding the performance of that surface in adhesive systems. Microscopy has been, and still probably remains, the most common technique employed for the characterization of surfaces. The magnification of surfaces to identify structure dates back to at least the 16th century. With simple lenses the features of surfaces could be magnified 100 times.

In the 1700's the optical microscope was developed, and it really enabled the effective characterization of surfaces. This microscope gave the person interested in surfaces his most effective tool, and it still remains that to this day. The ordinary optical microscope can yield detailed surface features at magnifications of about 500 and 1000 with the aid of oil immersion. Thus, the character and structure of grain boundaries in metals and alloys are readily identifiable.

The development of the electron microscope was a notable advance because it permitted magnifications from 10 to 100 000. For the first time atomistic features of surfaces were identifiable and rows of atoms on the surface could be readily seen. Today, electron microscopy is used routinely to identify and characterize dislocation structures in materials.

In the 1950's it became possible to characterize surface structures at the individual atom level with the development of the field ion microscope by Erwin Mueller (ref. 9). At this point in the development of research instrumentation, it must be said that, for structural analysis, the field ion microscope is the ultimate tool because it does identify individual atom sites on a solid surface. Thus, each individual white spot in the field ion micrograph of figure 15 represents an individual atom site with the rings representing atomic planes.

The field ion microscope has been adapted for use in adhesive studies to characterize surfaces. Figure 15 is a photomicrograph of a

tungsten surface. The micrograph reveals the atoms and planes. The ring just to the upper right of center is the (110) plane of tungsten. Each row out from the center ring represents the next nearest layer of atoms to the surface. The field ion microscope is so sensitive that it can detect the absence of a single atom from the surface or conversely the presence of extra or foreign atoms.

In recent years the atom probe has been developed to determine single atom chemistry. When used in conjunction with the field ion microscope, the atom probe can characterize the structural arrangement of individual atoms on a solid surface and also determine the chemistry of an individual atom present in the surface.

ETCHING

Etching is the interaction of surfaces with chemical agents such as acids or bases. With simple metals in the polycrystalline form, the crystallographic orientation at the surface of each adjacent grain varies. The energies of these surfaces vary and they, therefore, react at different rates with a particular chemical agent. Thus, in a crude way, one can distinguish the more atomically dense surface planes from the less dense. Since the more dense planes have lower surface energies, they are not as readily attacked as the less dense planes.

Etching can be and has been used very effectively to reveal grain boundaries in metals. Grain boundaries are sites of higher energy than are the surfaces of the individual grains and, therefore, they are preferentially attacked. Furthermore, different phases in alloys etch differently at the surface. The chemical reagents for such etching are available in standard metallurgical handbooks.

In addition to identifying orientation, grain boundaries, and phases, etchants can be used to identify atomistic defects such as dislocations, the line atomic defects in crystalline materials referred to earlier. The proper etchant can not only indicate the concentration of dislocations at the surface but can also reveal their

location. Furthermore, etchants reveal the atomic plane on which the dislocation lies.

A wealth of useful information can be acquired about a surface by using the optical microscope and etching techniques. Simple chemical spot tests used in conjunction with the foregoing can provide insight into the chemistry of the solid surface. These tests require using readily available chemical reagents which, when applied to the surface, reveal the metallic element present in the surface. Many standard college chemistry textbooks on inorganic qualitative analysis list the required materials.

The chemical spot test can be used to detect adhesive transfer to surfaces where dissimilar materials are in contact. A permanent pattern of an elements distribution on a surface can be obtained if the chemical reagents are impregnated in a porous paper such as filter paper. This paper is then pressed against the surface to be analyzed, and the paper is moistened. A map showing the location of the elements then appear on the paper.

ANALYTICAL SURFACE TOOLS

The field ion microscope and the atom probe have already been discussed. These tools have been used in adhesive studies to characterize surfaces before and after adhesive contacts.

Many analytical tools have been developed in recent years to characterize the real nature of solid surfaces. Some operate on the principle of atomic arrangement in the surface layers of crystalline solids. One such device is LEED (low-energy electron diffraction). This surface tool can be very useful to those interested in surfaces. It analyzes by an electron diffraction technique the general atomic arrangement of the outermost surface layers of a solid. A rudimentary understanding of atomic arrangement helps in understanding its mode of indicating surface structure.

With the exception of amorphous carbon, glasses, and some polymers, nearly all materials, including metals, alloys, ceramics, solid lubricants, and graphitic carbon, are crystalline. This means

that the atoms or molecules are arranged in accordance with particular structures that can readily be identified. These structures are mostly cubic and hexagonal. The cubic structure can be further subdivided into face centered cubic and body centered cubic.

Metals such as copper, nickel, silver, gold, platinum, and aluminum have a face-centered-cubic structure, while metals such as iron, tantalum, niobium, vanadium, and tungsten have a body-centered-cubic structure. A number of metals, including zinc, cadmium, cobalt, rhenium, zirconium, and titanium, have a hexagonal crystal structure.

The atoms making up the faces of the cube for the face-centered-cubic and the body-centered-cubic structures are referred to as the (100) surfaces. They constitute planes of atoms that can move relative to each other when the crystal is deformed plastically and are, therefore, also referred to as slip planes within the crystal. Under applied stresses these planes (the (100)) are frequently one of the sets of planes most commonly observed to slip over one another in the body-centered-cubic system.

The (111) planes are a third set of planes in the cubic system. These planes are the ones on which slip and cleavage in face-centered-cubic materials are most frequently observed. There are other planes that may be observed as well. For example, if one were to use X-ray diffraction, electron channeling, or some other technique to determine the crystallographic orientations in each grain of a polycrystalline sample analyzed, many different crystallographic planes would appear.

As already mentioned, the (111) planes in the face-centered-cubic crystal are the planes of closest atomic packing. The atoms occupy the least area for the number of planes involved. When this particular plane is present on a surface, it has the lowest surface energy in the face-centered-cubic system and, therefore, is the least likely to interact chemically with environmental constituents.

The (110) planes in the face-centered-cubic system are the least densely packed. The two outer rows of atoms as well as the center row are outermost with the two in-between rows below these. The (110)

planes have higher surface energies than the (111) planes and are, therefore, much more reactive. Furthermore, because they are less densely packed, their mechanical behavior such as elastic modulus and microhardness is also less than is observed on the (111) planes.

On any particular crystallographic plane present on the surface, the atomic packing can vary with direction of movement. For example, on a (111) surface two basic directional packing variations exist. Surface energies also vary in these two directions.

Low-Energy Electron Diffraction (LEED)

Low-energy electron diffraction (LEED) is a very widely used surface tool for characterizing of the surface atomic structure seen on crystalline solids. Because the device detects the surface crystal structure, single crystals are generally studied, although large-grained polycrystals can also be examined. Low-energy electrons in the range of 20 to 400 electron volts are diffracted from the surface crystal lattice producing a reciprocal image of the lattice on a phosphorus screen.

Figure 16 contains three LEED patterns from an iron (011) surface. The photograph and pattern in the upper left corner are for the iron surface with oxide removed. Upon oxide removal and heating of the iron in vacuum, the surface of the iron becomes covered with a film which produces a ring structure of diffraction spots on the surface. Auger electron spectroscopy analysis (which is discussed in the next section) identified the surface film to be graphitic carbon. Carbon segregates from the iron bulk to the surface.

When the iron is argon ion bombarded, the carbon disappears and four diffraction spots in a rectangular array representative of the clean iron (011) surface remains. The carbon has been removed by the argon ion bombardment. The iron diffraction spots are not sharp but rather are fuzzy and elongated because the argon bombardment strains the iron surface lattice. This strain can be removed by a very mild heating for a short period and then cooling to room temperature. This

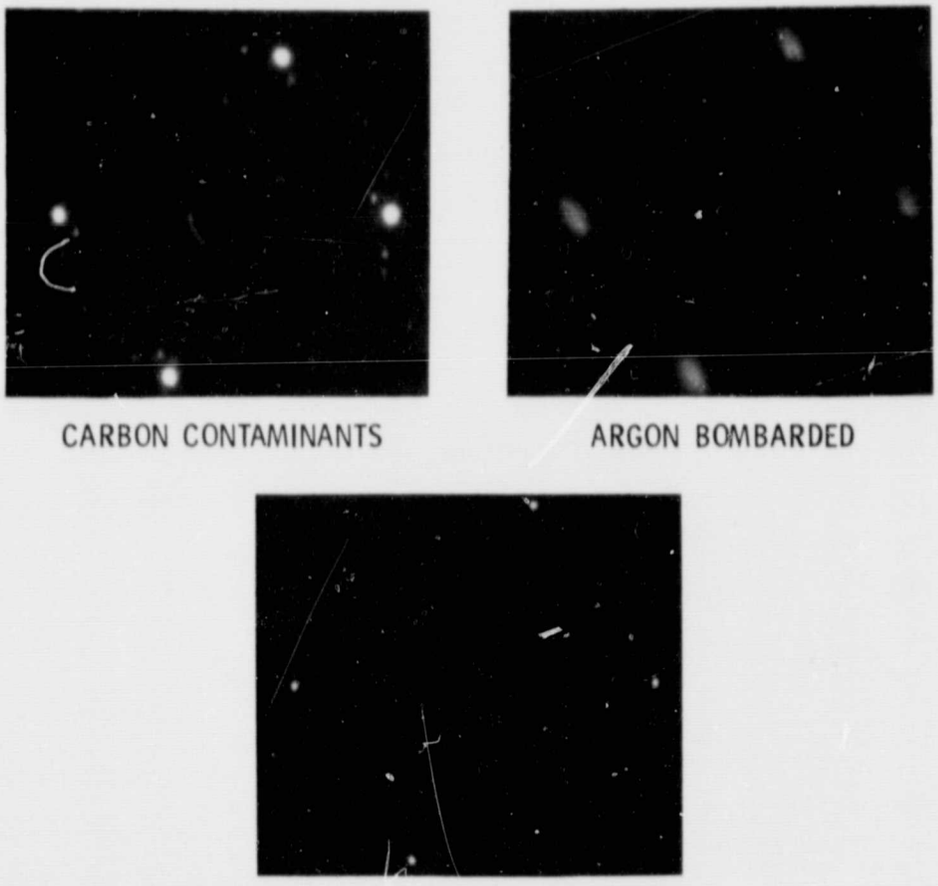

Figure 16. - LEED patterns of iron (011) surface.

produces the clean iron surface diffraction pattern of the lower photograph in figure 16.

LEED can, as indicated, be an effective tool in identifying a clean metal surface, its structure, and its condition or state. It can also be used to identify the structure of films formed on a clean surface. Two polymer forming hydrocarbon molecules produce entirely different structures when adsorbed to a clean iron surface. These films and their structures are presented in figure 17. The two molecules, ethylene oxide and vinyl chloride, each contain two carbon atoms; however, one molecule contains oxygen, and the other, chlorine. A close-packed structure of ethylene oxide completely covers the iron surface.

Auger Electron Spectroscopy

Although LEED is very useful for structural surface analysis, it does not give any indication of the chemistry of the surface. For this information other surface tools must be used. A very effective tool for this purpose is Auger emission spectroscopy analysis. It has the ability to analyze for all the elements present on a surface except for hydrogen and helium. It is sensitive to an element such as oxygen to surface coverages of as little as one-hundredth of a monolayer. It analyzes to a depth of four or five atomic layers.

The basic mechanism in Auger electron spectroscopy analysis involves the use of a beam of electrons just as with LEED, but the energy of the electron is higher than with LEED - usually 1500 to 3000 electron volts. The incident electrons strike the sample surface, penetrate the electron shells of the outermost surface atoms, and cause the ejection of a second electron called an Auger electron. The ejected electron carries with it an energy characteristic of the atom from which it came. Thus, if the energy of the ejected electron is measured, it is possible to identify its element source.

The electron energies detected can be recorded on a strip chart recorder or on an oscilloscope. The details of Auger emission

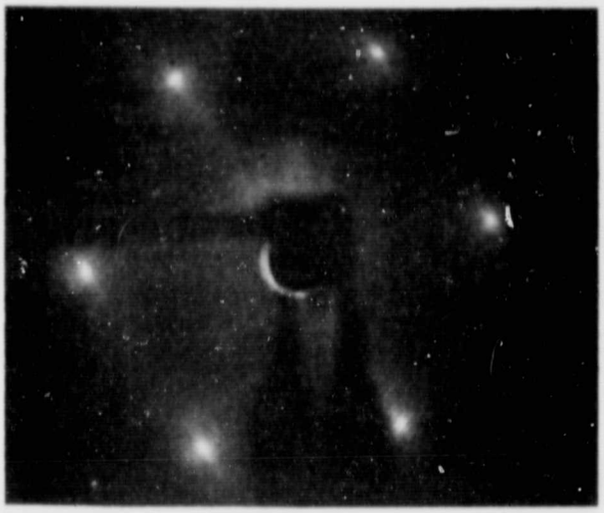

$CH_2 - CH_2$

$CH_2 = CHCl$

Figure 17. - LEED patterns obtained with two polymer forming hydrocarbons on iron (011) surface (1000-L exposure).

spectroscopy analysis and the type of data generated can be found in Kane and Larrabee (ref. 10).

Figure 18 presents an Auger spectrum for an iron (011) surface. An ordinary iron surface with normal surface contaminants present yields a spectrum such as that displayed in figure 18. The surface contains peaks for the elements sulfur, carbon, oxygen, and iron. The carbon and sulfur have two sources of possible origin: impurities in the bulk iron which have segregated to the surface or adsorbates from the environment. For example, the carbon can arrive on the surface as carbon monoxide or carbon dioxide or can diffuse to the surface from the bulk.

The oxygen peak in figure 18 can result from the iron oxides present on the surface or, again, from adsorbates such as carbon compounds or water vapor. The three iron peaks originate from the iron oxides and the iron metal.

If the surface represented by figure 18 is bombarded with argon ions, the surface contaminants sulfur, carbon, and oxygen would be knocked off, leaving only iron to be detected by the Auger spectrometer. A low-energy iron peak appears at the left end of the spectrum after the sulfur, carbon, and oxygen have been removed. This low-energy peak is easily lost when the surface is contaminated and is, therefore, usually seen when the surface is clean.

In addition to supplying information on the identity of elements present on a surface, Auger electron spectroscopy can give insight into the form in which an element exists on a surface. For example, carbon can arrive at a surface from many sources. It can diffuse from a bulk metal or alloy and segregate at the surface. It can be present as adsorbed carbon monoxide or it can exist in the crystalline form of graphite. The form of the carbon can be extremely important to adhesive bonding characteristics.

Analysis of the shapes of Auger peaks can provide considerable information about the source of an element such as, for example, carbon. Carbon peak shape analysis can indicate whether the carbon comes from the bulk solid carbide, adsorbed carbon containing gases (e.g., CO or CO_2), or graphite. The Auger peaks are all for carbon

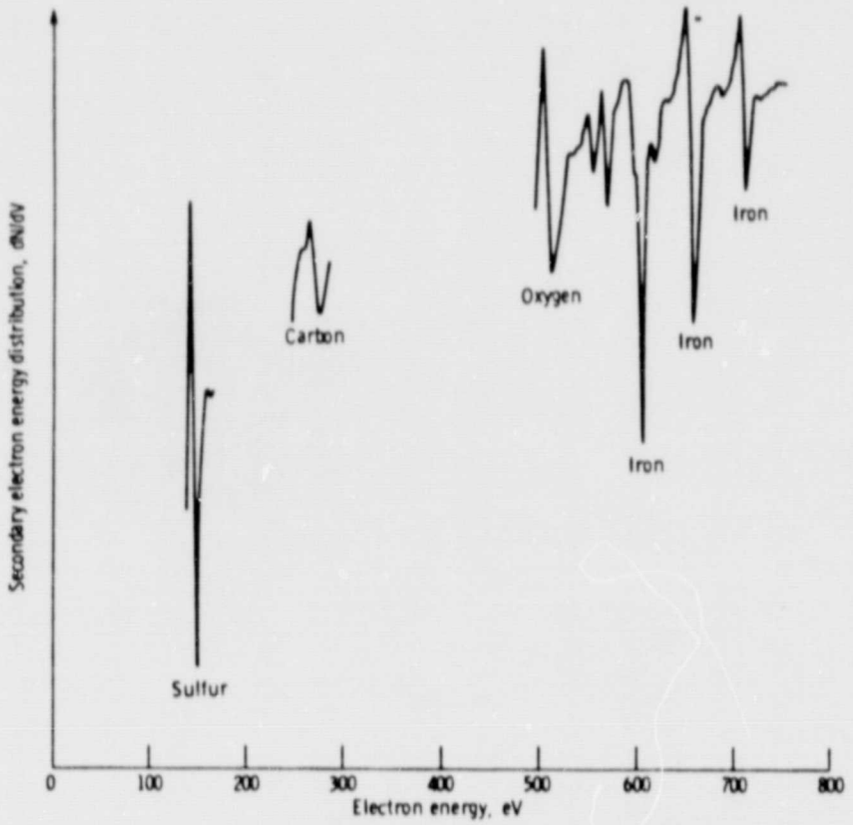

Figure 18. - AES analysis of iron (011) surface.

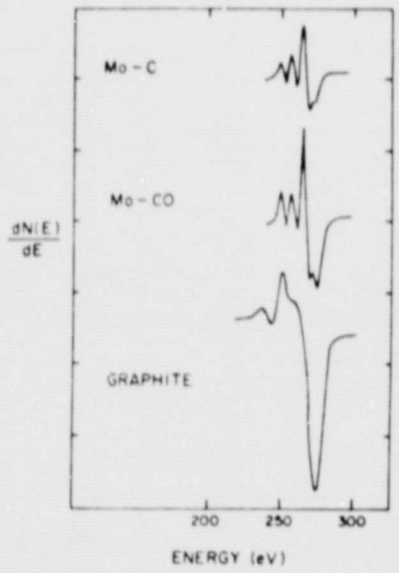

Figure 19. - AES of carbon segregated at a Mo (110) surface during initial cleaning, in CO on a clean Mo (110) surface (Mo-CO), and in graphite.

but their shape differences tend to identify the carbon source. These differences can be seen in figure 19 for the various forms of carbon on a iron surface.

X-Ray Photoemission Spectroscopy

While Auger electron spectroscopy can give some indication of the surface structure from which an element came, it is rather limited in this area. Its principal function is elemental surface analysis. There are other surface tools that can determine the molecular structure from which an element came. One such tool is X-ray photoemission spectroscopy.

With XPS an X-ray rather than an electron beam is used as the energy source. The X-ray beam is monochromatic, and it causes electrons with kinetic energies characteristic of the surface atoms to be ejected from the specimen. A spectrum containing the elements present is obtained by plotting the total number of electrons ejected from the surface as a function of kinetic energy. XPS gives binding energies of the elements, and from these binding energies it is possible to identify the nature of the compounds in which these elements exist. The binding energy of the electrons ejected from the surface is determined by the chemical environment and is roughly a function of the atomic charge.

The binding energy measured with XPS is altered by changing the particular elements bound to the element being examined. This is demonstrated for sulfur in the data of figure 20. Elemental sulfur (S^0) has a characteristic binding energy of 162.5 electron volts. Negatively charged sulfur (S^{-2}) has a readily measurable lower binding energy. When oxygen is bound to the sulfur, there is an increase in the sulfur binding energy. Furthermore, the amount of oxygen bound to the sulfur will affect the observed binding energy. The SO^{-2} structure has a greater binding energy than the SO^{-2} which can be used to distinguish between sulfur bound in these two states (ref. 11).

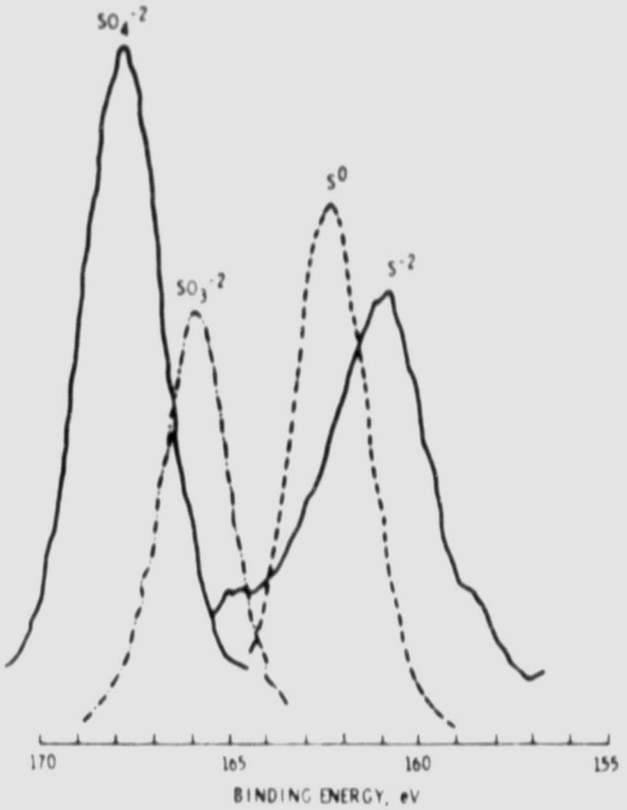

Figure 20. - Sulfur (2p) XPS of representative sulfur types.

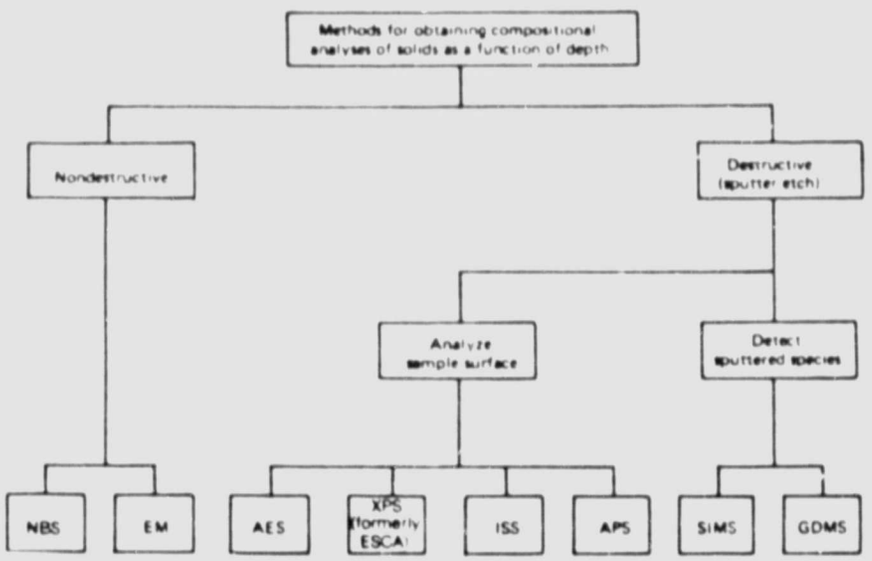

Figure 21. - Some techniques for chemical characterization of surfaces.

Other Techniques

A host of surface tools have been developed for the analysis and chemical characterization of surfaces. At the time of this writing, the author knows of over 70 such tools. The number will undoubtedly have increased by the time of publication of this thesis, and there is no doubt that the number will continue to grow. A few of the more commonly used techniques are indicated in figure 21. The techniques indicated are separated into destructive and nondestructive classes.

The nondestructive techniques are nuclear back-scattering spectroscopy (NBS) and electron microprobe (EM). Auger electron spectroscopy (AES), X-ray photoemission spectroscopy (XPS), ion-scattering spectroscopy (ISS), and appearance potential spectroscopy (APS) are destructive only if sputter etching or depth profiling is used.

Two techniques, which are definitely destructive to the surface, are secondary ion-mass spectroscopy (SIMS) and glow-discharge mass spectroscopy (GDMS). These techniques detect the species sputtered from the surface and thus analyze material that has been removed from the surface. The details of the operation of these devices can be found in reference 10.

The capabilities of the instruments presented in figure 21 are set forth generally in table I. All of these devices have certain limitations. Note that they can detect all elements except hydrogen and helium, can provide excellent chemical identification, have sensitivities of surface elements to as little as 0.01 monolayer, and give chemical information. Their disadvantage, not indicated in table I, is that they must be operated in a vacuum.

Probably the most versatile tool available for use on surfaces and the one requiring the least technical interpretation skill is the scanning electron microscope (SEM). It is extremely useful to the surface analyst because it allows him to view depth features on a surface such as the asperities or surface irregularities discussed earlier. It can also identify the topography of surfaces where adhesion has taken place with adhesives.

TABLE I. - COMPARATIVE TABLE FOR THE VARIOUS TECHNIQUES USED FOR THE CHEMICAL CHARACTERIZATION OF SURFACES

	NBS	EM	AES	XPS	ISS	SIMS	GDMS	APS
Destructive to sample (in general)	No	No	No	No	No	Yes	Yes	No
Element that can be detected	Heavy	$Z \geq 4$	$Z \geq 3$	$Z \geq 3$	$Z \geq 3$	All	All except He, Ne	$Z \geq 3$
Elemental identification[a]	F	G	E	E	E	G	G	E
Sensitivity (typical) in monolayers	50	5	~0.01	<0.01	~0.01	<1	~1	$\leq$0.1
Detectability (i.e., ppm)	NA[b]	100	<1	NA	NA	1	100	NA
Results are (in principle)	Absolute	Absolute	Absolute	Absolute	Absolute	Absolute	Absolute	Absolute
Depth probed (in Å)	10^4	10 to 10	15 to 20	15 to 75	3	$\sim 5 \times 10^4$	10 to 10	~10
Depth distribution of elements	Yes	Yes	Y/d[c]	Y/d	Yes	Yes	Yes	Y/d
Chemical (i.e., binding) information	No	Yes	Yes	Yes	No	No	No	Yes

[a]E, excellent; G, good, F, fair.
[b]NA, not applicable.
[c]Y/d, yes, if destructive.

When the SEM has incorporated into it X-ray energy dispersive analysis, both topography and chemistry can be determined. The X-ray analysis is not a surface analytical tool but it can provide considerable information where material transfer takes place as in adhesion. The effectiveness of this combination can be seen in figure 22 where gold contacted and transferred to a single-crystal silicon surface. The upper figure is an SEM photomicrograph of the transfer, while the lower is an X-ray map for gold and reveals that the white areas in the upper photomicrograph are gold.

ROLE OF ENVIRONMENT ON TRIBOLOGICAL BEHAVIOR

The environment surrounding practical tribological components can play a very strong role in the adhesion, friction, and wear behavior of these materials in solid-state contact. For this reason the lubrication or tribological system is frequently referred to as consisting of essentially three components. The material surfaces are the first to be lubricated whether they belong to a bearing, gear, seal, or some other mechanical device; then, there is the lubricant (liquid or solid) that provides the friction and wear reducing protective surface films; and finally there is the environment. The environment in many practical tribological systems can have a very strong influence on the behavior exhibited, and in some instances, the environmental constituents when present on surfaces can completely mask other effects such as those of the lubricants.

ADSORBATES AND OXIDES

In a conventional atmospheric environment, the oxygen present in the air interacts with freshly generated metal and alloy surfaces to produce surface films - namely, oxides. These oxides play a very strong role in the adhesion, friction, and wear behavior of metals and alloys. In the absence of these oxides, very strong adhesion, high friction coefficients, and ultimately cold welding of materials from one surface to another are observed. If, for example, two normal

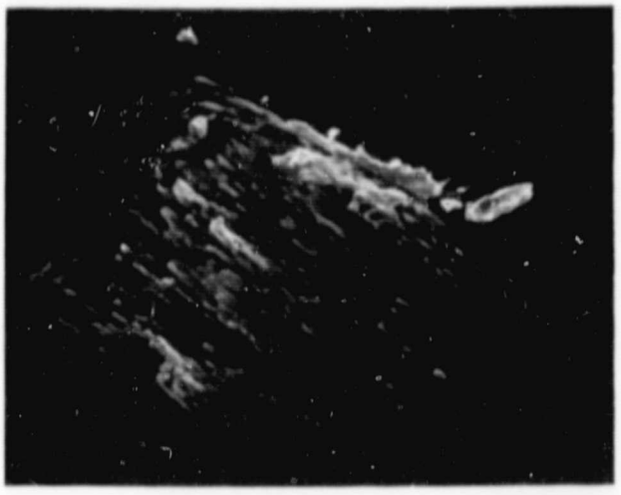

PHOTOMICROGRAPH

X-RAY MAP FOR GOLD

CS-78-709

Figure 22. - Silicon (111) surface after adhesive contact with gold (30 g; 23° C; 10^{-8} N(cm^2).

metal surfaces are taken and placed inside a vacuum environment with a system capable of achieving pressures to 10^{-10} torr and the surfaces are very carefully cleaned with argon ion bombardment and then brought into touch contact, adhesion immediately occurs of one surface to the other. Attempts at tangential motion cause a growth in the area adhered at the interface (i.e., in the real contact area) with an ultimate complete seizure of the surfaces one to another. With this occurrence, the surfaces are generally severely disrupted (refs. 12 and 13).

When adhered surfaces are separated, the adhesion at the interface between the two dissimilar solid surfaces is sufficiently strong so that fracture does not occur at the interface but generally in the cohesively weaker of the two materials in contact (ref. 14). An example of such behavior is shown in the photomicrograph in figure 23. The results shown in figure 23 are for an experiment conducted in a vacuum chamber where two solid surfaces were brought into contact and the surfaces had been cleaned in the vacuum environment. Adhesion occurred at the interface, and when separation of the solid surface was attempted, fracture occurred in one of the two materials, leaving material transferred to the opposite surface. The actual area of real contact at the interface can be seen in figure 23 by a careful examination of the interface region. There are what appear to be voids in the interface region where complete and intimate solid-state contact across the interface did not occur. However, a great portion of the interfacial area does reflect solid to solid contact in adhesive bonding. This adhesive bond, that of figure 23, was generated when attempting to slide one surface over the other. This resulted in growth in the adhered junctions at the interface leaving only a small area where there was no intimate contact of the two solid surfaces. On separation, the adhesive bond at the interface remained intact and fracture occurred in one of the solids as indicated in figure 23 by the rough piece which remained on the solid surface.

This type of adhesion and transfer behavior is observed for all clean metal surfaces and alloys in solid-state contact. That is, when the environmentally contributed surface films, namely the oxides, are

Figure 23. - Severe surface welding resulting from unlubricated sliding (2% Al-Ni alloy from 10^{-9} torr vacuum experiment.)

removed, such adhesion is observed with strong adhesion and friction coefficients measured in excess of 100 under such circumstances. The surfaces of solids such as metals and alloys are so sensitive to the microenvironment (i.e., the environment in the contact region) that the admission of very small concentrations of adsorbates from the environment to the solid surface are sufficient to markedly reduce adhesion and friction. For example, fractions of a monolayer on the solid surface produce a marked reduction in the adhesion and corresponding static friction coefficients for metals in contact (ref. 15).

The adhesion, friction, and wear behavior of nonmetallic materials is also markedly influenced by the presence of environmental constituents. For example, adsorbates on ceramic materials such as aluminum oxide have a pronounced influence on the friction coefficients measured for aluminum oxide (ref. 16).

Polymeric materials are also affected by environmental constituents on their surfaces. For example, nylon is a material which serves as a good, solid self-lubricating material in certain mechanical applications. Nylon, however, depends on the presence of adsorbed moisture for its effective lubrication - that is, for its low friction and wear properties. Without moisture, nylon does not lubricate effectively and thus is a poor tribological material (ref. 16).

Carbon materials, which are heavily used in mechanical devices such as dynamic seals, are extremely sensitive to environment and environmental constituents. It was established during World War II that the carbon generator brush materials of aircraft flying at high altitude received excessive wear. Careful analyses of the surfaces revealed that the excessive wear of carbon materials at high altitudes was due to a reduction in the ambient pressure and especially reduction of moisture in the environment. Carefully controlled experiments in the laboratory subsequently demonstrated that in the presence of moisture carbon lubricates effectively and exhibites low friction, low wear, and little tendency to adhere. In the absence of moisture, however, the carbon exhibits extremely heavy wear and

becomes a very poor friction and wear material. In fact, by simply reducing the ambient pressure from 760 torr of air to an ambient pressure of approximately 1 torr, a 1000-fold change in wear properties is observed. The wear increases 1000-fold with a reduction in ambient pressure and a loss of moisture from the environment on the wear properties of carbon. Thus, moisture is needed on these surfaces and at the interface between two carbon bodies in relative contact in motion or between the carbon body in some other material in solid state contact (ref. 16).

LUBRICANT STURCTURE

If one considers ordinary air as having vapors of hydrocarbons in addition to principally oxygen and nitrogen with some water vapor, then the particular hydrocarbon molecular structure that may be present in the environment can have a very pronounced influence on the adhesion, friction, and wear behavior of materials in contact. For example, careful cleaning of iron surfaces in a vacuum environment results in the generation of surfaces that are extremely energetic and that adhere to one another when brought into contact. If, however, a small amount of hydrocarbon gas is admitted to the vacuum chamber and allowed to adsorb on the clean iron surface, a structure develops on the solid surface that provides that surface with a protective film. Furthermore, clean iron surfaces chemibsorb nearly all hydrocarbons (ref. 17).

The presence of the hydrocarbon film reduces adhesion, friction, and wear because the surface energy has been reduced by the hydrocarbon molecules on the surface. The surface energy on the clean iron surface available for bonding across an interface to another solid surface has been taken up in the interaction of the clean iron surface with the lubricating molecules absorbing on the surface. The particular molecular structure, however, of the adsorbing hydrocarbon also affects tribological behavior; that is, a slight modification in the molecule produces sensitivities in adhesion, friction, and wear. These slight differences in the molecular structure producing a change

in adhesion, friction, and wear indicate extreme sensitivity in the tribological behavior of materials to environment and environmental constituents.

This effect can be demonstrated by the adsorption of a simple hydrocarbon such as ethylene oxide onto an iron surface and exposing that surface to a different simple hydrocarbon with a slightly modified molecular structure, something such as ethylene chloride or as is commonly called vinyl chloride. If clean iron single-crystal surfaces of the same orientation are exposed to equivalent concentrations of these two different simple hydrocarbons, namely ethylene oxide and vinyl chloride, entirely different surface structures result. These differences can be seen in the LEED patterns presented in figure 17 (p. 30). In this figure we see the molecular arrangement in the diffraction pattern for the adsorbed ethylene oxide and vinyl chloride on the iron surface in the two patterns. Equivalent concentrations of each specie were provided. Thus, everything is constant except for the particular molecular structure.

In ethylene oxide there is the basic ethylene structure with oxygen present in the molecule; in vinyl chloride there is essentially the same type of structure as that of ethylene but instead of having oxygen, chlorine is substituted. With this subtle difference in the structures, however, marked differences in surface coverage are observed in the LEED patterns (fig. 17). With the ethylene oxide, the six diffraction spots in an hexagonal array indicate that the ethylene oxide molecule was completely masked or covered with the iron surface. There are no diffraction spots seen from the iron in diffraction pattern in figure 17. The close packing of the molecules of ethylene oxide on the iron surface provides a very effective and continuous surface film.

In contrast, with the vinyl chloride, the structure is much more open with less than complete surface coverage and with bonding of vinyl chloride to the surface. The four bright diffraction spots seen in the rectangular array in figure 17 with vinyl chloride absorption are associated with the iron. Thus, vinyl chloride does not cover completely and nascent iron is still exposed at the surface. As one

might anticipate, differences in adhesion and friction behavior are observed with these two films present. With the ethylene oxide, the adhesive forces are appreciably reduced between two clean iron surfaces in contact. Furthermore, the friction forces are less for the ethylene oxide on the iron surface than is observed with the vinyl choloride present on the surface. Thus, slight differences in the molecular structure of hydrocarbons present in the microenvironment of solid surfaces in contact can influence the tribological behavior of those surfaces.

LUBRICANT - ENVIRONMENT INTERACTIONS

Once a lubricating film has been formed on a solid surface as a result of interactions with the environment or by the deliberate application of lubricating films to solid surfaces, the presence of a lubricant on a surface can be altered or modified by interactions of environmental constituents with the surface in the asperity contact regions. Sulfur is an element frequently used as an antiwear and antiseizure surface film material. When sulfur is present in organic molecules or organo-metallics, it can interact at the solid surface in metallic systems to form metal sulfides which provide a minimum of adhesion, friction, and wear for lubricated systems. In fact, many practical tribological devices rely very heavily on sulfur for the formation of protective surface films.

Metal sulfides, however, that may exist on the surfaces of solids as a result of the interaction of lubricating species with the solid surface are extremely sensitive to microenvironmental constituents such as oxygen. The presence of oxygen at a rubbing interface of two surfaces in sliding, rolling, or rubbing contact can change the nature of the surface chemistry. The interaction of the oxygen with the lubricated surface reduces the metal surface sulfides to form metal surface oxides. In fact, if a carefully controlled metal sulfide surface is exposed to oxygen, the oxygen can completely displace or remove the sulfur from the solid surface with an oxide replacing it. This effect is demonstrated in the data in figure 24.

In figure 24 the relative Auger peak intensities are plotted where an Auger spectrometer is used for monitoring the presence of sulfur and oxygen on a iron surface. The data in figure 24 were obtained by generating a sulfide film on an iron surface. This sulfide film represents basically a lubricating protective film. The iron surface was then exposed in a clean vacuum system to various concentrations of oxygen. As the concentration of oxygen in the system continuously increases (represented in fig. 24 by exposure in Langmuirs of oxygen), the Auger peak intensity for oxygen increases. With increasing exposures of oxygen, the sulfur peak intensity decreased as indicated by the data in the figure. Ultimately, at some exposure, the sulfur present on the iron surface was completely displaced from the solid surface by oxygen and was replaced by an oxide film. There is a gradual decrease in the concentration of sulfur on the surface and a gradual increase in the concentration of oxygen on the surface with continued exposures to oxygen. Thus, microenvironmental constituents such as oxygen at the interface between two surfaces in contact with sulfide films can completely erase the lubricating film that may be present.

MECHANICAL - ENVIRONMENTAL EFFECTS

In tribological systems, surfaces of two solids are generally in contact with either sliding, rolling, or some type of relative motion between the two surfaces. In addition, there is some velocity or rate of motion associated with the movement of the surfaces relative to each other. Furthermore, there is generally some mechanical loading applied to the surfaces in contact. The presence of these factors, namely, relative motion between the two surfaces and the imposition of loads on the surfaces in contact, can cause marked changes in the nature of the surface chemistry in the presence of certain environments, and the environment can affect the wear behavior of such systems. For example, for two solid iron or steel surfaces in contact in the presence of a liquid lubricant containing a sulfur additive, rubbing of the surfaces under relatively light loads results in the

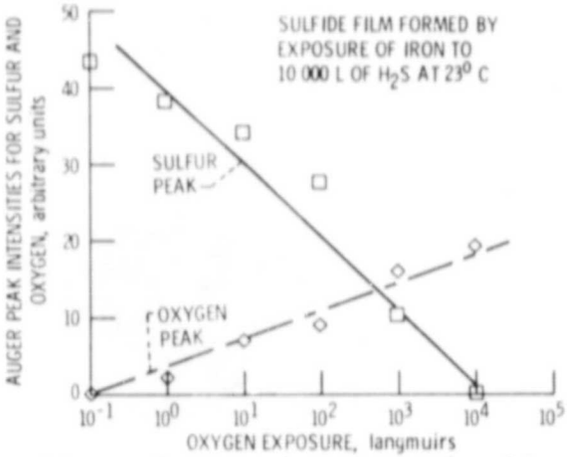

Figure 24. - AES evidence for displacement of sulfur from iron surface by oxygen.

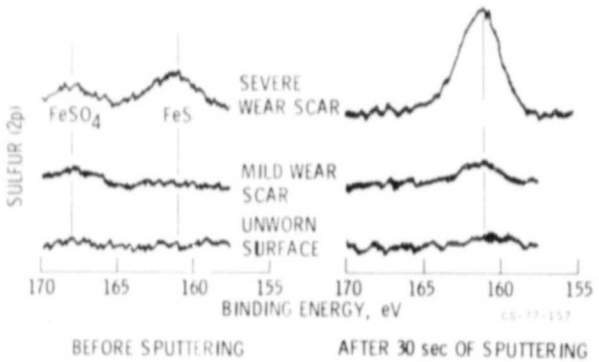

Figure 25. - Sulfur ESCA peaks from wear scars and unworn surface.

formation of surface films which are generally identified with XPS (X-ray photoelectron spectroscopy) as being principally surface oxides. With the mechanical activity of the surfaces, relatively low wear is observed in the presence of these surface oxides. If, however, the load is increased to the point where the sulfur-containing additive in the lubricant can interact with the nascent iron or steel surfaces as a result of disruption of surface oxides, sulfides are found on the surface. In the presence of these sulfides, the friction, adhesion, and wear behavior are much higher than they are in the presence of the oxides. This effect is demonstrated by the data of figure 25 where XPS data are presented for surfaces containing oxides and sulfides under three sets of conditions: (1) absence of rubbing, (2) mild wear conditions, and (3) severe wear conditions. Under mild wear conditions one type of surface film is present, while under severe wear conditions a completely different type of surface film is present. If the sulfur-containing surface film observed in the severe wear conditions is exposed to oxygen for either sufficently long periods of time or at sufficiently high concentrations of oxygen, data analogous to those obtained in figure 24 are observed for these particular films (ref. 18).

In the 1930's, Roscoe observed the interaction of the environment with metal surfaces. This interaction produced metal oxides which altered the mechanical behavior of the metals. In some experiments with cadmium crystals, Roscoe found that when cadmium oxide was present on the surface, as a result of interaction of the cadmium single crystal with oxygen, the mechanical properties were altered. The crystal became much less prone to plastic deformation increasing its hardness (ref. 6).

In contrast to the observations of Roscoe, Rehbinder and his colleagues in the 1940's in Russia observed that the presence of certain surface active organic molecules, such as organic acids on solid surfaces, made those surfaces much more prone to deformation. The surfaces strained more readily and at much lower stress levels

than they did in the absence of the surface active organic species (ref. 8).

The Rehbinder work and that of his colleagues have established that surface softening can occur for a number of classes of materials - metals as well as nonmetals. These surface interactions of environmental constituents with the solid surface not only influence mechanical properties but also tribological behavior (fig. 26). Figure 26(a) shows a schematic illustration of these surface effects (ref. 19). It is a plot of stress against strain for materials under normal conditions. It also presents data for surface films manifesting the Roscoe effect and surface active liquids representing or demonstrating the Rehbinder effect. Figure 26(a) shows that with a surface film present from the interaction of the environment with a solid surface, manifesting the Roscoe or surface hardening effect, the stress/strain curve shows an increase in the strength of the material. In contrast, however, where a surface active specie is present that produces a surface softening or a Rehbinder effect, a reduction in the stress required to produce strain is observed for materials when compared to the normal or the Roscoe effect (fig. 26).

The sensitivity of tribological behavior to the interaction of the environment with a solid surface is shown by the data in figure 26(b). In this figure a wear track width and friction coefficient are plotted for a zinc crystal surface, the basal orientation (0001) surface where a ruby ball slid on that surface in a <1010> direction. The sliding experiments were conducted in three different environments: (1) dry sliding, which represents the equivalent of the normal condition of figure 26(a); (2) sliding with an oxidized surface, which is analogous to the Roscoe effect in figure 26(a), bearing in mind that Roscoe observed the formation of oxides on cadmium while in figure 26(b) the oxides are present on zinc; and (3) sliding, friction, and wear behavior of the zinc surface in contact with the aluminum oxide in a 5-percent hydrocholoric acid solution. The 5-percent hydrochloric acid solution represents a surface-active liquid situation that would produce the Rehbinder effect.

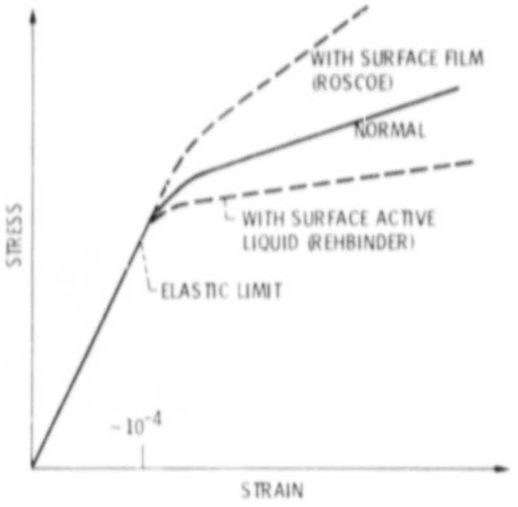

(a) SCHEMATIC ILLUSTRATION OF THE PRINCIPAL EXTRINSIC SURFACE EFFECTS (REF. 55).

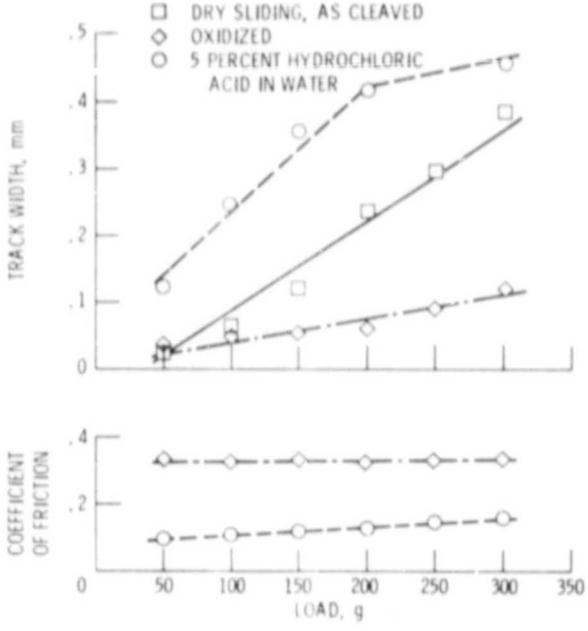

(b) WIDTH OF WEAR TRACK AND COEFFICIENT OF FRICTION PRODUCED WITH RUBY BALL SLIDING ON ZINC SINGLE CRYSTAL (100) SURFACE IN [10$\bar{1}$0] DIRECTION. (SLIDING VELOCITY, 1.4 mm/min; TEMPERATURE, 23^{0} C; DRY ARGON).

Figure 26. - Influence of surface active species on mechanical and tribological behavior.

The data of figure 26(b) indicate that the normal dry surface has a track width that is equivalent to the wear of the surface immediately between the surface oxidized to produce a surface hardening or Roscoe effect and the surface softened to produce the Rehbinder effect. The tribological results are analogous to the stress/strain data in figure 26(a).

With the oxide present on the surface in the sliding friction experiment, the track width is much smaller in size than it is in the absence of the surface hardening effect of the oxide. One observes a smaller track width because the surface has been hardened by the presence of the oxide (as was observed by Roscoe) and this hardening reduces the wear to the surface. In the presence of the surface active liquid, however, the surface becomes softer or more likely to deform plastically under a fixed load. Consequently, the wear track generated in the solid surface is much larger than it is in the normal case or in the case where the oxide is present on the solid surface. Thus, there is a distinct and definite relationship between the track widths observed in figure 26(b) and the stress/strain behavior observed in figure 26(a).

In sliding friction there are two components to the friction force or resistance to tangential motion which result in the measure of friction coefficients. There is the friction associated with the real area of contact in shear, and there is the friction associated with the amount of plowing of the surface that must take place. With the sapphire or ruby ball sliding on the zinc surface, there is a considerable amount of deformation that occurs to the zinc surface. The presence of the oxide reduces the amount of plastic deformation that may occur to the solid surface, but it increases the strength of the surficial layers which must be plowed. Consequently, the layers are more resistance to tangential motion, and this results in an increase in the fricton force. In contrast, in the presence of the surface active liquid - namely, the 5-percent hydrochloric acid (fig. 26(b)) - the increased plasticity of the surface reduces the resistance

to tangential motion and the plowing of the zinc by the ruby ball. Consequently, a lower friction coefficient is measured in the presence of the surface active liquid manifesting the Rehb'nder effect than is observed for the oxidized case representing the Roscoe effect. This difference was observed over a range of loads as shown by the data in figure 26(b). Thus, it is apparent, from the data in figure 26, that the interaction of environmental constituents with solid surfaces can produce changes in the mechanical behavior of the solid surfaces. Those changes in the mechanical behavior of the solid surface are reflected in changes in tribological behavior (such as friction and wear).

EFFECT OF ENVIRONMENT ON SOLID-FILM LUBRICATION

In addition to the environment influencing or altering the chemistry of solid surfaces and their adhesion, friction, wear, or mechanial behavior, the environmental constituents can interact also with lubricants (particularly with solid film lubricants) that may be present on surfaces to alter their observed behavior.

Molybdenum disulfide and graphite are two of the most common solid film lubricants used to reduce adhesion, friction, and wear of metals in solid-state contact. Yet, both of these materials are extremely sensitive to the microenvironment in their tribological performance. For example, molybdenum disulfide is a much better lubricant in a vacuum environment than it is in an air environment. In contrast, graphite, which lubricates very effectively in air at atmospheric pressure, is completely ineffective as a lubricant in a vacuum environment. These differences are due to environmental constituents - namely, water vapor - that are present on the surface of the solids.

The effect of atmospheric pressure on the friction performance of molybdenum disulfide and graphite is indicated by the data in figure 27. Friction coefficient is plotted as a function of ambient pressure for molybdenum disulfide and graphite. The data show that as

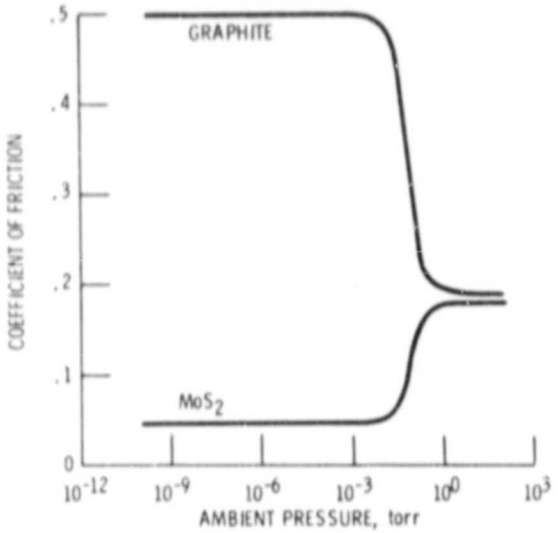

Figure 27. - Effect of ambient pressure on friction of graphite and MoS_2.

the ambient pressure is reduced toward that of a vacuum of 10^{-10} torr, molybdenum disulfide goes through a decrease or a marked reduction in friction coefficient. The presence of adsorbates, which have been pumped off the surface and identified by mass spectrometry, indicate that the water vapor that is present on the molybdenum disulfide crystallites is deterimental to its lubricating characteristics. The friction coefficients are markedly superior in the absence of the water vapor than they are in its presence.

In contrast to the behavior of molybdenum disulfide (in fig. 27), the friction coefficient for graphite increases as the ambient pressure is reduced from atmospheric to that of a good vacuum. In this instance, the water vapor is extremely beneficial for the lubricating solid surfaces with graphite. Physically adsorbed water on the graphite platelets improves friction characteristics. Using mass spectrometry shows that, in a vacuum system, water vapor is liberated by the graphite, and the friction coefficient of graphite increases markedly with a loss of the water from the solid surface. Ultimately, in a vacuum environment, very high friction coefficients comparable to those obtained for drying metal sliding are observed for the graphite. The graphite becomes ineffective as a solid film lubricant in the vacuum environment and therefore is never used as a lubricant for vacuum applications. Thus, it is apparent from the data in figure 27 that the lubricating properties of solid-film lubricants can be altered by a change in the microenvironment at the surface of solids in contact. Alterations in the atmospheric pressure and atmospheric constituents can destroy the lubricating properties of graphite but can improve the lubricating properties of molybdenum disulfide. The data in figure 27 again indicate the extreme importance of microenvironment on the behavior of tribological systems.

CONCLUSIONS CONCERNING ENVIRONMENT

It can be seen that the microenvironment plays a very strong role in tribological behavior of materials in contact. Oxygen from a normal air environment interacts with solid metal surfaces to provide

a continuously protective surface film and to keep metal surfaces from adhering to one another. Naturally occurring oxides are probably the best natural solid-film lubricants we have. They are provided to us by the environment.

Hydrocarbons adsorbed from the environment on solid surfaces alter adhesion, friction, and wear behavior, and minor differences in molecular structure produce marked differences in tribological behavior. Furthermore, environmental constituents can completely displace lubricating films from solid surfaces, thus altering adhesion, friction, and wear behavior.

Mechanical activity of solid surfaces in contact can produce interactions with environmental constituents to alter surface chemistry and mechanical behavior. This alteration in surface chemistry and in mechanical behavior alters tribological performance.

The presence of environmental constituents, such as water vapor, can markedly alter the lubricating characteristics of solid-film lubricant materials. Molybdenum disulfide can be improved in its lubricating characteristics by reducing ambient pressures and eliminating moisture from the environment. Graphite, however, becomes ineffective as a solid-film lubricant once moisture from the environment is removed.

SOLID-STATE INTERACTIONS

METAL TO METAL

Clean Metal Adhesion

Ferrous-base alloys are the most widely used materials in lubrication mechanism design and in engineering practice. Frequently, in such devices ferrous surfaces are contacted by nonferrous materials. The adhesion behavior of ferrous surfaces with nonferrous surfaces is therefore of practical as well as fundamental interest. Combining LEED with Auger emission analysis can provide insight into both the structural and chemical changes that take place on surfaces

as a result of the adhesion of various metals to iron. The nature of the adhesion process can be followed at the atomic level.

To gain insight into the interfacial bonding of metals to one another across an interface, iron was brought into solid-state contact with a variety of metals, and the adhesion behavior was studied. The metal surfaces were atomically cleared by ion bombardment prior to contact, and the surfaces were characterized by LEED and Auger analysis. Adhesion data for iron in contact with itself and various other metals together with other properties of the metals are presented in table II.

An examination of table II indicates that the strongest adhesion bond forces are found for iron adhering to itself. Thus, the bending forces of cohesion, the bonding of a metal to itself, are greater than the binding forces to other metals. It is of interest to note that even with metals such as lead where there is no solubility in iron, strong bonding occurs as it does with gold, which is a relatively nonsurface active metal.

Adhesion experiments were conducted with the (0001) surface of cobalt and the (111) surface of nickel contacting the iron (011) surface. Cobalt has a hexagonal-close-packed structure, and nickel has a face-centered-cubic structure. The adhesion results obtained together with some other properties of these metals are presented in table II. Both cobalt and nickel have approximately the same cohesive energy and atomic size. They have identical valency states. Cobalt exhibits 35-percent solubility before ordering in iron, and nickel has a solubility of 9.5 atomic percent (ref. 20).

Adhesion results indicate a greater bonding force for nickel to iron than for cobalt to iron. The iron surfaces were examined after adhesive contact with LEED and Auger analysis. Cobalt was found on the iron surface, indicating the fracture of cobalt cohesive bonds. Nickel was not found on the iron surface. A larger nickel (111) flat was used, and adhesive contact was made to the nickel (111) surface with a 3.0-millimeter-diameter iron (011) surface. The nickel surface was examined with LEED and Auger after adhesive contact, and iron was found to be present on the nickel surface.

TABLE II. - SOME PROPERTIES OF VARIOUS METALS AND FORCE OF ADHESION OF THESE METALS TO IRON

Metal	Cohesive energy,[a] kcal/g atom	Atomic size,[b] Å (10^{-10} m)	Valency states[b]	Solubility in iron,[c] at. %	Adhesion force to iron,[d] dynes
Iron	99.4	2.86	2,3	-----	>400
Cobalt	101.7	2.50	2,3	35	120
Nickel	102.3	2.49	2,3	9.5	160
Copper	80.8	2.551	1,2	<0.25	130
Silver	68.3	2.883	1	0.13	60
Gold	87.6	2.877	1	<1.5	50
Platinum	134.8	2.769	2,4	20	100
Aluminum	76.9	2.80	3	22	250
Lead	47.0	3.494	2,4	INS.	140
Tantalum	186.7	2.94	5	0.20	230

[a]Reference 21.
[b]Reference 22.
[c]Reference 20 and without ordering or introduction of other structures.
[d]Applied load, 20 dynes; temperature, 20° C; ambient pressure, 10^{-10} torr.

An examination of the cohesive energies for iron, cobalt, and nickel in table II indicates that they are nearly the same, but differences in adhesive forces to iron exist. The cohesive energies do not, however, reflect orientation effects. The values in table II reflect an average of the lattice cohesive energy for each of the metals. The minimum for cohesive energy in cobalt would exist between atoms in adjacent basal planes. This may account for the lower adhesive forces of cobalt to iron than for nickel to iron. The cohesive forces between (0001) planes in cobalt would be less than the forces between (111) planes in nickel.

The outer electron configuration and thus the electrons that would enter into adhesive bonding for these metals are iron $3d^6 4S^2$, cobalt $3d^7 4S^2$, and nickel $3d^8 4S^2$. For these metals it is primarily the 3d and 4S electrons that enter into adhesive bonding. It is these electrons that act as the glue in adhesion and impart the chemical activity to metal surfaces. Since cobalt transfers to iron, it may be assumed that the cohesive bonds in cobalt were weaker than the adhesive iron to cobalt bonds or the iron to iron cohesive bonds. With nickel, however, iron transferred to the nickel surface; this indicates that the iron to iron bonding was the weakest. The adhesive forces of nickel to iron were less than the forces of iron to itself. Since iron cohesive bonding is involved for both couples, the differences in adhesive forces must be the result of atomic packing, size factor, and lattice spacing at the interface, all of which would affect the amount of metal involved in interfacial bonding.

With respect to solubility, cobalt has greater solubility in iron than in nickel (see table II). If solid solubility influences adhesion, it would be anticipated that cobalt and not nickel would exhibit the higher adhesive forces to iron. The Hume-Rothery rules are more closely met with nickel. Yet, the data indicate just the opposite.

Adhesion of Noble Metals to Iron

Copper, silver, and gold were brought into adhesive contact with the (011) surface of iron. The noble metal plane contacting the iron was the (111). Adhesion results obtained are presented in table II. Copper, the most chemically active of the noble metals, exhibited greater than twice the adhesive force to iron than did the other two metals.

While all three noble metals are hyperelectronic (excess of electrons) and should develop strong bonds with either hypoelectronic (electron deficient) or buffer elements, there is a difference in the degree of interaction or chemical activity with iron. Copper exists in valency states of both 1 and 2, the latter being the more common, while silver and gold exist primarily in a valency state of 1 (table II). Copper, silver, and gold transferred to a clean iron (011) surface. All three noble metals transferred to iron in an orderly manner with the surface structure being the same for all three noble metals as indicated by the LEED patterns in figure 28.

The solubility of these three noble metals in iron is relatively low (table II). Despite the very limited solubility of these elements in iron, their adherence to a clean iron surface was very strong. It varied from 2.5 times the applied normal load for gold to 6.5 times the applied load for copper.

A platinum (111) surface was brought into adhesive contact with the iron (011) surface, and the adhesion forces measured are presented in table II. While having a relatively good solubility in iron, the adhesive force measured was appreciably less than that measured for nickel where the solubility is less than half that of platinum in iron. Platinum, however, is not as chemically active as nickel.

The very chemically active metal, aluminum, was brought into adhesive contact with iron, the (111) surface of aluminum contacting the (011) surface of iron. The adhesive forces measured were very large (table II). The force of adhesion was 12.5 times the applied load. The forces of adhesion measured between iron and aluminum were greater than those between iron and any other metal examined in

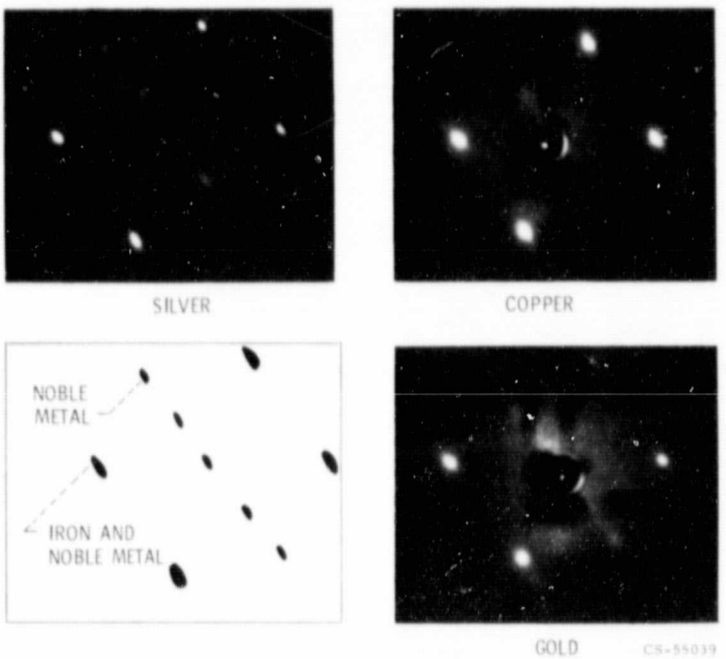

Figure 28. - LEED photographs of iron (011) surface after adhesion of noble metals.

table I with the exception of iron itself. Aluminum is a hypoelectronic element, and strong interaction of hypoelectronic elements with iron might be expected.

The cohesive energy for aluminum in table II indicated that it is in the same general range as copper and silver and, consequently, the contact area with deformation under load might not be too greatly different. This is particularly true since all three are face-centered-cubic metals with the same surface orientation. The adhesion values are, however, markedly different. The adhesive forces of aluminum to iron were greater than four times the value for silver and nearly twice the value observed for copper. The difference in these three face-centered-cubic metals is the chemical reactivity of the surfaces. Aluminum is more reactive than copper, which in turn is more reactive than silver. This is reflected in the valency states of these metals in table II. Aluminum has a normal valency state of 3, copper 1 and 2, and silver normally 1.

The solubility of aluminum in iron is 22 atomic percent. The solubility of platinum in iron is 20 atomic percent. Despite this similarity of solubility in iron, the adhesive forces of aluminum to iron were 2.5 times the adhesive force of platinum to iron. The differences in cohesive energies for the two metals would indicate a greater contact area for aluminum than for platinum. It is of interest to note that, even where aluminum is insoluble in an element, surface interactions can take place with stable bonding. Ordered phase surface structures as a result of bonding of aluminum to silicon occur. This structure forms despite the fact that the aluminum is nearly insoluble in silicon. This again argues against using bulk properties to predict surface behavior.

Active Metal

A number of adhesion experiments were conducted with the face-centered-cubic metal lead contacting the clean iron (011) surface. The adhesion forces measured for the various applied loads are presented in figure 29. With increasing load, an increase in the

force to fracture the adhesive junction is observed. The increase in force to fracture with increasing load reflects the effect of the increase in true contact area. With the larger applied loads, the real area of contact has increased, and with this increase is associated an increase in the number of adhesive bonds developed across the interface.

When a tensile force is applied to the adhesive junction between iron and lead, fracture in the interfacial region is to be expected in the area of weakest bonding. This would exist in the lead to iron bonds or in the cohesive bonds of lead. An Auger trace was made of the iron (011) surface after adhesive contact with lead, and the results obtained are presented in figure 30. The Auger analysis indicates a transfer of lead to the iron surface. This indicates that the zone of fracture in tension was in the cohesive lead bonds. The adhesive bonds of lead to iron were stronger than were the cohesive lead bonds.

Iron and lead are mutually insoluble (ref. 20). Despite the mutual insolubility, the adhesive bonds developed between the two clean metal surfaces were in excess of 47.0 kilocalories per mole, the cohesive bonding energy of the lead (ref. 21).

The bonding of lead to elements with which it is not soluble is not limited to iron in adhesion studies. Lead deposited on a silicon surface in a monolayer had an interatomic lead atom to lead atom distance of 3.3 Å. The bond distance in bulk lead is 3.5 Å. The interatomic contraction in the lead is a result of the strong adhesive bonds developed between the lead and silicon. The adhesive bonds between the lead and silicon are stronger than are the cohesive lead bonds. These strong bonds exist despite the insolubility of lead in silicon.

A tantalum (011) surface was brought into adhesive contact with the clean iron (011) surface. The adhesion force measured for an applied load of 20 dynes was 230 dynes. Tantalum, much like aluminum, exhibited strong bond forces to iron (see table II). Tantalum, like aluminum, is hypoelectronic and should develop strong bonds with iron. The cohesive energy of tantalum is very high, indicating that

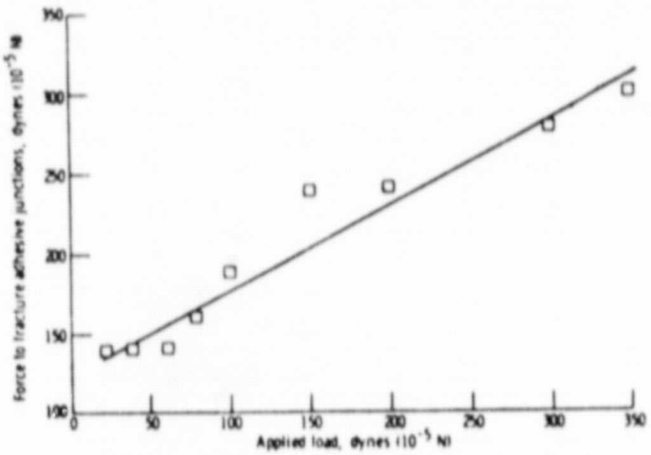

Figure 29. - Adhesion of lead crystal to clean iron (011) surface. Ambient pressure, 10^{-10} torr at 20° C.

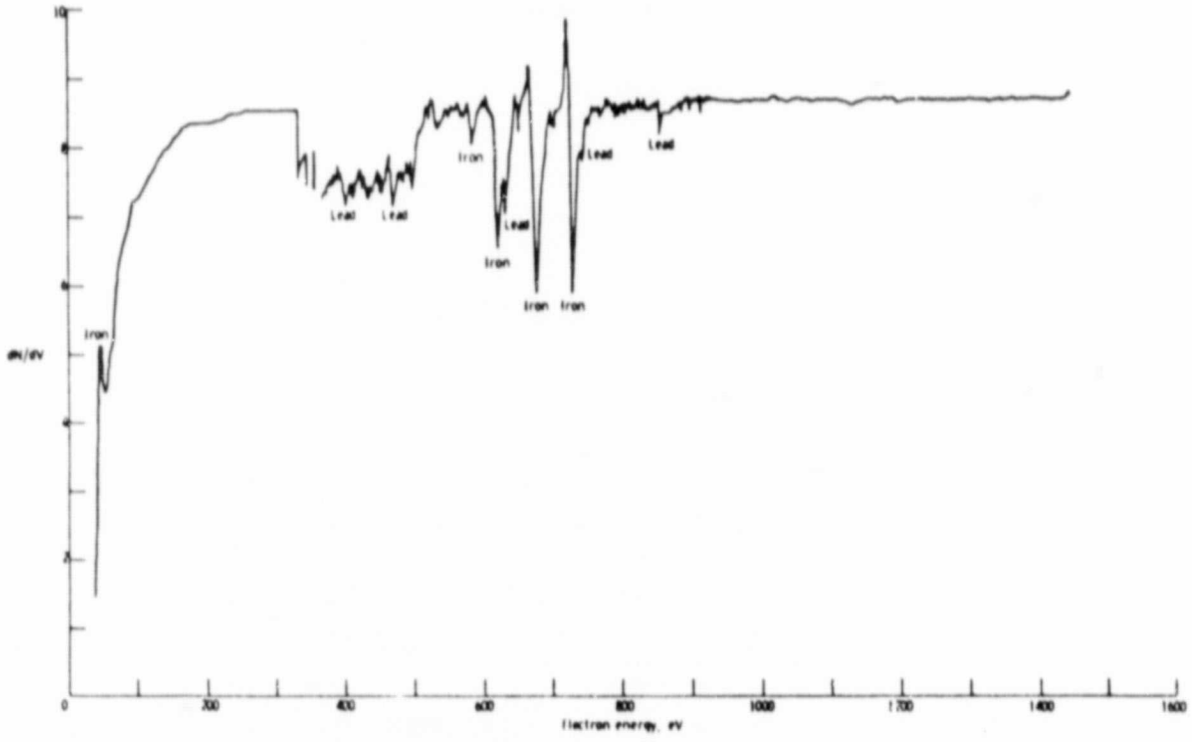

Figure 30. - Auger emission spectrometer trace of iron (011) surface with adhered lead.

with loading the iron rather than the tantalum may be undergoing deformation.

Surface Films

If a clean iron (Fe) surface is heated to 500° C and held at that temperature for a period of time, sufficient sulfur (S) diffuses from within the iron to the surface to produce a Fe(011) c(2 x 4)-S structure. Auger analysis substantiates that it is sulfur. The sulfur has 2 times the lattice spacing of the iron in the [20] direction and 4 times the lattice spacing in the [02] direction.

The structure Fe(011) c(2 x 4)-S defines the substrate structure, the arrangement of the sulfur, and the lattice spacing of the sulfur with respect to the iron. The Fe(011) indicates the high-atomic-density iron atomic plane (011). The c in the surface structure designation indicates that the sulfur structure is centered. The (2 x 4) designation indicates that sulfur has $2a_0$ lattice spacing in the [20] direction and $4\sqrt{2a_0}$ in the [02] direction. The S following the (2 x 4) simply indicates that the species is sulfur. The nomenclature used herein to describe surface films is widely used in the literature.

Adhesive contact was made to the Fe(011) c(2 x 4)-S structure. The first effect observed with the sulfur present on the surface was that it appreciably reduced the adhesive force of iron to itself. The second observation was that the adhesive force measured was relatively independent of load over the range of loads examined. The data for adhesive forces measured at various applied forces are shown in figure 31 (see curve for Fe(011) c(2 x 4)-S). It would appear that small amounts of bulk contaminants in a metal such as iron can, when diffused to the surface, markedly alter adhesion behavior.

A clean iron surface exposed to various amounts of oxygen gas produces the same surface concentration of oxygen on the iron (011) surface as that with sulfur present. After a number of unsuccessful attempts with too much or too little oxygen on the surface and an exposure of 0.1 Langmuir, a Fe(011) c(2 x 4)-O structure was obtained

and adhesive contact to that surface was made. The adhesion results obtained for various applied forces are presented in figure 31. The adhesion forces measured for the oxygen-containing surface were higher at all applied forces than were the values obtained on the sulfur-containing surface. Furthermore, an increase in applied force on contact resulted in an increased force required for separation. This dependency of adhesion force on applied force indicates that an increase in iron cohesive bonding has occurred across the interface with increasing loads. The insensitivity of the sulfur-containing surface to applied loads may indicate that the atomic size of the surface-contaminating atom may exert some influence on adhesive behavior. The sulfur atom is more than twice the size of the oxygen atom, and since both have a 2 x 4 structure on the iron, the amount of exposed iron per unit area available for cohesive bonding with sulfur present on the surface could be expected to be less.

Hydrogen sulfide gas was admitted to a vacuum system in a sufficient amount to produce a 2 x 4 structure. The exposure required to obtain the 2 x 4 structure was 1.0 Langmuir. The exposure in terms of coverage is influenced very markedly by the position of the gas outlet tube with respect to the crystal surface. When the gas outlet tube is placed very close to the crystal surface, a Langmuir value for a specific surface coverage is markedly different from that obtained when the tube outlet is positioned in the chamber such that the incoming gas does not directly impinge on the crystal surface.

Sufficient hydrogen sulfide was admitted to the system to produce a Fe(011) c(2 x 4)-H_2S structure. Adhesive contact was made to the surface, and the LEED pattern after adhesive contact was obtained. A considerable change in background intensity occurred as a result of adhesive contact.

Adhesive forces were measured at various applied forces for the Fe(011) c(2 x 4)-H_2S structure, and the results obtained are presented in figure 32 (see curve for Fe(011) c(2 x 4)-H_2S). The force of adhesion increased with increasing load. This result should be compared with that obtained for sulfur in the surficial layer and

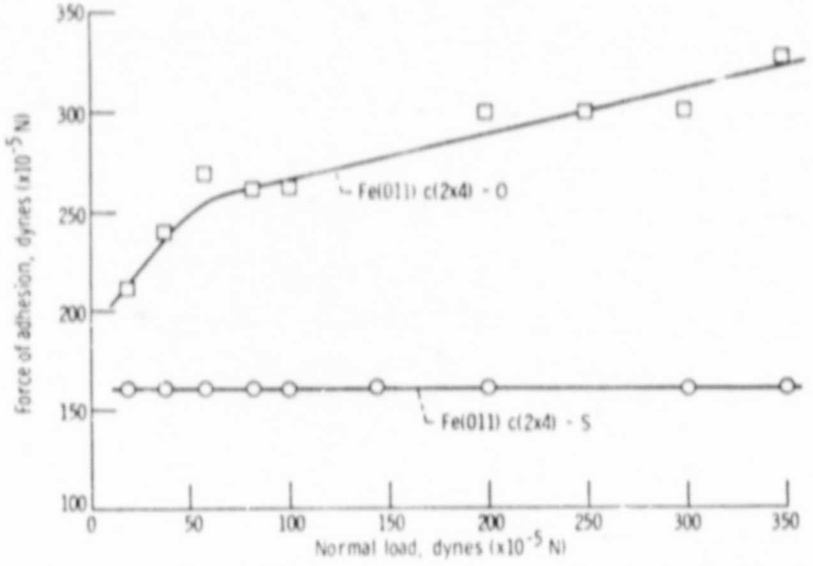

Figure 31. - Effect of oxygen and sulfur on adhesion of iron (011) to itself. Diameter of contacting flat, 3.0 millimeters; contact time, 10 seconds.

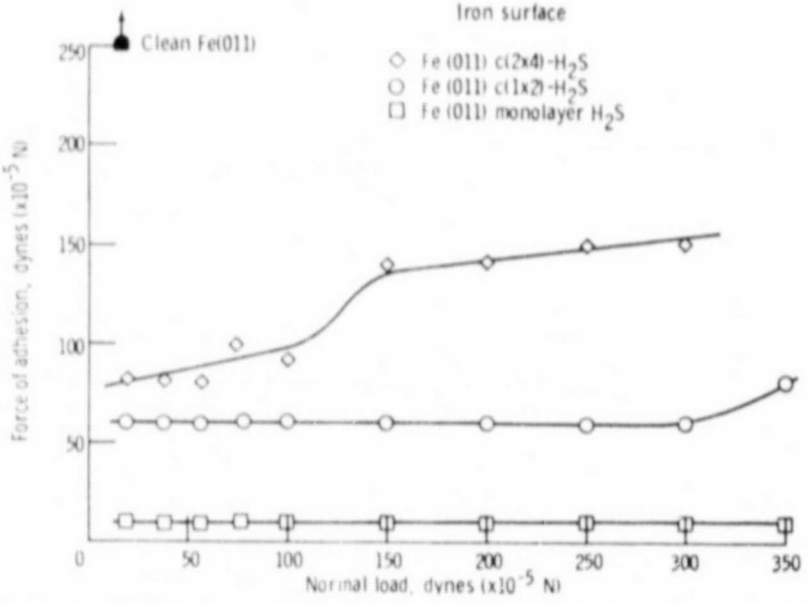

Figure 32. - Influence of hydrogen sulfide adsorption on adhesion of iron (011) surfaces. Diameter of contacting flat, 3.0 millimeters; contact time, 10 seconds.

oxygen on the surface in figure 31. It appears that, for equivalent surface coverages, namely, a (2 x 4) structure on the (011) surface of iron, chemisorbed hydrogen sulfide affords the greatest surface resistance to adhesion. Sulfur offers intermediate surface protection, and oxygen the least surface protection.

The lower adhesive forces of iron bonding to iron in the presence of hydrogen sulfide may in part be a steric effect. An examination of atomic attractive energy between like atoms reveals that it is a function of interatomic spacing (ref. 22). The iron (011) surface next received a hydrogen sulfide exposure of 10 Langmuirs. Adhesion measurements were made for this surface at various loads, and the results obtained are presented in figure 32 (see curve for Fe(011) c(1 x 2)-H_2S). With greater surface coverage, the adhesive force decreased from the values obtained with the (2 x 4) surface coverage, as might be anticipated. Furthermore, there appears to be a greater independence to the contact force applied.

With prolonged exposures of the iron surface to hydrogen sulfide (50 Langmuirs), full monolayer coverage of the iron (011) surface was observed. The surface structure produced a close-packed surface arrangement. The suggested arrangement of the hydrogen sulfide on the iron (011) surface is shown in figure 33. Further exposures to as much as 100 Langmuirs produced no change in the surface structure. The adhesion forces to this surface were the least of those measured, as shown by the data in figure 32. These data indicate that adhesive force is a function of surface coverage - the greater the coverage, the lower the adhesive force.

Subsequent heating of the Fe(011)-(1 x 1)-H_2S surface to 500° C did not produce a change in the surface arrangement but simply intensified the diffraction spots. Heating to this temperature should produce a decomposition of the hydrogen sulfide to form iron sulfide and liberate hydrogen. The pressure in the system rose, and diffraction peak intensities changed, indicating the liberation of hydrogen. Adhesion measurements revealed no change in the adhesion forces. These results suggest that the adsorbed close-packed monolayer of hydrogen sulfide is present on the iron (011) surface

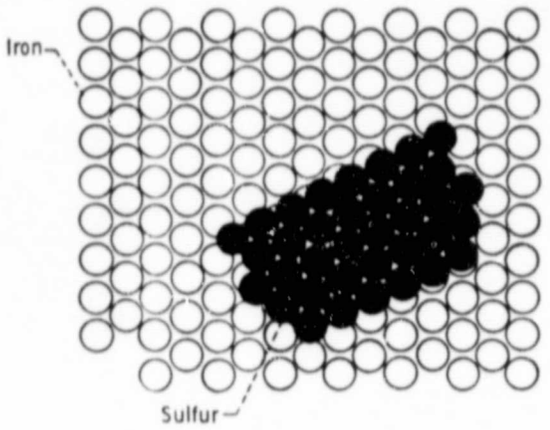

Figure 33. - Suggested arrangement of hydrogen sulfide on iron (011) surface with monolayer coverage. Sulfur coverage is over entire surface although only small portion is shown.

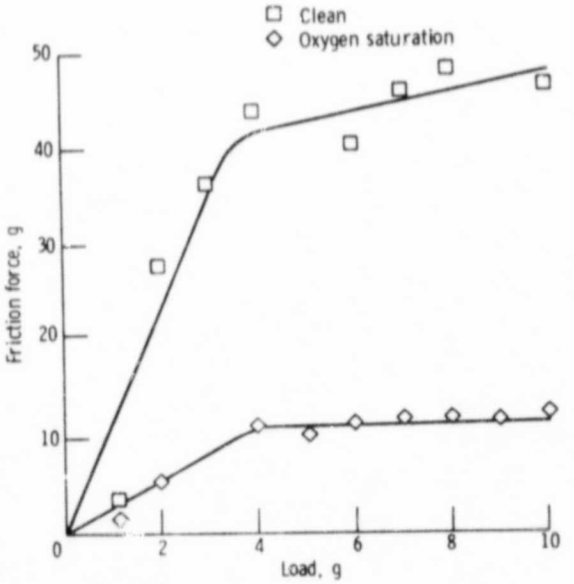

Figure 34. - Friction force as function of load for gold (111) single crystal sliding on platinum (111) single crystal. Sliding velocity, 0.7 millimeter per minute; ambient pressure, 1.33×10^{-8} newton per square meter (10^{-10} torr); and temperature, 23° C.

with the sulfur directly in contact with the iron and the hydrogen in an upper layer. Decomposition simply removes the hydrogen layer and leaves the sulfur close-packed layer on the iron surface.

Friction and Surface Films

In addition to the adhesive behavior of metals in solid-state contact, the resistance to tangential motion of such surfaces is of interest. The effect of surface contaminants and or lubricants on that resistance is also important.

The members of the platinum metals family offer properties amenable to both friction and lubrication studies. The metals of the platinum metals family of elements and their alloys have been used extensively in electrical contacts - both the make and break type and sliding or rubbing contacts (ref. 23). The elements involved are ruthenium, rhodium, palladium, osmium, iridium, and platinum. Their atomic numbers are, respectively, 44, 45, 46, 76, 77, and 78.

The platinum metals, in general, are not very reactive with environmental constituents and lubricants. They are good catalysts and have been found in electrical contact studies to initiate polymerization of environmental organic vapors (ref. 24). The adhesion, friction, and lubricated behavior of these metals as a group has not been explored. Such a study could facilitate the proper selection of these metals in contact applications.

In practical electrical contact systems these metals are generally not used in contact with themselves but rather in contact with some other metal or alloy. Many of these systems used in the aerospace industry must operate in a vacuum. Frequently, the contacting mating surface is either copper or one of the other noble metals, gold or silver.

The data in figure 34 were for gold sliding on clean platinum. The Auger spectroscopic analysis of the platinum surface after sliding indicated the transfer of gold to the platinum surface with single pass sliding. Thus, the friction data (clean) in figure 34 are a reflection of the shear behavior of gold. The adhesive interfacial

bond strength was stronger than the cohesive gold bond strength. Such results are consistent with the properties for these two metals and the properties normally associated with tangential shear behavior.

To determine surface film effects on friction, the clean platinum was exposed to oxygen at a pressure of 6.65×10^{3} newtons per square meter (50 torr) after the ion pump was turned off for 30 minutes. The system was then evacuated to 1.33×10^{-8} newton per square meter (10^{-10} torr), an Auger spectroscopic analysis was made to confirm the presence of oxygen on the platinum surface, and a friction experiment was conducted at various loads. The Auger trace showing the oxygen peak therein is presented in figure 35. The friction results obtained are presented in figure 34.

Figure 34 shows a marked decrease in the friction force with load for platinum (111) covered with oxygen. Furthermore, beyond a 4-gram load no change in friction force was observed with further load increases to 10 grams. The amount of oxygen on the surface at saturation is a monolayer or less.

A LEED analysis of the surface revealed a diffuse pattern. A (2 x 2)-O surface structure as defined in reference 25 has been observed for oxygen on platinum (ref. 26).

Both platinum and palladium are chemically more active than ruthenium, rhodium, and iridium. While surface species such as oxygen bonded more readily to metals such as platinum and palladium, they showed very weak or no bonding to the other metals as evidenced by LEED and Auger emission spectroscopy analysis. The adsorption characteristics and friction behavior of the platinum metals with various surface conditions are presented in table III.

As the atomic number in period 5 containing the elements ruthenium, rhodium, and palladium is increased, the contribution to bonding of d electrons is increased. Likewise, a similar behavior is observed in period 6 with the elements osmium, iridium, and platinum. Thus, stronger bonding of gold to platinum and palladium would be anticipated from the valence-bond model when that model is applied to metallic systems. There is no reason not to apply it to metal systems

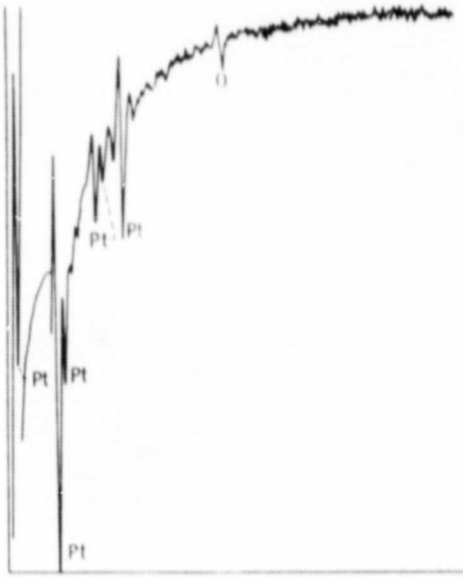

Figure 35. - Auger spectrometer trace of platinum (111) surface after exposure to oxygen. Total oxygen exposure, 6.65×10^{3} newtons per square meter (50 torr) for 30 minutes; spectrum obtained at 23° C and 1.33×10^{-8} newton per square meter (10^{-10} torr).

TABLE III. - FRICTION COEFFICIENTS OF PLATINUM METALS

Metal	Metal surface condition			
	Clean	Oxygen	Vinyl chloride	Methyl mercaptan
	Friction coefficient			
Ruthenium (0001)	1.0	[a]1.0	[a]1.0	[a]1.0
Rhodium (111)	1.0	1.0	1.0	.8
Palladium (111)	2.2	.18	.16	.15
Iridium (111)	.4	.4	[a].4	[a].4
Platinum (111)	4.0	1.0	.8	.7

[a]Did not absorb.

since it involves the same basic electronic bonding that is involved in other systems for which the model was originally developed.

In considering the transition elements a knowledge of the contribution of d electrons to metallic bonding is necessary. An examination of the heats of atomization of the elements in the periodic table clearly indicates the importance of the d electrons to bonding. The most stable metallic structures are those which use as many d electrons as possible in bonding.

A consideration of the adsorption of various species to the surface of members of the platinum metals family was made. Attempts were made to adsorb oxygen, vinyl chloride, and methyl mercaptan to these surfaces and to measure the effect of these films on friction behavior. The results obtained in these experiments are presented in table III.

Examining table III indicates that variations in friction behavior exist for the metals in the clean state and with the surface film present where adsorption occurred. With ruthenium, where LEED and Auger analysis failed to reveal the adsorption of any of the molecules on the surface, the friction coefficient was essentially the same as that for the clean surface as might be anticipated.

With rhodium, the adsorption of oxygen and vinyl chloride did not reduce friction while the adsorption of methyl mercaptan did cause a decrease in the observed friction coefficient. The presence of oxygen on the iridium surface did not influence friction behavior but that same film on platinum produced a fourfold reduction in friction coefficient as indicated by the data of table III and the friction force in figure 33.

METAL TO SEMICONDUCTORS

Clean Surfaces

When two solid surfaces, a metal and a semiconductor, are brought together, contact occurs at the asperity tips as already indicated. Either under the weight of the solids or when a load is applied,

depending on the materials, first elastic and then plastic deformation occurs in the asperities. Deformation continues until the real asperity contact area is sufficient to support the load; then, at this point, deformation ceases, and the resultant real area of contact is a small percentage of the apparent area of contact.

At sufficiently light loads and depending on the materials, the surface films present may not be disrupted by the deformation process. With most materials, however, disruption of these films occurs with the result that nascent solid surface contact takes place. The extent of the contact depends on the properties of the solid as well as those of the film.

The removal of adsorbed films and oxide layers from surfaces, such as metallic surfaces, results in very strong interfacial adhesion when two such solids are brought into contact as already demonstrated. It also occurs with metals in contact with nonmetals. For example, when a clean gold surface is brought into contact with a clean semiconductor surface such as silicon, the adhesive bonds formed at the solid to solid interface are sufficiently strong so that a fracture of the cohesive bonds in the gold and a transfer of gold to the silicon surface result. This is indicated in the photomicrograph and X-ray map presented in figure 36.

In general, when two solid surfaces are brought into contact and adhesion occurs, the interfacial bond is stronger than the cohesive bond in the cohesively weaker of the two materials. On separation of the two solids this results in the transfer of the cohesively weaker material to the cohesively stronger. Thus, gold transfers to the cohesively stronger silicon (fig. 36).

Silicon and germanium are both semiconductors with many similar properties. One property in which they differ, however, is their cohesive binding energy, germanium being much weaker than silicon and having a cohesive binding energy comparable with that of gold. If the adhesion experiment in figure 36 is repeated with germanium substituted for the silicon, the results presented in figure 37 are obtained.

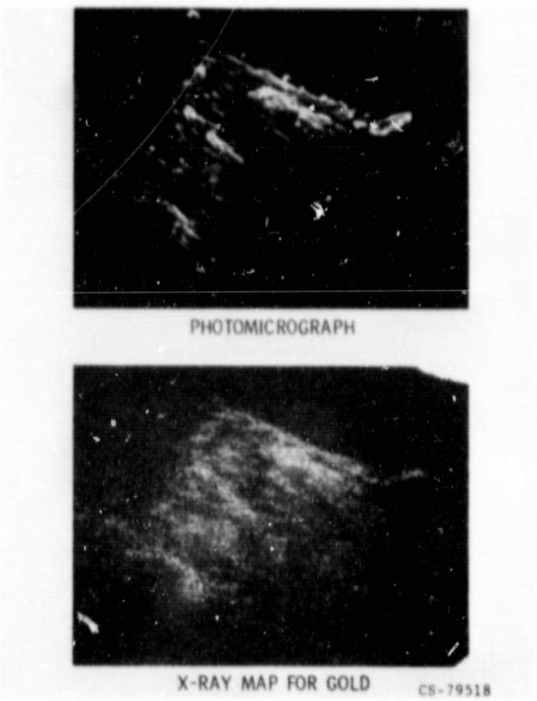

Figure 36. - Gold transferred to silicon (111) surface after adhesive contact. Load, 30 grams; sputter-cleaned surfaces; temperature, 23° C; pressure, 10^{-8} newton per square meter.

The photomicrographs in figure 37 indicate the contact region between the gold and germanium surfaces. Instead of gold transferring to the germanium, fracture occurs in the germanium with transfer of germanium to the gold. The photomicrograph at a higher magnification indicates chevron-shaped fracture cracks have developed in the (111) crystal surface of the germanium. Thus, the behavior of metal to nonmetal contacts is similar to that observed for metal to metal contacts.

Iron is cohesively much stronger than germanium and gold. When a similar adhesion experiment is conducted with iron in place of gold, germanium, as would be predicted, transfers to the iron. Furthermore, if a tangential force is applied to the iron-germanium contact, the resistance to the tangential motion (friction force) reflects the fracture behavior.

Figure 38 presents the friction force recorded with time for the iron sliding (tangentially) along the germanium surface. The trace has a sawtooth appearance, reflecting what is commonly referred to as stick-slip behavior. The stick portion is the adhesion of the solid surfaces at the interface which accounts for the gradually rising value of the friction force shown in figure 38. At the point where the applied tangential force exceeds the adhesive bond strength or the cohesive strength of the cohesively weaker of the two materials, as in this case, fracture occurs in the germanium and sliding commences. The slip portion reflects this and is indicated in figure 38 by the periodic sharp drop in the friction force.

The adhesive bonding force measured for two solids in contact is, as already discussed, a function of the cohesive binding energy of the cohesively weaker of the two materials. It is also a function of the real area of contact. The greater the load, the greater the plastic and elastic deformation and the larger the real area of contact. The adhesive force increases with increasing load.

When tangential motion or sliding is initiated between two clean surfaces in contact, the resultant applied forces in the materials can produce material changes other than those associated with adhesion and principally tensile fracture. For example, prolific cracking can

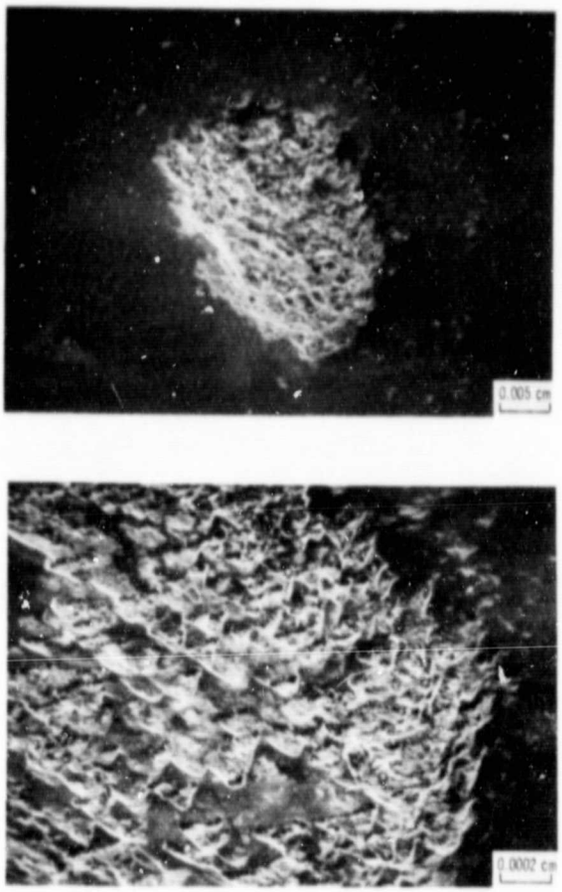

CS-78-708

Figure 37. - Adhesion of (111) gold surface to (111) germanium surface. Load, 30 grams; temperature, 23° C; pressure, 10^{-8} newton per square meter. Fracture occurs in germanium.

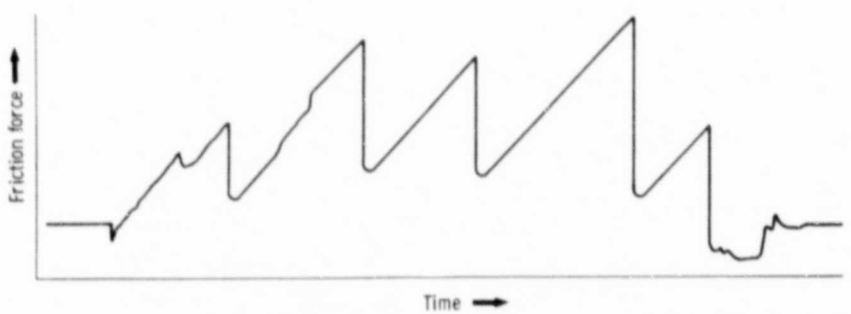

Figure 38. - Friction trace for single-crystal iron (110) sliding on germanium (111) single-crystal surface. Sliding velocity, 0.7 millimeter per minute; load, 30 grams; temperature, 23° C; pressure, 10^{-8} newton per square meter.

occur in a relatively brittle material such as silicon. This fracture cracking has been for a single-crystal (111) silicon surface after a single-crystal (110) iron surface slid across it.

Surface Films

Since adhesion plays a role in silicon undergoing brittle fracture, lubricating the surface to reduce adhesion should reduce crack formation in the silicon. Friction experiments were conducted with the silicon surface lubricated with 0.2-percent oleic acid in mineral oil. The friction coefficients measured for the lubricated iron-silicon contacts at various loads are presented in figure 39.

The friction coefficient for the lubricated surface was relatively unaffected by load. Sliding was extremely smooth with no evidence of stick-slip behavior. Furthermore, an examination of the silicon surface revealed a complete absence of fracture cracks. Etch pitting the surface disclosed a band of dislocations generated in the sliding contact region. These are shown in the photomicrograph in figure 40 by a series of delta-shaped etch pits. Slip bands also appear to the right of the etch pits.

Plastic deformation of silicon and germanium occurred in sliding friction experiments conducted at room temperature. Both silicon and germanium are brittle at room temperature, and deformation experiments on these materials are usually conducted at elevated temperatures (refs. 27 to 29). This is true even in the easy-slip stage (ref. 30). Furthermore, with silicon, bond rupture occurs more easily than bond shear at room temperature (ref. 31). The dislocations generated herein with sliding at room temperature are, therefore, unusual.

Examination of the entire specimen surface revealed a complete absence of fracture cracks, indicating entirely plastic behavior of the silicon. The only other occurrence we could find of plastic deformation behavior of these materials at room temperature was in abrasion studies of silicon (ref. 32). In the abrasion studies, damage varied with orientation. In some instances, only dislocations

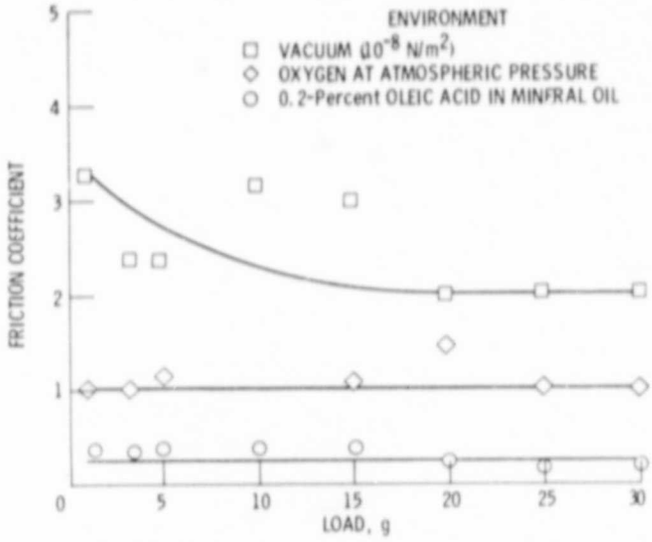

Figure 39. - Friction coefficient as function of load for single-crystal iron (110) sliding on a single-crystal silicon (111) surface in vacuum and in oxygen and lubricated with 0.2-percent oleic acid in mineral oil. Sliding velocity, 0.7 millimeter per minute; temperature, 23° C.

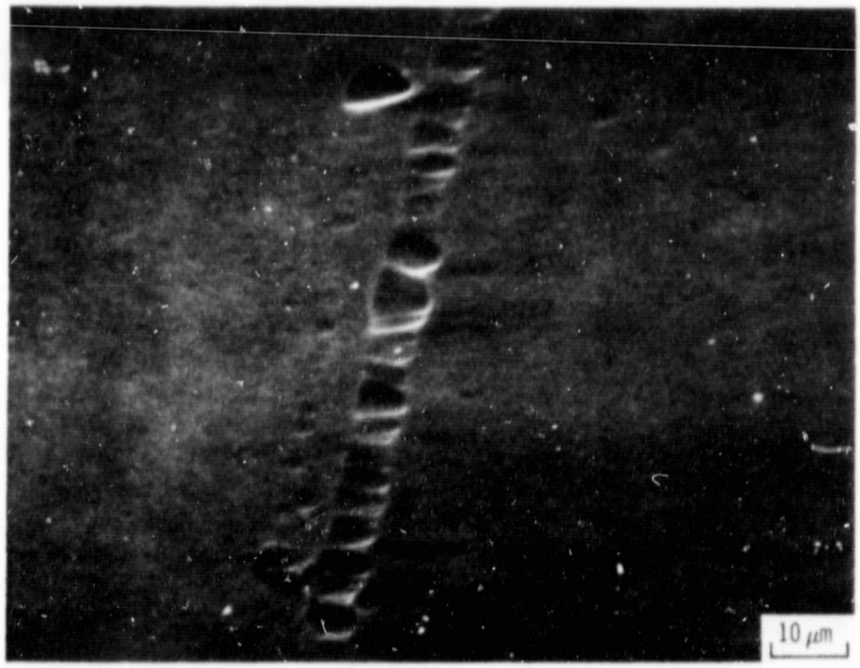

Figure 40. - Etch-pitted wear track made by single-crystal iron (110) sliding across silicon (111) surface, which was lubricated by mineral oil containing 0.2-percent oleic acid. Sliding velocity, 0.7 millimeter per minute; load, 30 grams; temperature, 23° C; environment, argon at atmospheric pressure.

were generated; in other instances, chips and cracks formed in addition to dislocations.

Data for oxygen adsorbed to the iron and silicon surfaces are also presented in figure 39. The presence of oxygen reduces the adhesion and correspondingly the friction coefficient from that observed for the materials in the clean state. Dry sliding still produces higher adhesion forces and friction than does liquid lubrication as indicated by the data in figure 39. Consequently, the friction at various loads with oxygen is intermediate between the clean state and the lubricated state. This result is, in general, consistent with the observations for metals in contact with metals.

METAL TO GLASSES AND CERAMICS

Certain properties of glasses and ceramics set them apart from metals and polymers with respect to adhesion, friction, and wear behavior. In general, metals and polymers deform plastically, while glasses and ceramics are normally brittle and exhibit little evidence for plastic flow. Plasticity affects the real area of contact for two solid bodies pressed together. In turn, the real area of contact affects adhesive forces, friction forces, and the propensity for adhesive wear to occur.

In a wide variety of situations, glasses and ceramics are not in contact with themselves but rather in contact with other materials and frequently metals. It is important to understand which of the materials in contact is contributing to friction and wear and by what mechanism.

The load or force with which two glass surfaces are pressed into contact affects the real contact area and corresponding friction force. In figure 41 the friction force for glass sliding on glass is presented as a function of load in two environments, air saturated with water vapor and a vacuum of 10^{-10} torr. Friction is proportional to load in both environments. This basic law of friction was first recognized by Leonardo de Vinci (1452-1519).

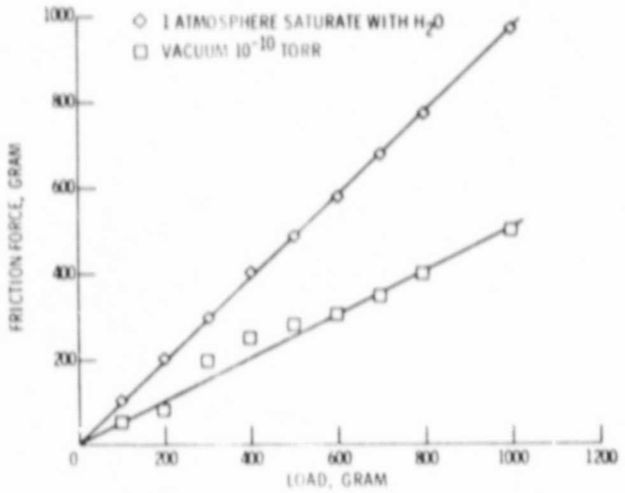

Figure 41. - Friction force as function of load for glass sliding on glass. Sliding velocity, 30 centimeters per minute; load, 100 grams; temperature, 23° C.

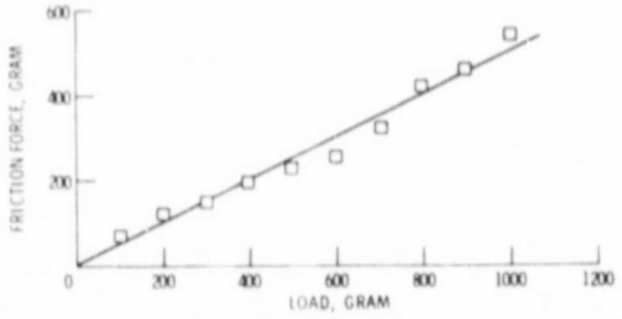

Figure 42. - Friction force as function of load for aluminum sliding on glass. Sliding velocity, 30 centimeters per minute; load, 100 grams; temperature, 23° C.

In figure 42, friction force is plotted as a function of load for aluminum sliding on glass in vacuum. The curve can be superimposed over the one obtained in vacuum in figure 41. The friction force at any particular load is essentially the same for glass sliding on glass and aluminum sliding on glass. Similar results have been obtained with other metals, such as iron sliding on glass. This is explained by examining the surfaces after sliding. When sliding on metal, the glass undergoes wear just as it does when sliding on glass. Microscopic examination of the metal surface indicates transfer of glass into the metal surface. Thus, in a vacuum, the metal surface becomes charged with glass and ultimately glass is sliding on glass. This is because initially the metal adheres to the glass. With tangential motion, fracture takes place in the weakest zone. Both the adhesive bond and the shear strength of aluminum are greater than the force necessary to fracture glass. Thus, glass transfers to the metal. What would appear to be an abrasive wear process from an examination of only the glass surface is in fact an adhesive wear process. Besides the load effect, other mechanical parameters, such as sliding velocity, affect friction behavior.

Most materials are extremely sensitive in their adhesion, friction, and wear behavior to the environment (refs. 16 and 33 to 36). Glasses are no exception. At a 1000-gram load the friction force of glass on glass in vacuum is one-half the value obtained in saturated air (fig. 41).

The results in figure 41 are unusual, however. For most materials, adhesion, friction, and wear are greater in a vacuum environment; this is the case with metals, carbons, and ceramics.

The anomalous behavior of glass with respect to friction can be explained on the basis of increased adhesion of glass in the presence of water vapor. The adhesion force for glass in the presence of water is more than three times that for glass in the presence of octane (ref. 33).

Metals in sliding contact with glass in moist air are observed to transfer to glass. Friction coefficients are then typically from 0.5 to 0.7, depending on the shear properties of the metal involved. In

vacuum, glass transfers to the metal, and friction coefficients are approximately 0.5. Thus, while the friction coefficients are not markedly different in the two cases, the mechanism is. The difference lies in the fracture properties of glass, which are strongly affected by water (ref. 37). Water impedes fracture and is a manifestation of the Joffe effect in an amorphous solid. From the transfer characteristics observed with metals sliding on glass, it must be concluded that the strength of glass under these circumstances is less in the absence of water vapor.

The marked difference in elastic and plastic deformation of ceramics and metals can result in plowing being the principal contributor to measured friction forces. This demonstrated by figure 43. A spherical rider of sapphire was slid on a single-crystal copper flat. Then, a single-crystal copper rider was slid over a sapphire flat. The coefficient of friction for the sapphire sliding on copper was 1.5, and for with copper sliding on sapphire, it was 0.2. In both instances, adhesion of copper to sapphire occurred. The differences in friction coefficient are due to the effects of plowing.

Surface chemistry also plays a role. Various metals were slid over a sapphire flat with the sapphire basal plane parallel to the sliding interface. With metals that form stable oxides, such as copper, nickel, rhenium, cobalt and beryllium, adhesion of the metal occurred to the surface oxygen ions of the sapphire.

With these metals fracture took place along the sapphire basal cleavage plane. This resulted in plucking out of large particles. This indicates that the strength along the basal plane was less than the bond strength and the metal coherence. The friction coefficient for all of the metals with sapphire was essentially the same, 0.2; this was dictated by the cleavage strength of the sapphire (fig. 44).

Metals examined in sliding contact with polycrystalline aluminum oxide showed friction coefficients greater than those obtained when metals slid on sapphire, exceptions being rhenium and lanthanum. The reason was that shear took place in the surface layers of the metal rather than fracture occurring in the aluminum oxide, as was observed with the single-crystal sapphire experiments. Metal transferred to

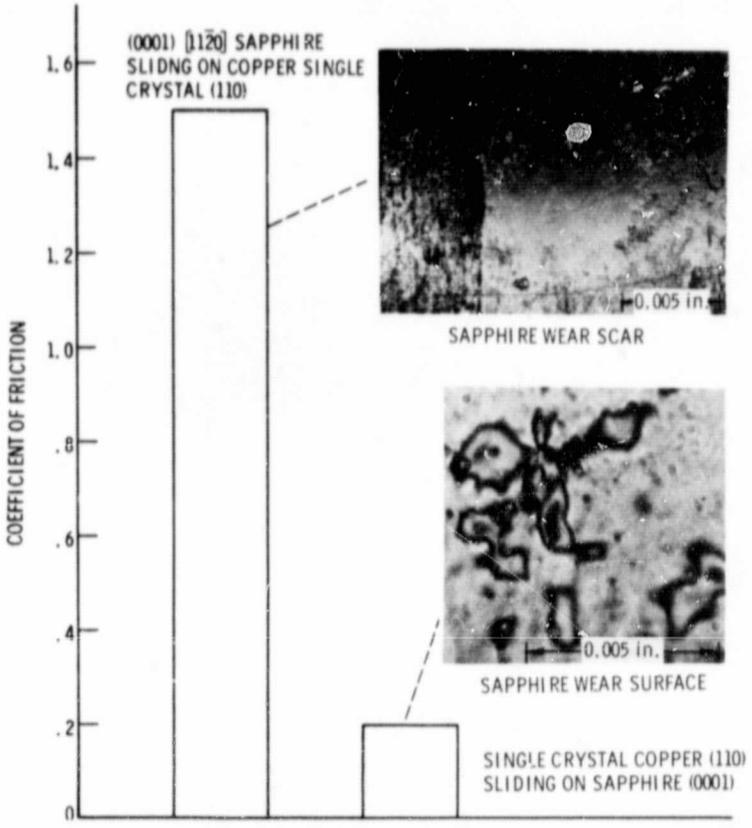

Figure 43. - Coefficient of friction for copper in sliding contact with sapphire in vacuum (10^{-10} torr). Load, 100 grams; sliding velocity, 0.013 centimeter per second.

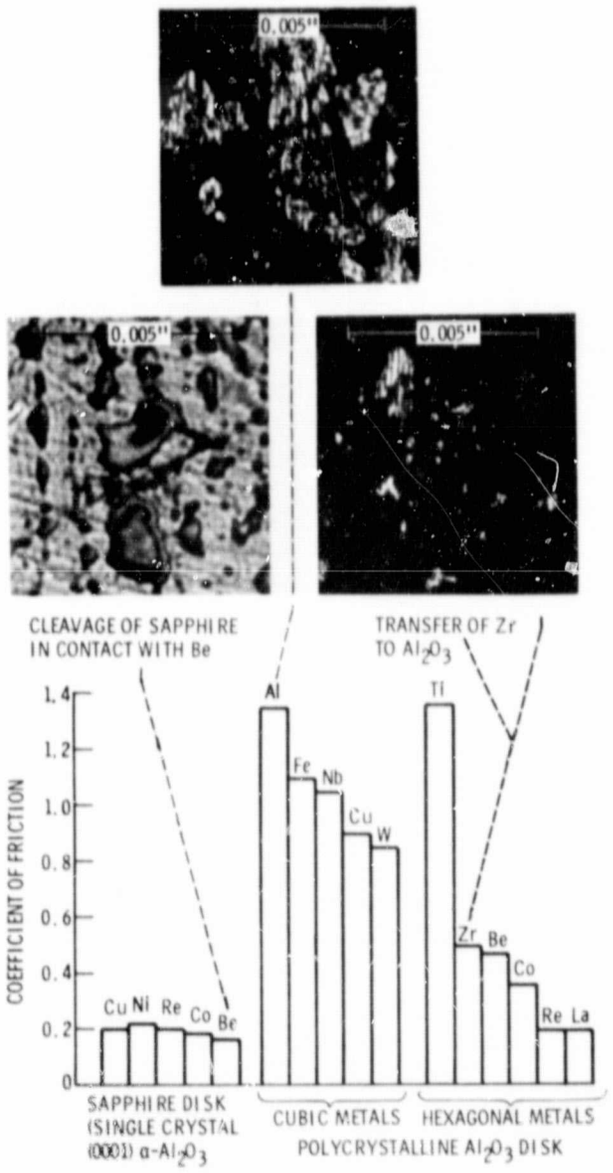

Figure 44. - Coefficient of friction for various metals sliding on Al_2O_3 in vacuum (10^{-10} torr). Load, 1000 grams; sliding velocity, 0.013 centimeter per minute; duration of experiment, 1 hour.

the polycrystalline aluminum oxide disk surface. The shear properties of the metal were therefore determining the friction force.

Differences in the friction coefficients for hexagonal and cubic metals in figure 44 occurred because of the differences in the slip and shear behavior of the metals. In general, hexagonal metals have fewer operable slip systems, shear more readily, and do not work harden rapidly; as a consequence, they exhibit lower friction coefficients than cubic metals. Titanium shows complex slip, making it behave more like a cubic than a hexagonal metal, which accounts for its striking friction behavior.

If a metal does not form a stable oxide, the observed friction coefficient is lower. With both gold and silver (fig. 45) the friction coefficient of sapphire in vacuum was 0.1 or one-half that obtained with the oxide-forming metals. The sapphire surface after sliding revealed no evidence of fracture. The lack of strong interfacial bonding between these metals and sapphire resulted in shearing of the bonds. From a practical point of view, this is the most desirable area for shear, since both friction and wear are least.

The crystallographic nature of the metal exerts a marked influence on friction beyond simply the crystal structure discussed in reference to figure 44. Even with a single metal, changes in surface orientation with sliding and the accompanying changes in associated slip systems affect friction.

From the foregoing it is apparent that adhesive wear, which is one of the most severe types of wear encountered with metals, also occurs with ceramics and is most pronounced where metals are in contact with glasses or ionic solids. In air, metal is generally observed to transfer to the glass. In vacuum, where the surficial strength of the glass appears to be reduced, glass transfers to metal with the result that glass is sliding essentially on glass.

The adhesive wear behavior of ionic solids in contact with metals is strongly dependent on the particular ionic solid involved and on its form. With sapphire, for example, adhesion to metals resulted in fracture along basal planes in the sapphire and wear to the sapphire.

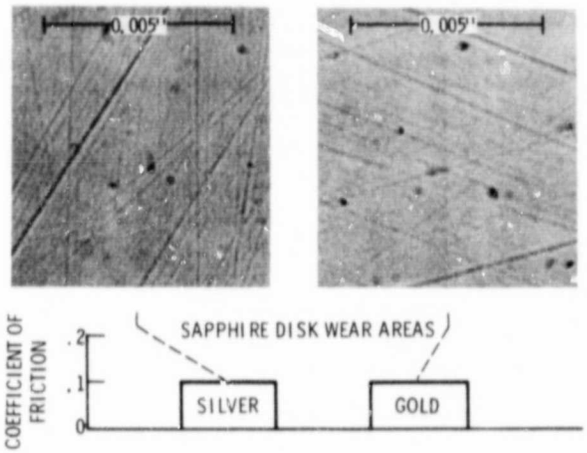

Figure 45. - Coefficient of friction for gold and silver riders sliding on sapphire in vacuum (10^{-10} torr). Sliding velocity, 0.013 centimeter per minute; ambient temperature, 25° C; duration of experiment, 1 hour.

With polycrystalline aluminum oxide, shear took place in the metal and the metal underwent wear.

The adhesive bonding of the metals to aluminum oxide can be related to the orbited energies of the metals and aluminum oxide. For the sake of simplicity, it is easier to consider the aluminum oxide in the form of sapphire. One may consider the binding electrons involved across an interface for metals in contact with sapphire as being that of the antibonding electrons (as has been done K. Johnson of MIT).

The orbital energies for the metals, iron, nickel, copper, and silver are presented together with that for sapphire in figure 46. From a consideration of the data in figure 46 one would anticipate stronger bonding of iron to aluminum oxide than of copper to aluminum oxide. The friction data in figure 44 indicate a higher coefficient of friction for aluminum oxide in the polycrystalline form with iron than with copper. This may result from two effects: first, the higher shear strength of iron, and second, the stronger adhesion resulting from less involvement of antibonding electrons (as indicated in fig. 46 for iron).

A comparison of the friction results (fig. 44) for copper in contact with sapphire and those (fig. 45) for silver in contact with sapphire indicates that the friction coefficient for copper is twice that for silver. Figure 44 shows that the strong interfacial bonding fracture occurs in the sapphire, as already stated, and figure 45 shows that it occurs for silver at the interface. Thus, the bonding is weaker for silver to sapphire, and this is consistent with the orbital energies and antibonding of figure 46. Silver has less antibonding energy than copper.

METAL TO POLYMER

Adhesion

The adhesion of polymers to metal surfaces is of interest with respect to both two-body and single-body adhesion - that is, where the polymer is the adhesive. Polytetrafluoroethylene (PTFE) has an

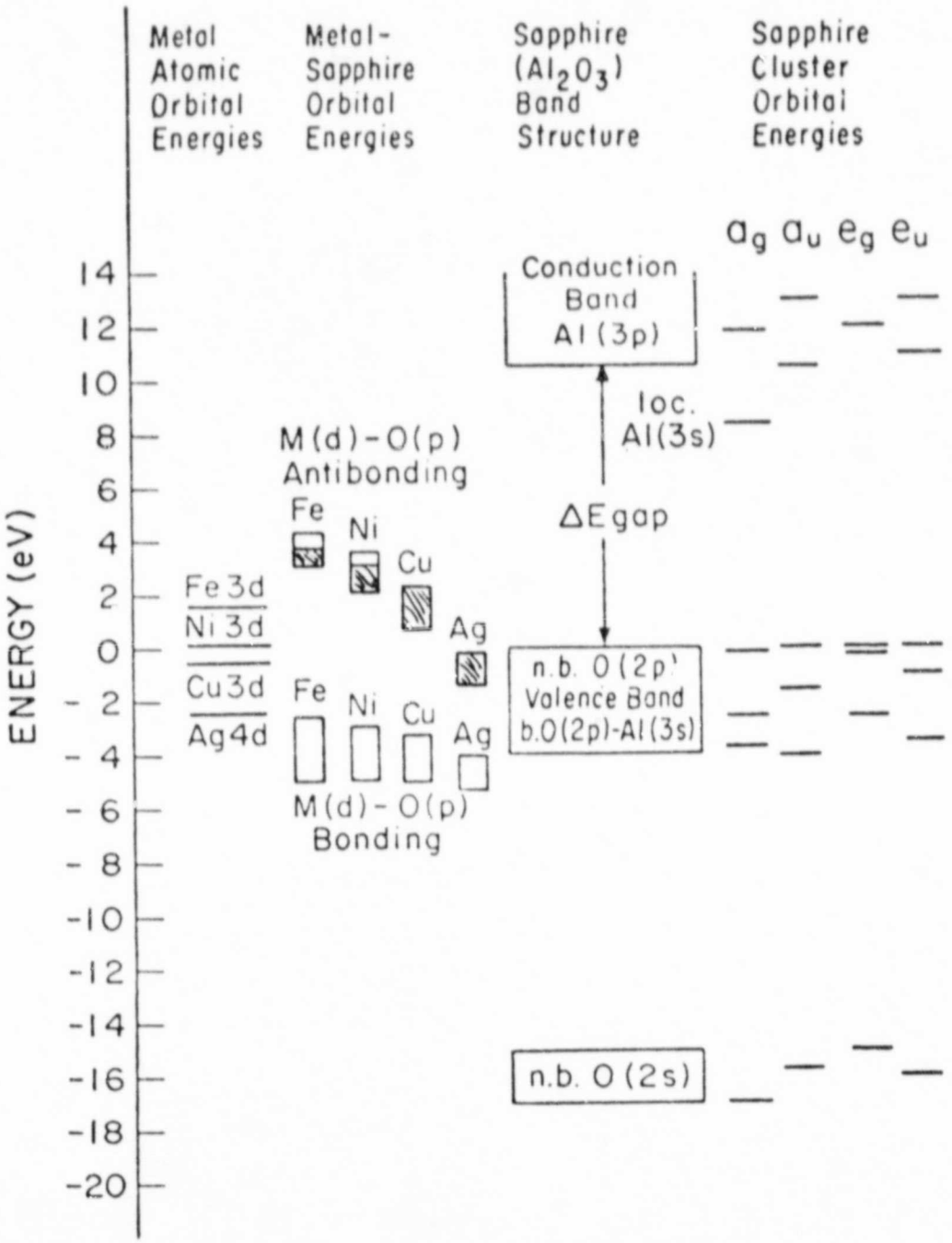

Figure 46. - Binding energies for metals in contact with sapphire.

extremely low-surface energy, is difficult to get to adhere to metal surfaces, and is, therefore, an ideal polymer to measure adhesion to metals.

The field ion microscope (FIM) is a powerful tool for studying the adhesion process, particularly of polymers to metals. A combination of high magnification and a resolution of 2 to 3 Å permits the adhesion process to be studied in atomic detail.

A series of PTFE-tungsten contacts was made with atomically clean tungsten contacting PTFE at loads between 20 and 30 grams, and the force of adhesion was measured. Figure 15 is a FIM picture of a clean tungsten tip. Figure 47 is a FIM picture taken after contact for a few seconds with PTFE. Many extra image points are apparent on the post-contact micrograph, particularly on the (110) plane shown in this figure. Adsorbed or adhered atoms can be observed because the geometry of the extra atoms on the surface of the flat creates points of localized field enhancement resulting in increased probability of ionization and hence greater brightness. Thus, clusters visible in the figure are fragments of PTFE which adhered to the tungsten surface after separation occurred. The other bright image spots also represent PTFE on the metal surface but their clusterlike nature cannot be resolved. The fragments of PTFE have the appearance of the end of a PTFE chain that is normal to the (110) plane. The fact that the fragments are stable at the very high electric field required for helium-ion imaging implies that the bond between the PTFE and tungsten is very strong; otherwise, field desorption of the adhered PTFE would occur.

To obtain a measure of the bonding between the PTFE and tungsten, the forces of adhesion were measured in terms of an adhesion coefficient for a number of contacts over varying periods of contact time. The results are summarized in figure 48. For short contact times the forces of adhesion were immeasurably small. After 2 minutes, however, the force of adhesion increased markedly. At contact times of 4 to 6 minutes, adhesion coefficients approching those for clean metals in contact were obtained.

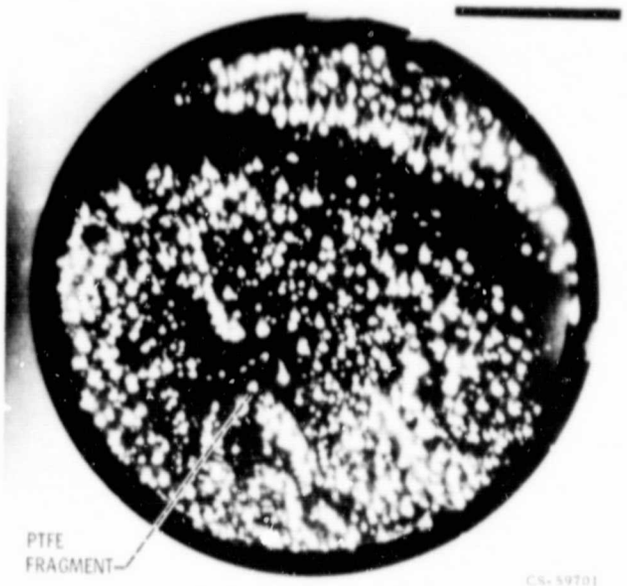

Figure 47. - Result of contact of tungsten FIM tip with PTFE.

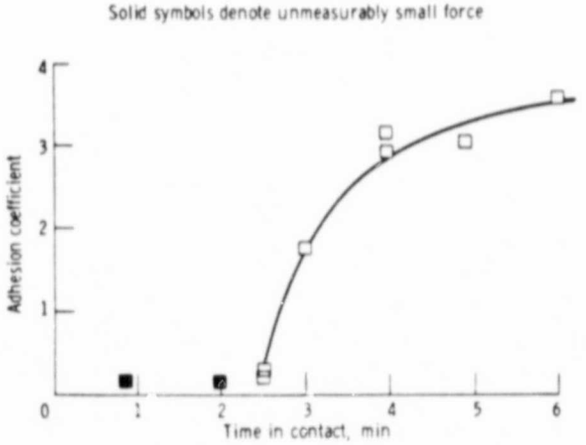

Figure 48. - Adhesion of PTFE to tungsten as a function of contact time.

A negligible adhesive force was obtained when a second contact was made with a previously contacted tip. This indicates that the adhesive polymer to metal bond is stronger than the cohesive polymer bond. Polymer radicals can be expected to occur as a result of the breaking of chains by the chemical interaction of polymer and metal. Thus, for PTFE contacting a clean tungsten surface, the possibility of reactive valence states of carbon atoms in PTFE bonding to tungsten exists.

A heavily loaded tungsten-PTFE (approximately three times more load, ~1 mg) contact gave the rather surprising result that extensive deformation of the tungsten occurred. The deformation extended far into the bulk of the material.

Mechanical contacts with a polyimide polymer contacting tungsten tips were made in vacuum of 10^{-9} torr with both light and heavy loads. At light loads the results obtained were analogous to those obtained with PTFE. Random distribution of bright spots were visible, indicative of polymer fragments adhering to the tungsten. The spots (polymer fragments) were particularly heavily clustered on the (110) surface, as was observed with PTFE.

From the data in figures 47 and 48, it is obvious that, with a low-surface energy polymer such as PTFE, strong adhesive bonding to metal surfaces can occur when the metal surface is clean and contact pressure is very high. Surface analytical tools such as those described earlier are very useful in identifying the degree of surface cleanliness.

Strong adhesive bond forces can develop between polymer and metal surfaces even when the metal surface is not atomically clean. The application of compressive surface forces can act to bring about strong adhesive bonding. The pressing of polymeric materials between metal foils can cause strong adhesive bonding of polymers to metals with normal oxides present on the metal surfaces.

When high-density polyethylene is pressed against aluminum foil, ESCA or XPS analysis of the surface reveals transfer of the polyethylene to the aluminum surface. This transfer is demonstrated by the data in figure 49. In the figure there are two XPS spectra.

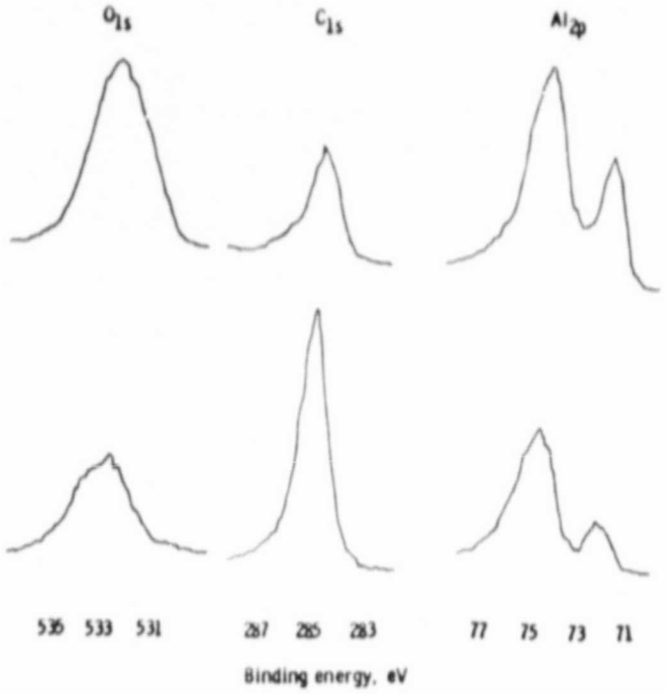

Figure 49. - XPS spectroscopy data.

The upper one is for the aluminum surface before being pressed by the high-density polyethylene, and the lower spectrum is for that same surface after it was peeled away from the high-density polyethylene.

The main points that emerge from these studies are that the oxide layer in commercially produced foil is typically ~20 Å thick and that a tenaciously held hydrocarbon-type layer is present at the surface that is not readily removed by either degreasing treatment or by heating under very high vacuum conditions. XPS, therefore, provides a convenient tool for investigating the nature of the peeled surfaces. Figure 49 shows the O_{1s}, C_{1s}, and Al_{2p} levels for the surface of the aluminum foil used for pressing the polyethylene sample b of figure 11(b). (It should be stated that no trace of Al_{2p} core levels could be detected on sample b.) The most significant feature is that both the aluminum and oxygen core levels are of appreciable intensity in the peeled foil, and this can only be interpreted on the basis that failure occurs very close to the aluminum surface. From the relative increase in the intensity of the peak due to the C_{1s} levels (taken in conjunction with an escape depth of 10 Å for electrons with kinetic energy of ~968 eV), a reasonable estimate for the thickness of polymer adhering to the peeled foil would be ~10 Å.

The adhesion of PTFE to tungsten in the atomically clean state has already been discussed. It has been found that a rubbing action between a metal and PTFE surface results in the adhesive transfer of polymer (PTFE) to the metal. With the polyethylene in contact with aluminum foils, adhesion of polymer to metal was achieved in the presence of surface oxides because of compressive loading, a mechanical activation of the adhesion process. A similar effect can be brought about by tangential motion of PTFE on the metal surface [11].

In figure 50 the PTFE film thickness is observed to increase with increased rubbing speed. An XPS analysis of the PTFE film transferred to the nickel surface revealed that the PTFE adhered to the nickel as a film and that the film was of the same composition as the bulk PTFE polymer. A small amount (<1 percent) of nickel fluoride (NiF_2) was

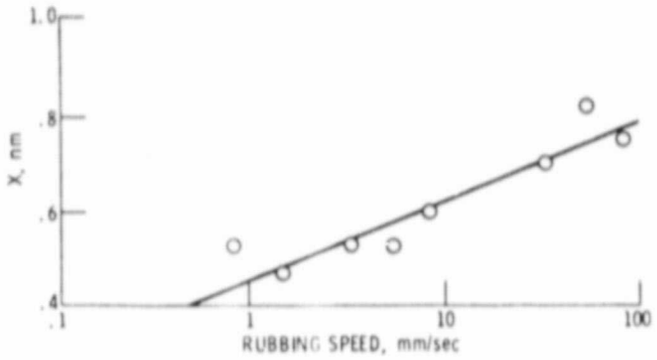

Figure 50. - PTFE film thickness as function of rubbing speed on nickel surface.

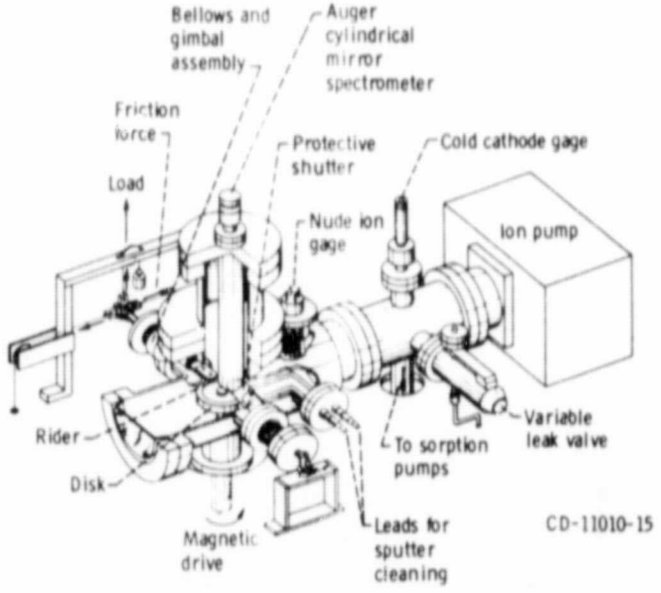

Figure 51. - Friction apparatus with Auger spectrometer.

present on the surface of the nickel, reflecting a chemical reaction to a limited extent of the PTFE with the nickel surface.

Static and Dynamic Friction Contact

Auger emission spectroscopy (AES) provides a technique for determining the chemical composition of a surface for elements heavier than helium with a high degree of sensitivity (i.e., 1/100th of a monolayer). AES was used in conjunction with a vacuum friction apparatus to provide an instantaneous chemical analysis of a metal surface during both static and dynamic contact with PTFE. The experimental apparatus is shown in figure 51, and further details on the technique and equipment are available in the literature (ref. 38).

Transfer of PTFE to atomically clean metals by static contact was observed for all metals brought into contact with PTFE. These included iron, tungsten, aluminum, and gold. An Auger spectroscopy analysis showed the transfer of PTFE to these surface.

The possibility that the transfer of PTFE to metal might be adversely affected by the presence of an oxide film on the metal was investigated by two methods. In the first method, high-purity oxygen was admitted to the chamber after the disk surface had been sputter cleaned with the oxygen being chemisorbed on the surface to monolayer coverage. Static contact was then initiated, and again transfer of PTFE was observed. Thus, the presence of a monolayer of chemisorbed oxygen does not prevent the transfer observed.

The second method involved using a preoxidized aluminum disk. It is known that the natural oxide layer on aluminum is many layers thick. Removing the normally present adsorbed carbon dioxide and carbon monoxide by a short sputtering (20 min) exposed the "clean" aluminum oxide layer. Static contact was again initiated, and again PTFE was found on the surface. Thus, PTFE transfers to the oxide of aluminum as well as to the clean metal. This implies that the chemical activity of the substrate was not an important factor in the transfer observed in these static contact experiments.

Figure 52 shows the curve of friction coefficient as a function of number of passes of the disk for PTFE sliding on atomically clean tungsten and aluminum. The value of 0.08 obtained for PTFE on tungsten is consistent with the values usually reported for PTFE sliding on metals in air. The friction for PTFE on aluminum, however, rose drastically from 0.08 at the start to over 0.5 in less than one complete revolution. Severe "machining" of the aluminum disk occurred: metal cut from the weak track was seen at the rider-disk contact zone and chips of aluminum were seen covering the surface. The severe scoring of the aluminum occurred in both the presence and absence of an oxide film.

The results of the study with PTFE polymer in contact with tungsten indicate that polymer transfers to a clean metal surface on simple touch contact. The transferred polymer at the high field for helium ion imaging implies that the bond of the polymer to the metal surface is chemical in nature. With PTFE it is hypothesized that the bonding is that of carbon to the metal surface because the carbon to carbon bond is the weakest bond in the PTFE structure and the one most frequently seen broken on polymer scission. Furthermore, the carbon could readily interact with the clean tungsten to form bonds stable at the imaging and field evaporation voltages applied in the field ion microscope.

The chemical bonding of the polymers to the clean metal surface necessitates breaking bonds in the organic molecule. Subsequently, metal to carbon, fluorine, or oxygen bonds form. Breaking organic bonds by metal surfaces is observed with hydrocarbons contacting metals in the field of catalysis. The tendency for such reactions should be increased when the metal surface is atomically clean because of the enhanced surface activity of the metal.

The effect of loading in the transfer of polymers was examined. Larger amounts of polymers were observed with an increase in load. The polymer appears to remain on the tungsten surface in longer chain fragments. This indicates that fracture occurred deeper in the polymer body than was observed at light loads. When field evaporation

C-2

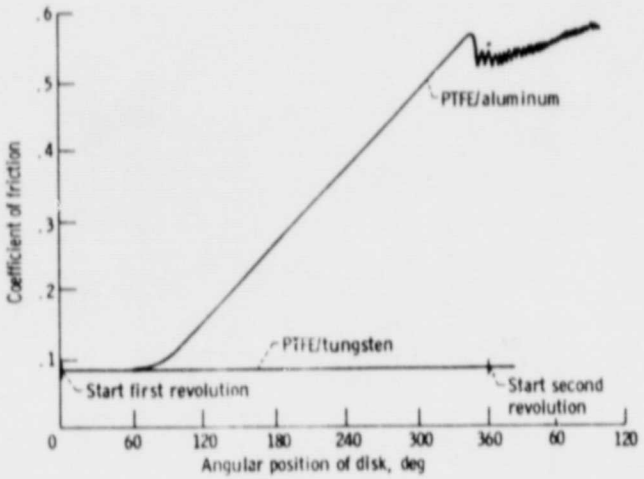

Figure 52. - Coefficient of friction of PTFE on aluminum and tungsten disks in vacuum. Sliding velocity, 0.07 centimeter per second; load, 250 grams.

was conducted, the polymer chain length that adhered to the tungsten could be reduced to that observed with light loads.

It is of interest also to note that preferred orientation of the polymer chains toward the zone of contact has occurred. This resulted when the tungsten was pressed into the polymer under load. Adhesion of polymer occurred to the tungsten surface. Polymer bonds were broken in the bulk and the relative tangential motion of the polymer body along the radius of the tungsten tip resulted in texturing (preferred orientation of chain fragments).

Polymers and polymer composites are being used increasingly in place of metals in many industries (ref. 39). Consequently, the friction and wear behavior of polymers and those properties which influence friction and wear are increasing in importance. Properties of polymers investigated in relation to their effect on polymer friction and wear have included film forming tendencies (ref. 40), polar nature (ref. 41), deformation behavior (ref. 42), bulk mechanical properties (ref. 43), molecular structure (ref. 44), transfer behavior (45), and crystalline transitions (ref. 46).

Most polymeric materials used in components of lubrication systems can and do vary in molecular weight. Furthermore, the molecular weight distribution can be different for different lots of the same material. It would therefore be desirable to know what effect, if any, molecular weight has on the friction and wear behavior of polymers.

Experiments were conducted to examine the effect of molecular weight on the friction and wear behavior of a polymer (polyethylene oxide) in contact with itself and iron for a range of molecular weights (from 100,000 to 5,000,000). Friction and wear experiments were conducted with a hemispherical rider sliding in reciprocal motion on a flat disk surface. Reciprocal sliding was at velocities of 0.1 and 5 centimeters per minute, loads of 25 to 250 grams, and a temperature of 23° C in a dry (<20 ppm H_2O) argon atmosphere.

When in contact with iron in one set of experiments, the rider was iron and the flat was polymer; and in the second set of

experiments, the rider was polymer and the flat was iron. The results obtained in these experiments are presented in figure 53.

Examining figure 53 reveals that with all three specimen combinations the friction coefficient decreased with the increasing molecular weight of the polyethylene oxide. The greatest reduction occurred with the lower molecular weights. It is apparent from figure 53 that, with polyethylene oxide, the higher the molecular weight, the lower the friction. A similar behavior may exist for other polymers.

The friction coefficient for the polymer sliding on itself in figure 53 is higher than it is for the polymer in contact with iron. Examinations of the wear surfaces revealed some differences in wear behavior.

With the polyethylene oxide sliding on itself a number of events are seen to take place in the contact zone of the surface. In some regions a surface glaze appeared, and this indicated some localized surface melting of the polymer during sliding. This is localized, and it does not occur over the entire contact region. Two forms of polymer removal are also observed. In the first, ribbons of polymer material were generated from the surface. These ribbons stand above the flat surface of the polymer. Cavities or pits are also observed in the rubbing surface. It appears that particles of polymer are removed from the bulk.

In contrast, where the polymer is in sliding contact with both iron riders and iron flats, a high degree of localized surface melting of the polymer occurs. Surface melting occurred over most of the contact zone.

Likewise, with the polymer rider sliding against the iron flat surface, melting of the polymer occurs. When the polymer was in sliding contact with the iron, there was no evidence of polymer ribbon formation or plucking out of polymer from the bulk as was observed with the polymer sliding on itself.

The differences in friction behavior seen in figure 53 may be explained by the differences in the surface generated. Where iron contacts polymer and melting occurs, lower friction would be observed than when plucking out of the polymer takes place. Thus, lower

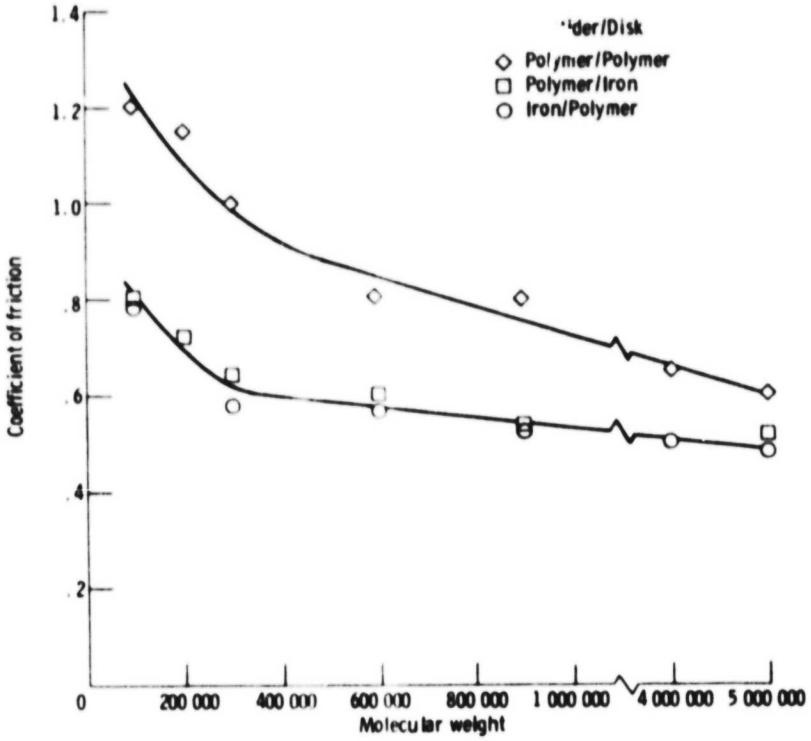

Figure 53. - Average coefficient of friction for polyethylene oxide polymer sliding on itself and iron as function of molecular weight. Sliding velocity, 0.1 centimeter per minute; load, 25 grams; temperature, 23° C; argon atmosphere.

friction might reasonably be anticipated with the polymer in contact with iron, as shown by the data in figure 53.

METAL TO CARBON

Graphitized Carbon

Graphite and carbon-graphite bodies are widely used in the field of lubrication. Graphite is used as a solid lubricant (refs. 47 to 49). Carbon-graphite bodies are used as components in such devices as mechanical seals (ref. 50) and electrical brushes (refs. 24 and 51). Thus, the fundamental adhesion, friction, and wear behavior of these materials are of interest.

It has been demonstrated in many problem areas that the metal surfaces against which carbon materials run can exert a considerable influence on the friction and wear. It was decided, therefore, to explore the role of varied mating metals for 100-percent electrographitized carbon sliding in vacuum. The results obtained in these experiments can be seen in figure 54. The lowest coefficients of friction were obtained for the carbon sliding on electrolytic iron and electrolytic copper. The best wear results, however, were obtained with 100-percent electrographitized carbon sliding on 440-C stainless steel. The greatest wear to carbon surfaces was obtained with gold plate and electrolytic silver as mating surfaces. This is significant because it was with these two metals that no visual evidence of a transferred carbon film to the metal surface was obtained. All the other metal surfaces are "oxide formers," and, with all of them, carbon transfer films were present. Such transfer films have been shown to be essential for effective lubrication by graphite materials (ref. 52). Although these experiments were conducted in vacuum, residual metal oxides present on the surface have low enough evaporation rates to be retained on the metal surface.

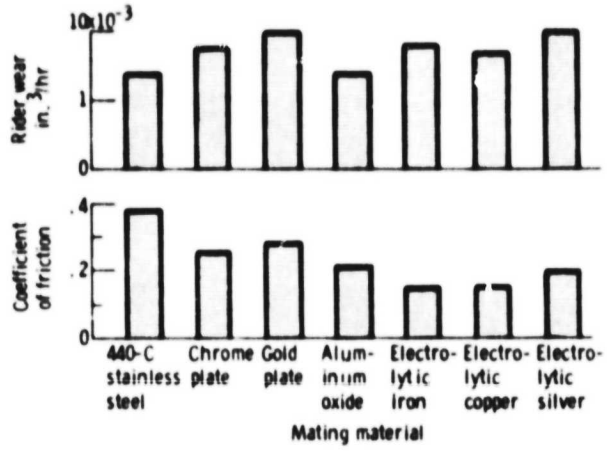

Figure 54. - Effect of mating materials on coefficient of friction and rider wear for 100-percent electrographitized carbon in vacuum (10^{-7} torr). Sliding velocity, 156 centimeters per second; load, 1000 grams; duration of experiment, 1 hour.

Mechanism of Adsorption

There exist two possible types of bonding of carbon to the metal: first, direct bonding with the formation of metal carbides (ref. 53), and second, the chemisorption of carbon and carbon oxides to the metal oxides. The formation of metal carbides requires intimate contact of carbon and metal. This is not possible at ordinary temperatures and pressures because metal and carbon oxides are present on both surfaces and the oxides are thermodynamically more stable than the carbides. The chemisorption of carbon and carbon oxides to metal oxides is more likely than direct bonding (ref. 54). Chemisorption proceeds without extremely high temperatures or pressures. In addition, numerous references in the literature indicate the presence of adsorbed films on both carbons and metals (refs. 22 and 55 to 62).

The chemisorption of carbon (C) to the metal oxide (O-M) may be achieved with the formation of a complex with carbon being bonded to a metal oxide (-C-C-O-M). If the bonds between carbon and oxygen and between carbon and the metal are resonating double or triple bonds similar to those in the carbonyls, the bond energy binding the carbon to the surface is considerably higher. This type of attachment may occur for nascent surfaces generated in the process of sliding.

When oxygen is chemisorbed on the carbon surface, as is generally the case, the adsorption may occur by the mechanism considered in references 57 and 62. The adsorption of a carbon monoxide type structure (resulting from the chemisorption of a single oxygen atom on carbon within the carbon surface) on an oxygenated surface (metal oxide) may occur in the following manner:

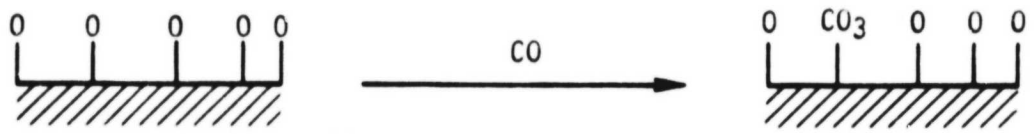

Metal disk surface — From carbon body — Metal disk surface

The adsorption of a carbon dioxide type of structure (resulting from the chemisorption of two oxygen atoms on a carbon atom within the carbon surface) on an oxygenated surface (metal oxide) may occur in the following manner:

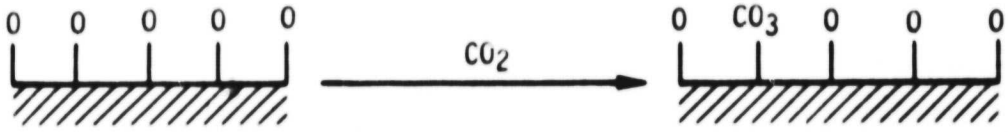

Metal disk surface From carbon body Metal disk surface

The chemisorption of a carbon monoxide type of structure results in the formation of a carbonate with a new site on the metal surface exposed for further reaction of the metal with oxygen or other gases. The chemisorption of a carbon dioxide type of structure also involves the formation of a carbonate on the metal surface; with the adsorption of a carbon dioxide type of structure, however, no additional sites on the metal surface are exposed for reaction or adsorption.

Adsorption of the carbon monoxide type of structure from the carbon body may occur on metal oxides in a reversible manner. With this reversible adsorption, the carbon monoxide type of structure can be desorbed. Often, however, depending on the surface to which the carbon monoxide is adsorbed, desorption only occurs by removing oxygen from the metal oxide - that is, by the desorption of carbon dioxide. The latter type of reaction is irreversible and can leave a nascent metal surface.

Removing these chemisorbed structures from metals like copper, nickel, cobalt, iron, and chromium can involve energy levels of 20 to 100 kilocalories per mole (ref. 63). The wide range of adsorption energies results from the type of bond, which depends on the nature of both the metal and the adsorbing species. Once all the active oxygen sites on the metal surface have been occupied by carbon atoms or carbon complexes, a carbon film can be established on the metal surface and the sliding process can become one of carbon sliding on carbon rather than carbon on metal.

Pyrolytic Graphite

Pyrolytic graphite prepared by the high temperature decomposition of hydrocarbons affords a source of high purity carbon in graphite form. Orientation effects can readily be studied with this material. Furthermore, it has many properties which make it an ideal material for use in lubrication systems.

Generally, as already indicated, the solid-state contact of carbon-graphite bodies is not against itself in lubricating devices but rather against metals. The interactions of metals with graphite carbon of differing orientations and the effect of surface films on those interactions are, therefore, important.

Studies with pyrolytic graphite were to determine the effect of (1) orientation, (2) reactivity of the metal, and (3) the effect of surface films on the friction and wear of metals in contact with pyrolytic graphite. Low energy electron diffraction (LEED), Auger emission spectroscopy analysis, scanning electron microscopy (SEM), and energy dispersive X-ray analysis (EDXA) were used to characterize and monitor surface changes. Gold was the metal selected for study. It does not reach chemically with carbon.

The pyrolytic graphite used was electronic grade prepared from vapor deposition. It was prepared from the decomposition of methane at 2100° C and was then compression annealed at 3000° C under a pressure of 200 kilograms per square centimeter. It was machined into cylinders 8.0 millimeters in diameter by 5.0 millimeters in length with the basal orientation parallel to the cylinder axis (prismatic orientation) or perpendicular to the axis (basal orientation) as desired. A fresh surface was prepared by polishing with 600 grit abrasive paper. A basal surface was also prepared by cleavage with a razor blade.

The metal pin specimens contacting the pyrolytic graphite were single crystal gold. The pins were cylindrical with a 2-millimeter diameter and a 2.0-millimeter radius on the end (the contacting surface). The gold was 99.99 percent pure. With gold the (111) plane

was parallel to the contacting interface to within ±2°. The metal crystal contacting radius was electropolished prior to use.

An apparatus used in this kind of investigation was a vacuum system with the capability of measuring adhesion, load, and friction, and also performing Auger and LEED surface analysis. A diagram of the apparatus for measuring adhesion, loading, and friction is shown in figure 55.

A gimbal mounted beam projects into the vacuum system. The beam contains two flats machined normal to each other with strain gages mounted thereon. The gold, iron, and tantalum single-crystal pin specimens are mounted on the end of the beam. A load is applied by moving the beam toward the disk. Load is measured by the strain gage. Adhesive forces are measured by moving the beam in the direction opposite to which the load was applied (see fig. 55).

Tangential motion of the pin along the disk surface is accomplished through the gimbal assembly. Friction force is measured by the strain gage normal to that used to measure load. In the present study, full-scale deflection on a conventional strip chart recorder resulted from a 10-gram load.

Multiple wear tracks could be generated on the disk surface by translating the beam containing the pin. Pin sliding was in the vertical direction in figure 55.

In addition to the friction apparatus, the experimental chamber also had a LEED diffraction system and an Auger spectrometer. The electron beam of both could be focused on any disk site.

The vacuum system was a conventional vacsorb and ion pumped system capable of readily achieving pressures of 10^{-8} newton per square meter as measured by a nude ionization gage. Sublimation pumping was also used.

It has been generally accepted for some time that the surface of graphite contains adsorbed oxygen which can only be removed as CO and CO_2 by heating to 1000° C in vacuum (see refs. 64 and 65 for summaries). Most of these studies concluded that oxygen was present on the graphite surface from indirect measurements such as mass spectrometry. The XPS studies of references 66 and 67 indicate

chemisorption of oxygen to the surface of graphite with the amount adsorbed being sensitive to both oxygen pressure and the temperature.

Auger spectroscopic analyses of the basal and prismatic orientations of pyrolytic graphite were conducted. The results are presented in figure 56. With both spectra the only Auger peak detected was that of carbon. The carbon Auger peak occurs at 272 electron volts and the oxygen at 511 electron volts. If oxygen were present on either surface, a peak would occur to the right of the carbon peak in figure 56.

It should be indicated that Auger spectroscopy analysis is sensitive to oxygen surface coverage to as low as 0.01 monolayer (ref. 68). Thus, if oxygen is present on either the prismatic or basal orientation of pyrolytic graphite, it is less than 0.1 monolayer. These results are consistent with the observations of Hart et al. (ref. 69) who found an absence of oxygen chemisorption to graphite.

Sliding friction experiments were conducted with gold as a metal in contact with graphite.

Gold

Gold was selected as a pin material because it is nonreactive with carbon and can be easily cleaned. The gold pin was heated to 700° C for 1 hour and then cooled to room temperature in vacuum to anneal it and remove any adsorbed film. It was slid on the two orientations of pyrolytic graphite in separate experiments. Experiments were conducted at 23° C for various loads and at temperatures to 700° C. The friction results are presented in figure 57.

In figure 57(a) the coefficient of friction is unaffected by load, but it is higher for the prismatic orientation at all loads. The friction coefficient on the basal orientation exceeds 0.4, and for the prismatic orientation it is 0.6. SEM photographs of the two surfaces after sliding are presented in figure 58.

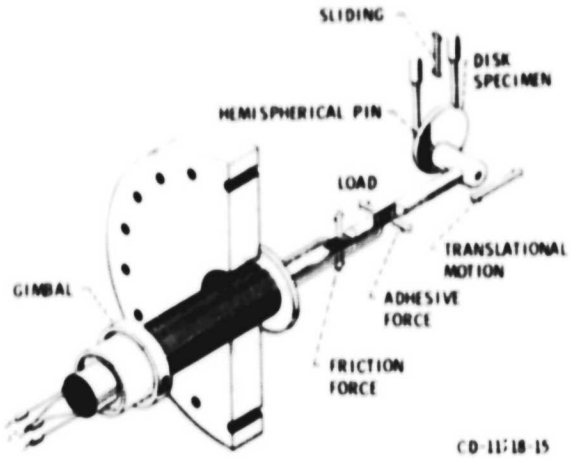

Figure 55. - High-vacuum friction and wear apparatus.

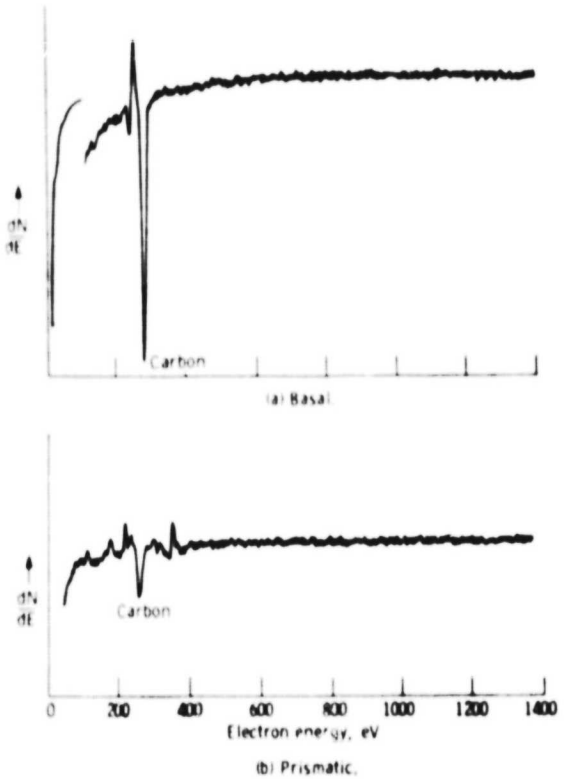

Figure 56. - Auger spectra for basal and prismatic orientations of pyrolytic graphite.

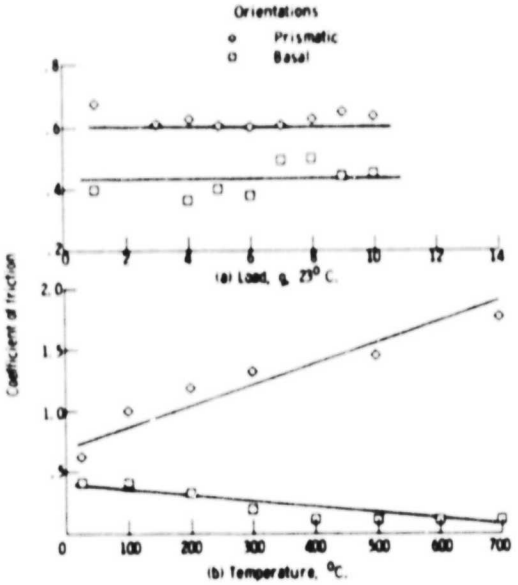

Figure 57. - Coefficient of friction as function of load and temperature for gold (111) sliding on pyrolytic graphite. Sliding velocity, 0.7 millimeter per minute; pressure, 10^{-8} newton per square meter.

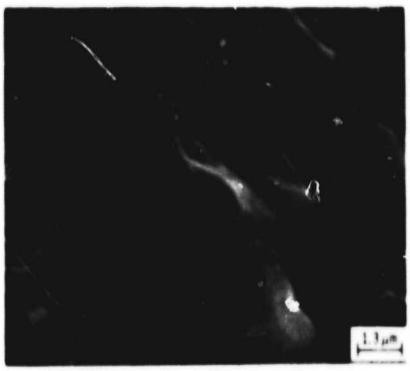

(a) BASAL ORIENTATION

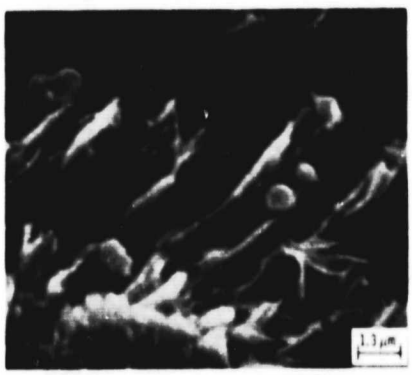

(b) PRISMATIC ORIENTATION

CS-77-165

Figure 58. - Scanning electron micrographs of basal and prismatic orientations of graphite after sliding of gold pin across surface of both orientations. Sliding velocity, 0.7 millimeter per minute; load, 10 grams; pressure, 10^{-8} newton per square meter; temperature, 23° C.

Figure 58(a) indicates the basal orientation of pyrolytic graphite after sliding. There was an absence of gold. On the prismatic orientation, however, small spheres of transferred gold were observed (see fig. 58(b)). Note the exposed edges of the graphite prismatic orientation in figure 58(b).

The prismatic orientation of graphite is from 500 to 10^3 times more chemically active than is the basal orientation (ref. 70). It has been indicated that the surface energy for the basal orientation of graphite is only a few hundred ergs per square centimeter while that for the prismatic orientation is 5000 ergs per square centimeter (ref. 71). When the basal orientation of graphite is decorated with gold to study vacancy loops, the gold is found to migrate on the surface to steps (ref. 72). The steps are higher energy sites (exposure of prismatic planes), and therefore the migration indicates stronger binding interaction of the gold with the prismatic planes than with the basal planes.

The difference in friction coefficients with the two orientations of pyrolytic graphite in figure 57(a) and the transfer of gold to the prismatic orientation must be related to binding energies. The reason for this relationship is that metal transfer to this orientation does not occur in the presence of physically adsorbed films.

The friction behavior of gold in contact with the two orientations of pyrolytic graphite at various temperatures is presented in figure 57(b). The friction coefficient for the basal orientation continuously decreases with increases in temperature while the friction for the prismatic orientation increases with increases in temperature. The friction coefficient for the basal orientation at 700° C is less than half the value at 23° C, while for the prismatic orientation the friction has increased twofold over the same temperature range.

Diamond

Another form of carbon which is of interest to the tribologist is diamond. Diamond, the hardest known material, is generally used for

machining nonferrous alloys, as abrasive materials (such as presintered carbides and ceramics), graphite, fiberglass, and rubber. It is also widely used in the electronics and jewelry industries for very light turning operations on precious metals.

To gain a fundamental understanding of the material removal process with diamond, it is extremely important to consider its basic material and tribological properties. Those properties that determine and influence material removal should be considered.

It is extremely difficult to expose (111) diamond faces by cleavage in the vacuum chamber for study in situ, and no entirely satisfactory cleaning procedure has yet been established for diamond. It has been suggested by Lurie and Wilson (ref. 73), on the basis of Auger electron spectroscopic and electron energy-loss measurements, that, when diamonds are bombarded with argon ions, their surfaces become graphitized. Thomas and Evans (ref. 74), however, believed that this treatment merely cleaned the surface. If Lurie and Wilson's conclusions were true, surface graphitization of diamond would profoundly influence the tribological properties of the ion-bombarded diamond surface.

The main features in the vicinity of the carbon Auger peaks of the Auger spectra from diamond are shown in figure 59. An Auger emission spectroscopy spectrum of the single-crystal diamond (111) plane obtained before argon ion bombardment is shown in figure 59(a). The crystal was in the as-received state after it had been baked out in the vacuum system. A carbon contamination peak is evident, and the spectrum is similar to that of an amorphous carbon. The surface was next argon ion bombarded at a 3-kilovolt potential under a pressure of approximately 7×10^{-4} pascal for 15, 30, 45, and 60 minutes. The spectrum of the surface after 15 minutes has three peaks; this is characteristic of graphite. The spectra of the surface after 30, 45, and 60 minutes have four peaks; this is characteristic of diamond as has been demonstrated and as indicated in reference 76. The peaks have been labelled A_0 to A_3, where A is used to denote an Auger peak. The energies of the peaks in this experiment were 267 to 269 for A_0, 252 to 254 electron volts for A_1, 240 electron volts

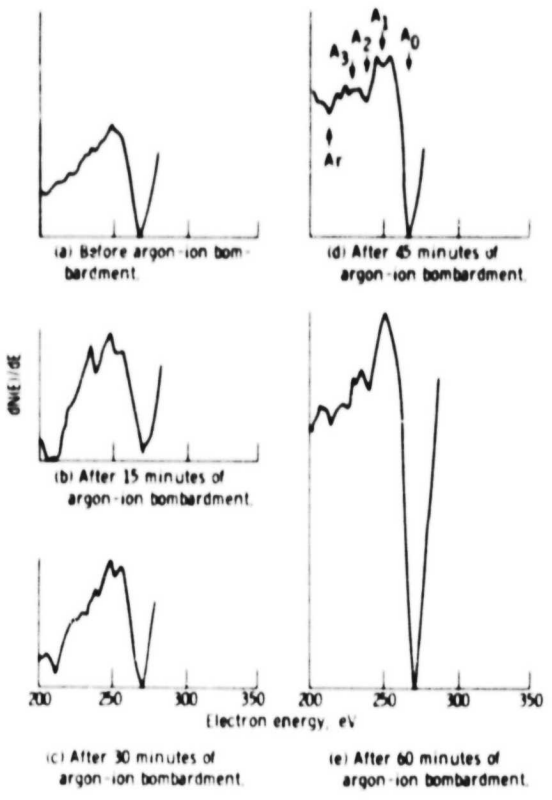

Figure 59. - Comparison of fine structure of the carbon Auger emission spectra for diamond.

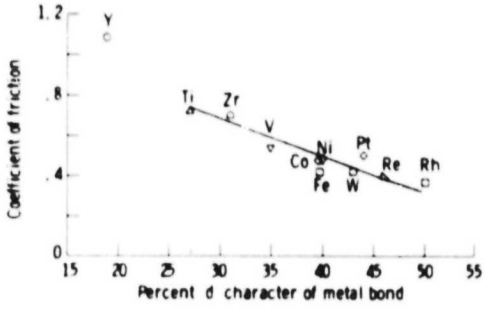

Figure 60. - Coefficient of friction as function of percent of metal d-bond character for single-crystal diamond {111} surface in sliding contact with transition metals in vacuum. Sliding direction, $\langle 1\bar{1}0 \rangle$; sliding velocity, 3×10^{-3} meter per minute; load, 0.05 to 0.3 newton; room temperature; vacuum pressure, 10^{-8} pascal.

for A_2, and 230 to 232 electron volts for A_3. The Auger spectrum of figure 59(d) is essentially the same as that obtained by Lurie for a clean surface (ref. 76).

Thus, for the adhesion and friction experiments reported herein, the surfaces of the diamond were argon ion bombarded for 45 to 60 minutes under a pressure of approximately 7×10^{-4} pascal. After this treatment the Auger spectra of the surfaces were very similar to that shown in figure 59(d).

In the 1940's Pauling (ref. 76) recognized differences in the amount of a d-bond character associated with transition metals. Since the d-valence bands are not completely filled in the transition metals, the filling of d-electron band is responsible for physical and chemical properties such as adhesive energy, shear modulus, chemical stability, and magnetic properties. The greater the amount or percentage of d-bond character that the metal possesses, the less active its surface should be. The adhesion and friction of metals in contact with themselves can be related to the chemical activity of the metal surfaces (ref. 77). The more active the metal, the higher the coefficient of friction. The d-valence bond character of the metal influences the coefficient of friction for metals in contact with silicon carbide, or manganese - zinc ferrite, just as it does for metals in contact with themselves (ref. 78).

The data in figure 60 indicate the coefficients of friction for some of the transition metals in contact with a single-crystal diamond (111) surface as a function of the d-bond character of the metal. The data indicate a decrease in friction with an increase in d-bond character. Titanium and zirconium, which are chemically very active, when in contact with diamond exhibit very strong interfacial adhesive bonding to diamond. In contrast, rhodium and rhenium, which have a very high percentage of d-bond character, have relatively low coefficients of friction. Figure 60 also presents the friction data for a diamond surface in sliding contact with a yttrium surface. Yttrium gives a higher coefficient of friction than that estimated from data of other metals. This may be due to the effect of oxygen. An argon-sputter-cleaned yttrium surface seems to be covered by an

oxide surface layer. It is very difficult to remove the oxide surface layer from yttrium by argon sputter cleaning for 30 to 60 minutes. The effects of oxygen in increasing the friction is related to the relative chemical thermodynamic properties and bonding of carbon to oxygen. The greater the degree of bonding across the interface, the higher the coefficient of friction. In the case of yttrium, oxygen on the surface tends to strongly chemically bond the yttrium to the diamond surface (ref. 79).

All the metals examined transferred to the surface of diamond in sliding. This reflects the strength of the diamond covalent bond. All of the metals have lower cohesive energies than the interfacial carbon to metal adhesive bond or the carbon to carbon covalent bond.

SURFACE METALLURGICAL PROPERTIES AFFECTING ADHESION, FRICTION, AND WEAR

SURFACE ENERGY

If one cleaves a crystalline solid along its cleavage plane, two highly chemically active surfaces are generated. The cleavage process causes the fracture of cohesive bonds across the cleavage interface, and these fractured bonds leave the surface in a highly energetic state. The energy of the surface is dependent on both the elemental nature of the bonds broken and the coordination number of the atoms in the resultant two surface layers. As a result, surface energy is a function of the material (ref. 80) as well as the surface orientation (refs. 81 to 86).

There is no question but that surface energy is important in the tribological behavior of materials. It influences adhesive bonds for solids in contact and hence friction and adhesive wear. In addition, it determines the nature of the interaction of lubricants with solids. The lubricant may either (1) physically adsorb, (2) chemisorb, or (3) undergo decomposition, as has been observed for some hydrocarbons with a clean metal surface (ref. 87). Surface

energy has been used in the formulation of an adhesive wear mechanism (ref. 36).

While surface energy can be very helpful in understanding the adhesion friction, wear, and lubrication behavior of materials, its present usefulness is very limited. The principle restriction has been the inability to obtain accurate experimental surface energy values.

An examination of the surface energy literature reveals wide disparities in reported values for any one material. Table IV indicates the minimum and maximum surface energy values that can be found in the literature for some of the elemental metals. These data were taken from a summary by Wawra (ref. 80).

While the broad range of values obtained are of concern, the fact that, for example, the minimum to maximum for some metals such as iron and chromium fall within the range found for tungsten are of even greater concern. It would be difficult, based on reported experimental data, to identify differences in the surface energy for iron, chromium, and tungsten.

As has already been indicated, the surface energy of solids such as metals is sensitive to crystallographic orientation. Most researchers conversant in the subject of surface energy readily agree that this is the case. Differences arise, however, when actual results are compared. The research results of three different investigators who have measured the surface energies for various planes of face-centered-cubic metals are presented in table V. The results are presented as the ratio of the surface energies for the various planes over that for the (111) surface.

The results of table V indicate that not only does the value vary with the investigator but more importantly the relative order of the metals as well (ref. 88).

One of the most significant reasons for the wide disparity in the surface energy values reported by various investigators has been inadequate control over the impurities in the materials. Small surface concentrations of such contaminants on hydrocarbon can have a pronounced effect (ref. 17). Small concentration of impurities in the

TABLE IV. - VARIATION IN VALUES OF REPORTED SURFACE ENERGIES

Element	Surface energy, ergs/cm^2		Temperature, °C
	Maximum	Minimum	
Cu	4258	950	-273
Ag	2493	600	-273
Au	2540	590	-273
Fe	5267	1980	-273
Ti	2730	1330	25,-273
Cr	4061	1515	-273
W	9410	1497	3370

TABLE V. - STRUCTURAL DEPENDENCE OF SURFACE ENERGY ON FACE-CENTERED-CUBIC METALS

Plane	Face-centered-cubic metals		
	Au,Ag,Cu,Ni (a)	Au (b)	Ni (c)
(111)	1.00	1.00	1.00
(100)	1.047	1.072	.95
(311)	1.119	1.065	1.00
(110)	1.15	1.047	1.01
(210)	1.16	1.055	1.00

[a]Reference 84.
[b]Reference 86.
[c]Reference 83.

bulk as well can markedly alter the measured surface energy of a material. This is indicated by the data in figure 61 for sulfur in iron. With an increase in concentration of sulfur, there is an accompanying decrease in surface energy (fig. 61).

Extremely small concentrations of bulk contaminant in a metal such as iron can have a pronounced effect in contaminating a surface. For example, as little as 8 ppm of carbon in iron diffuses to the surface, segregates there, and contaminates it (ref. 17). This segregation undoubtedly affects measured surface energies.

The use of high purity materials and the careful characterization of solid surfaces should result in the future acquisition of meaningful surface energy values. Surface analytical tools are currently being used for the needed surface characterization. One which has proven especially useful in this regard is the field ion microscope (refs. 85, 89, and 90). When used in conjunction with the atom probe, its contribution is enchanced. Alone it gives the atom by atom structural arrangement on a solid surface, but with the atom probe, it gives an atom by atom chemical analysis.

The significant reduction in the energy of the iron surface (fig. 61) with the presence of as little as 0.5-weight-precent sulfur is extremely significant. Iron-base alloys nearly all contain as bulk contaminants small amounts of carbon and/or sulfur. Both of these elements can segregate on the surface of the iron as the sulfur does (see fig. 61). What effect does such surface segregation from the bulk to the surface with the corresponding reduction in surface energy have on tribological behavior?

A number of years ago the author prepared some simple binary alloys of iron with sulfur and examined their friction and wear behavior in a vacuum environment. The object was to see what effect (if any) the sulfur would have on friction and wear behavior. The alloys contained up to 0.45-weight-percent sulfur. Friction and wear data for these alloys are presented in figure 62.

In figure 62 the addition of as little as 0.05-weight-percent sulfur reduced friction from complete seizure to a value of 0.3. Further additions of sulfur to the iron did not further reduce

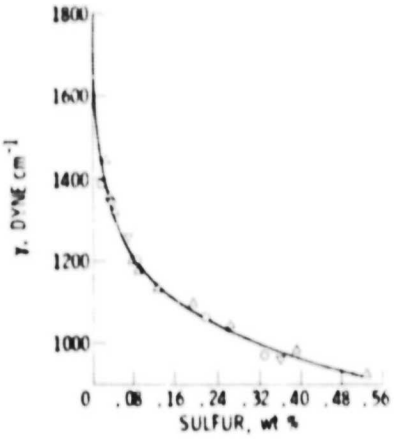

Figure 61. - Dependence of surface energy of liquid iron on sulfur content (ref. 82).

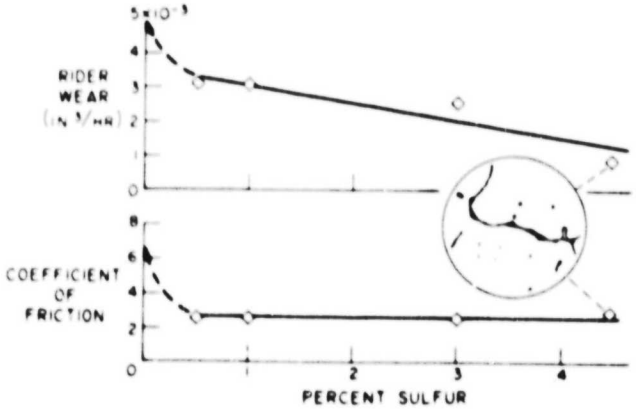

Figure 62. - Friction and wear of sulfur-iron alloys in vacuum. Sliding velocity, 170 centimeters per second; load, 1000 grams; ambient pressure, 10^{-9} torr; duration of run, 1 hour.

friction. The surface, as was learned by the author with the use of Auger emission spectroscopy, was already completely protected with a layer of sulfur at 0.05 weight percent. The wear of the iron, however, continued to decrease with increases in the sulfur content (fig. 62).

The friction and wear data of figure 62 were obtained with a rider sliding on a disk. The results for the disks and riders after sliding are presented in figure 63. The iron surfaces show evidence of adhesion and adhesive transfer. The surfaces of the sulfur containing alloy, however, indicate a relatively smooth sliding surfaces. Thus, the presence of sulfur has a very definite effect on friction and wear behavior.

AMORPHOUS METALS

In 1960 it was shown that amorphous solid phases could be formed by very rapid quenching of certain alloy compositions from the melt. This discovery launched a new field of research activity such that now there are well over 200 alloy systems that have been identified as being capable of quenching into the amorphous state (ref. 91). These alloys are referred to as metallic glasses (refs. 92 and 93).

From a tribological point of view, these amorphous alloys or metallic glasses have some very interesting properties. They are as hard as standard steels, yet they, unlike silicate glasses, possess substantial plasticity, are among the strongest known engineering materials, and are tough (resist the propagation of cracks through them). Their tribological behavior has not yet been studied.

Studies were conducted to determine the influence of the amorphous state of certain metallic alloys on tribological characteristics. Sliding friction experiments were conducted with three ferrous-base metallic glass compositions (both lubricated and unlubricated) in vacuum and argon. Riders of aluminum oxide, copper, and 52100 bearing steel were made to slide on the metallic glass surfaces under loads of 0.01 to 0.25 newton and over a range of

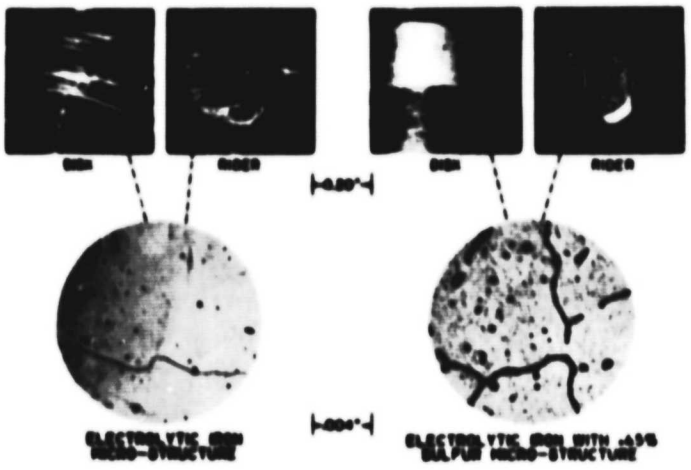

Figure 63. - Influence of sulfur on iron on sliding behavior in vacuum. Ambient pressure, 10^{-4} torr.

TABLE VI. - PROPERTIES OF METALLIC GLASSES[a]

Alloy composition	Crystallization temperature, °C	Density, g/cm^3	Hardness, GPa	Ultimate tensile strength, GPa	Bend ductility[b]
$Fe_{67}Co_{18}B_{14}Si_2$	430	7.56	10	1.5	1
$Fe_{81}B_{13.5}Si_{3.5}C_2$	480	7.3	10.3	.7	9×10^3
$Fe_{40}Ni_{38}Mo_4B_{13}$	410	8.02	10.5	1.38	1

[a]Reference 92.
[b]$\epsilon = t/(d-t)$: ribbon thickness, t; micrometer spacing at band fracture, d.

sliding velocities of 0.2 to 10 centimeters per minute. The vacuum experiments were conducted over a temperature range of 25° to 800° C.

Three metallic glass compositions were examined. These compositions and some of their properties are presented in table VI. The alloys were foils (0.05 mm thick) used in the cast condition except for heat treatments. The riders that were made to slide on the foils were single-crystal aluminum oxide (sapphire), 99.999 percent copper, and 52100 bearing steel.

Friction experiments were conducted in argon and in a 10^{-8} pascal vacuum. The coefficients of friction reported herein were obtained by averaging three to five measurements. The standard deviations of the data are within ±4 percent of the average value.

In an argon atmosphere, the foils of the metallic glasses and the rider specimen surfaces were scrubbed with levigated alumina and then rinsed with tap water, distilled water, and finally ehtyl alcohol. After drying the surface with argon gas, the foils were placed in the experimental apparatus. The specimen surfaces were brought into contact and loaded, and then the friction experiment was started.

With those experiments conducted in the vacuum chambers, XPS data were obtained on the specimen surface before and after sputter cleaning. The specimens were heated to the various experimental temperatures by resistance heating, and the temperature of each specimen was monitored with a thermocouple.

Table VII summarizes the surface conditions of the foils analyzed by XPS. Generally the XPS results indicate that the surface of the as-received $Fe_{67}Co_{18}B_{14}Si_1$ foil consists of a layer of oxides of iron, cobalt, boron, and silicon as well as a simple, adsorbed film of oxygen and carbon. The argon-sputter-cleaned surface consists of iron, cobalt, boron, silicon, and carbon. The surface heated to 350° C consists primarily of a layer of the alloy, boric oxide, and silicon oxide.

The XPS spectra obtained from the $Fe_{81}B_{13.5}Si_{3.5}C_2$ foil surface are summarized in table VII. The surface conditions of the foil are basically the same as those of the $Fe_{67}Co_{18}B_{14}Si_1$ already mentioned. Generally the surface of the as-received

TABLE VII. - SURFACES OF METALLIC GLASSES

Alloy composition	Surfaces		
	As-received	Argon sputter cleaned	Heated to 350° C
$Fe_{67}Co_{18}B_{14}Si_1$	Oxides of Fe, Co, B, Si, and C, adsorbed film of oxygen and carbon	Alloy, small amount of oxides	Alloy, boric oxides and silicon oxides migrated from bulk
$Fe_{81}B_{13.5}Si_{3.5}C_2$	Oxides of Fe, B, Si, and C, adsorbed film of oxygen and carbon	Alloy, small amount of oxides	Alloy, boric oxides and silicon oxide migrated from bulk

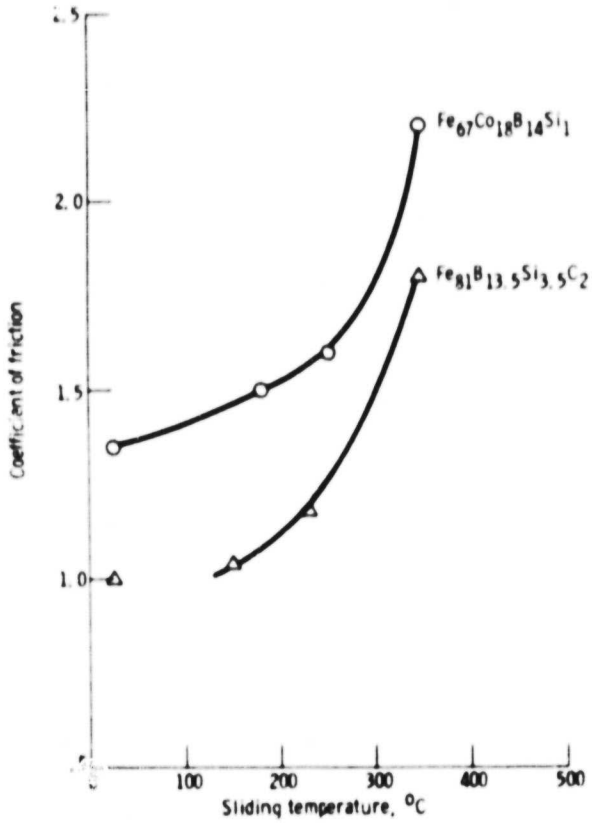

Figure 64. - Coefficient of friction as function of temperature for aluminum oxide sliding on $Fe_{67}Co_{18}B_{14}Si_1$ and $Fe_{81}B_{13.5}Si_{3.5}C_2$ alloys in vacuum. Normal load, 0.2 newton; sliding velocity, 3 millimeters per minute; vacuum, 10^{-8} pascal.

$Fe_{81}B_{13.5}Si_{3.5}C_2$ foil contains a layer of the oxides of iron, boron, silicon, and carbon as well as a simple, adsorbed film of oxygen and carbon. The argon-sputter-cleaned surface consists of the alloy and a small amount of oxides. The surface heated to 350° C contains primarily the metallic elemental constituents boric oxide and silicon oxide.

In situ friction experiments were conducted in a UHV system with the surface-treated foil specimens over a temperature range of room to 350° C. To obtain consistent experimental conditions, the time in contact before sliding was 30 seconds. Both the load and friction force were continuously monitored during a friction experiment. Sliding velocity was $3x10^{-3}$ meter per minute with a total sliding distance of $2x10^{-3}$ to $3x10^{-3}$ meter.

Experiments were conducted with the foils having the composition $Fe_{67}Co_{18}B_{14}Si_1$ and $Fe_{81}B_{13.5}Si_{3.5}C_2$ in contact with a aluminum oxide spherical rider at temperatures to 350° C with a pressure of 10^{-8} pascal. The coefficient of friction as a function of temperature for the foils is presented in figure 64. The foils and riders were sputter cleaned at room temperature before heating. The coefficient of friction generally increases with increasing temperature from about 1.4 for $Fe_{67}Co_{18}B_{14}Si_1$ and 1.0 for $Fe_{81}B_{13.5}Si_{3.5}C_2$ at room temperature to 2.2 and 1.7 at 350° C. Although the coefficient of friction remained low below 250° C, it increased rapidly with increasing temperature in the range of 250° to 350° C. The rapid increase in friction at temperatures from 250° to 350° C may be attributed to an increase in adhesion resulting from (1) crystallization of the foil and (2) the segregation of boric oxide and silicon oxide to the surface of the alloy.

The experiments herein started with a nearly amorphous surface containing some very small crystallites. Crystallization occurs for the foil with increasing temperatures. Crystallized foils are less resistant to adhesion and plastic flow than are the amorphous surfaces. The general increase in friction at elevated temperatures is then due to the increased adhesion and plastic flow in the contact area.

As already mentioned, at 350° C the foil surface was contaminated with boric oxide and silicon dioxide which had migrated from the bulk of the foil specimen to the surface. The oxide to oxide (Al_2O_3 rider) interactions produce stronger bondings than do the oxide to metal interactions (refs. 94 and 79). The increase in friction at elevated temperatures is due to the increased adhesion - that is, the increased bonding associated with oxidation of the foil surface.

Sliding friction experiments were also conducted in argon with normal residual surface oxides present on the amorphous foil having the composition $Fe_{67}Co_{18}B_{14}Si_1$ over a range of loads. The results obtained in these experiments are presented in figure 65.

At a very light load of 0.01 newton, the coefficient of friction was extremely high. The friction coefficient decreased with increasing load to a value of 0.35 at a load of 0.02 newton and remained there.

To determine the effect of the presence and absence of crystallinity on friction behaviors, foils were heated to 650° C for 2 hours in a vacuum furnace, cooled to room temperature, cleaned, and then examined in friction experiments. The results are presented in figure 65 together with those already described for the metal in the amorphous state.

At all loads the friction coefficient for the alloy in the amorphous state is less than it is for the same alloy in the crystalline state (fig. 65). Thus, the absence of crystallinity results in lower friction properties.

There was a complete absence of any visible wear track on the amorphous foil. A visible wear track was present on the crystallized surface. The amount of surface oxide was greater in the wear track of the crystalline sample. This is as might be anticipated, since the crystalline surface would be a higher energy surface.

To establish the exact crystalline state of the foils used in the experiments of figure 65, transmission electron diffraction patterns were obtained on the as-received foils and the foils after having been subjected to the heat treatment above the recrystallization temperature.

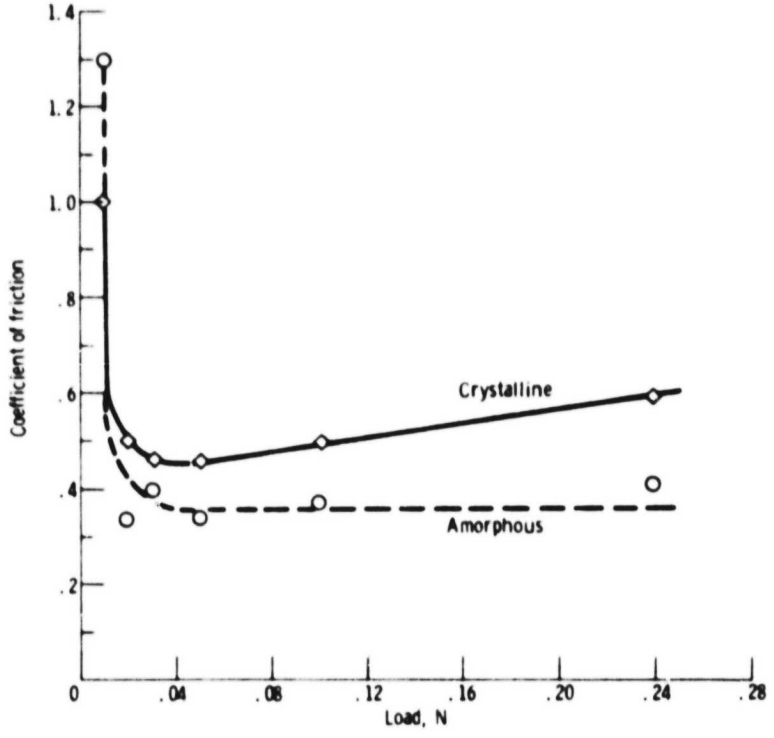

Figure 65. - Coefficient of friction as function of load for aluminum oxide sliding on $Fe_{67}Co_{18}B_{14}Si_1$ alloy in argon. Sliding velocity, 2.0 centimeters per minute.

The pattern of as-received foil indicated that the foil was not completely amorphous but contained grains of an extremely small size, approximately a few nonometers. The annealed foil had a general grain size after recrystallization of 0.3 to 1.0 micrometer.

The alloy composition shown in figure 65 is a metallic glass, and an obvious question would be how it compares in friction characteristics to conventionally used alloys. Friction experiments were conducted with 304 stainless steel foils under the identical conditions to those used in figure 65. From the data obtained, there appears to be very little difference in friction behavior of the two alloys. The wear results were, however, markedly different. There was essentially no detectable wear on the surface of the amorphous alloy. There was, however, considerable wear to the 304 stainless-steel surface. There was considerable plastic flow and oxide debris generated on the 304 stainless steel. Lumps of metal appeared in the wear track. Thus, while very little difference in friction coefficient was observed for the two alloys, marked differences in wear were found.

GRAIN BOUNDARIES

When going from the amorphous state of material to the crystalline state, there are, unless the material is a single crystal, grain boundaries. These boundaries are high energy sites which contribute to the overall surface energy and correspondingly to tribological behavior.

To examine this effect, it was decided to conduct friction experiments in vacuum with an oriented single crystal of sapphire sliding on a large-grained tungsten disk with known grain orientations. Data for sapphire in the literature indicate a dependence of wear of various surfaces on crystallographic orientation (refs. 95 to 98). With large grains in a polycrystalline matrix, the influence of crossing grain boundaries on slip behavior can be determined. This situation does not exist in single crystals.

The large-grain tungsten used in this investigation was prepared by electron beam melting. A chemical analysis of the material used indicated 5 ppm carbon, 3 ppm oxygen, less than 3 ppm nitrogen, and small percentages (less than 2 ppm) of the metallic elements calcium, chromium, cobalt, copper, iron, and nickel. The specimen was cut, finish ground, and lapped before electropolishing. The specimen was then electropolished in a sodium hydroxide solution to remove the worked layer. After electropolishing, the specimen was mounted in a fixture and Laue patterns of the various grains were obtained. The orientations obtained are shown in figure 66(a), and their positions on the unit triangle are shown in figure 66(b). The actual specimen is shown by the photograph at the top of figure 66(a); the diagrammatic sketch below the photograph indicates the orientations. In addition to crystallographic planes, directions are indicated in figure 66(a). Planes are given in parentheses and directions in brackets.

The single crystals of sapphire used in this study consisted of 1.0-centimeter-diameter balls. The balls were initially oriented with polarized light to locate the optical axis, and then X-ray determinations were made for plane and direction. The balls were locked on a stainless-steel holder similar to that described in reference 98. The orientations were then rechecked.

After the specimens were mounted in the vacuum system, the system was evacuated, and the tungsten disk specimen was electron bombarded for 4 hours to remove adsorbed gases and surface oxides. The disk temperature at this time was 500° C. The specimens were cooled to room temperature before friction experiments.

In working with various crystallographic planes, marked differences in oxidation rates do occur. Reference 99 shows this difference for tungsten. With repeated passes over the same track, these differences in oxidation rate could influence friction properties. The (100) surface of tungsten oxidizes more rapidly than the (111) and (110) surfaces.

Friction data for the (0001) plane, [1010] direction of sapphire sliding on the large grains of a tungsten disk specimen in a vacuum of

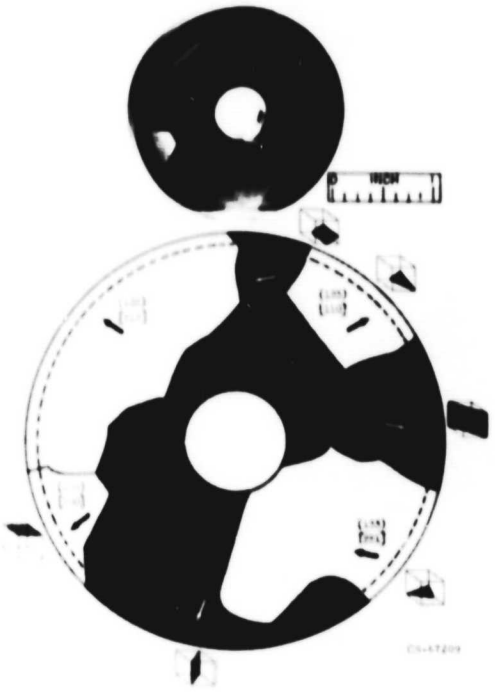

(a) Tungsten disk.

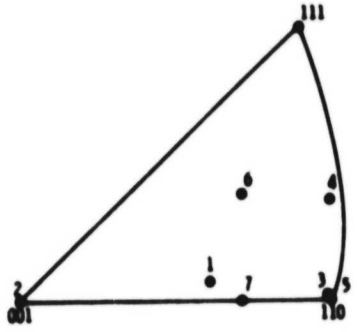

(b) Unit triangle.

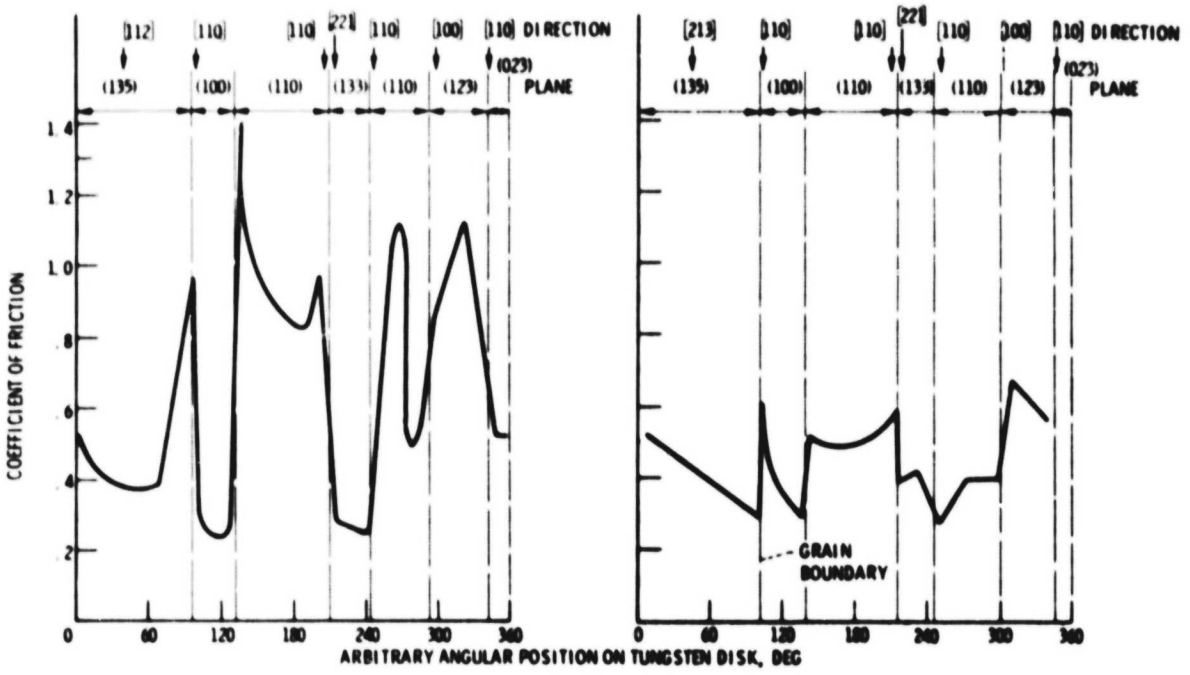

(c) In vacuum (10^{-10} torr).

(d) In air (760 torr).

Figure 66. - Coefficient of friction of sapphire ($10\bar{1}0$) plane sliding in [0001] direction on polycrystalline tungsten. Load, 500 grams; sliding velocity, 0.013 centimeter per second.

10^{-10} torr, a load of 500 grams, and speed of 0.013 centimeter per second are presented in figure 66(c). Light loads and low speeds were used to avoid high interface temperatures, which can cause surface recrystallization. The friction data are plotted as a function of arbitrary angular position. The crystallographic planes and the directions for each grain are indicated at the top of the figure and the position at which the grain boundaries in the tungsten disk surface were crossed by the sapphire slider are indicated by vertical lines.

The most obvious result of figure 66(c) is the marked change in friction properties with a change in slip systems in moving from one grain to another. Furthermore, on any particular plane a change in direction results in a change in friction.

The effect of plane on friction can be seen from an examination of friction on various planes in a particular crystallographic direction of figure 66(c). Changing direction on a particular plane does appreciably influence friction; for example, on the (100) plane moving from the [110] to the [100] direction gave a coefficient of friction of 1.23 while moving in the [100] direction decreased the coefficient to about 0.8. This difference is significant.

It is interesting to note that for the (100), (110), and (023) planes the maximum in friction is observed in the [110] direction. On both (110) planes, the maximum in friction (1.3 to 1.35) was in the [110] direction and a minimum (0.7 to 0.75) was about 45° to 50° from the [110] direction (fig. 66(c)).

Hardness measurements were made on the (100) plane of tungsten in two crystallographic directions, [100] and [110]. Hardness is lowest in the [110] direction and maximum in the [100] direction. When the friction data from the (100) plane of figure 66(c) are compared to the hardness data, a correlation between hardness and coefficient of friction is readily seen. An increase in hardness is accompanied by a decrease in friction coefficient. Figure 66(c) shows that for the (110) plane friction was high in the [110] direction and near the minimum in the [100].

Resolved shear-stress calculations and yield-strength data obtained from reference 100 were examined for the (110) plane in the body-centered-cubic system. If the shear stress to yield pressure relation is used, a maximum in friction should be anticipated at about 22.5° from either the [100] or the [110] direction. This probability could explain, in part, the pulses in friction noted between the [110] and the [100] direction. Hardness data obtained on the (110) plane in the [100] and [110] directions show a marked increase in hardness in the [100] direction over the hardness values obtained in the [110] direction. These results are in agreement with friction data and further indicate the anisotropic behavior of tungsten.

In vacuum, the adhesion of tungsten to sapphire can markedly influence the friction data obtained, because a thin transfer film of tungsten (to sapphire) could be sliding on itself. In air, however, an appreciable thickness of tungsten oxide is present, and this oxide inhibits metal transfer to sapphire and thereby reduces friction coefficients. Furthermore, various crystal planes of tungsten exhibit different oxidation rates, which could also influence the observed friction results.

A friction experiment was conducted in air with the sapphire (1010) plane sliding in the [0001] direction on the large-grain tungsten disk specimen. The results obtained are presented in figure 66(d). The most marked effect, as might be anticipated, is a general reduction in the friction coefficient on all crystallographic planes of tungsten. It is interesting to note, for example, that, on the (100) plane, the difference in friction between the [110] and [100] directions represents a change in friction coefficient from 0.6 to 0.3. For the same plane and in the same directions in vacuum with surfaces cleaned by electron bombardment, the friction decreased from 0.96 to 0.24. The friction in these two directions differed by a factor of 2 in air and 4 in vacuum; this indicates that the oxide plays a role other than a simple equivalent reduction of adhesion of the tungsten to sapphire in different crystallographic directions. A similar effect is noted for the (110) plane.

The friction characteristics observed in this investigation indicate a marked dependence of friction on crystallographic direction and orientation. With the aluminum oxide rider specimen sliding on the (100) plane of tungsten, a minimum in friction was noted when sliding in the [100] direction and a maximum when sliding in the [110] direction. Any examination of the (100) plane of the body-centered-cubic crystal indicates that the atomic density is greatest in the [100] direction and least in the [110] direction on the (100) plane. Hardness measurements also indicate this same dependence on direction.

Further evidence for possible dependence of friction coefficient on atomic density is gained from an examination of the friction data on the (110) planes in the [110] and [100] directions. On the (110) plane the coefficient of friction is greatest in the [110] direction and least in the [100] direction or approaching the [100] direction. Again in the body-centered-cubic system, atomic density would be least in the [110] direction and grestest in the [100] direction.

In summary, the tungsten studies reported herein indicate that marked changes were observed in friction characteristics as grain boundaries of tungsten were crossed. These changes are due to the changes in crystallographic slip systems in moving out of a grain, across the boundary, and into another grain.

Friction studies with metals other than tungsten also indicate a grain boundary effect. The effect is not only observed to influence friction but surface fracture and wear as well. Studies with a polycrystalline slider moving across a copper bicrystal (one grain the (111) and the other the (210) orientation) resulted in differences in friction not only on the surface of the grains but also in the grain boundary region as was observed with tungsten. This effect is shown by the data in figure 67.

In figure 67(a), in sliding from the (210) grain to the (111) grain, friction is higher on the (210) plane and in the grain boundary region than it is on the (111) plane. Grain boundary effects can be seen much more readily when sliding is initiated on the (111) surface as indicated in figure 67(b). There is a pronounced increase in the friction for the slider - grain boundary interface. The grain

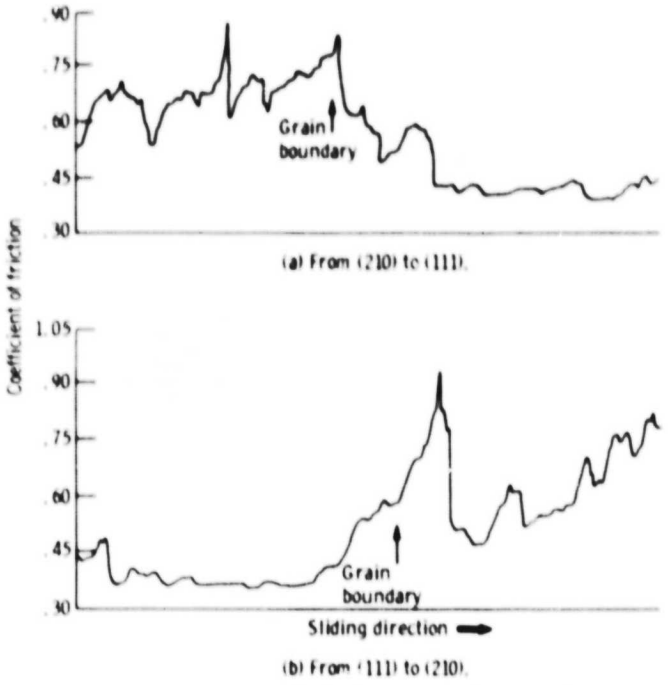

Figure 67. - Recorder tracings of friction force for copper slider sliding across grain boundary on copper bicrystal. Load, 100 grams; sliding speed, 1.4 millimeters per minute.

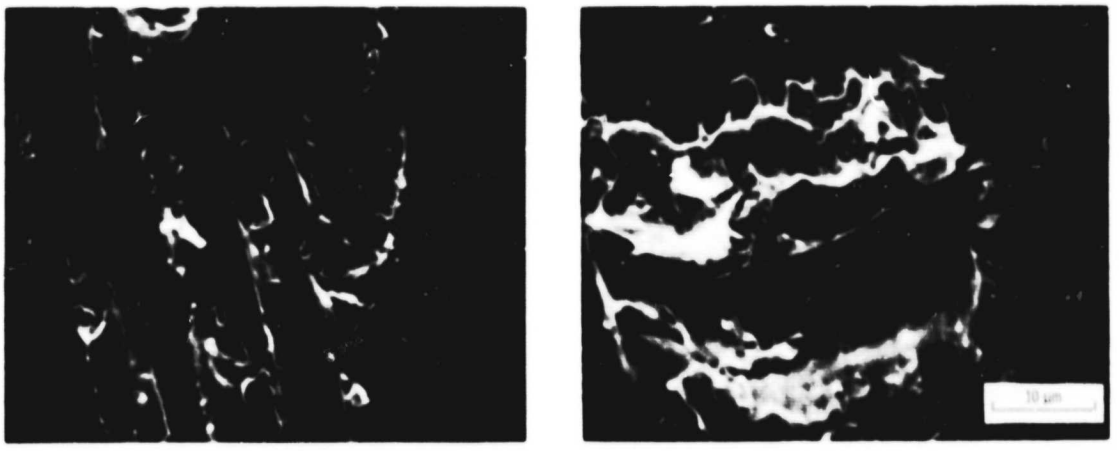

Figure 68. - Wear tracks on bicrystal grains. Copper slider; load, 100 grams; sliding speed, 1.4 millimeters per minute.

boundary is atomically less dense than the grain surfaces on either side of that boundary.

Examination with scanning electron microscopy of the (111) and (210) grain surfaces after sliding and a single pass of the slider across the surface revealed severe surface disturbance as a result of the contact as indicated by the micrographs in figure 68. The micrographs for contacted surface area on both grains are at the same magnification.

Fracture tracks are observed on both grain surfaces in figure 68. These cracks are surface initiated. The wear face of the cracks is extremely smooth, which indicates crack initiation along slip bands. As indicated in the micrographs, the cracks are much larger on the (210) surface than on the (111) surface. Sectioning the wear track and measuring the crack angle of orientation relative to the surface orientation indicate that the fracture cracks do form along slip bands in the copper grains.

A wake of metal just ahead of the fracture crack stands above the surface of the grain. This occurs for both grain surfaces, but again, the amount of metal standing above the surface is greater for the (210) than for the (111) grain.

The metal to metal interfacial adhesion mechanism responsible for the manifested friction behavior shown in figure 67 and the surface conditions shown in figure 68 can best be explained with the aid of figure 69. This figure schematically reveals the surface events.

When the copper slider is first brought into touch contact with either grain surface and a load is applied, deformation of surface asperities results in penetration of surface contaminating films and metal to metal interface formation with strong adhesive bonding. As tangential motion begins, fracture must occur in the weakest interfacial region. The weakest region is not at the interface but rather in the cohesive bonds between adjacent slip planes in the individual copper grains. Thus, with tangential force atomic bonds in the copper slip plane fracture, resulting in the formation of a surface initiated crack (fig. 69).

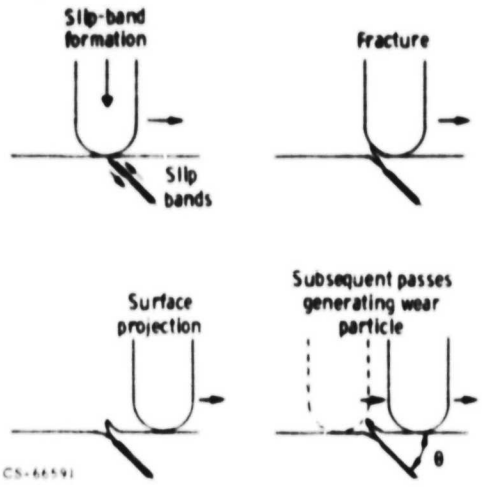

Figure 69. - Origin of surface fracture and formation of wear particle.

With a continued application of a tangential force, at some point the applied force is sufficient to exceed that of the interfacial slider to grain bond and fracture of that interfacial bonding occurs. The slider moves on until adhesion again occurs.

After the interfacial slider to grain bond has fractured, a wake or curl of metal remains above the plane of the grain surface (fig. 69). Subsequent passes result in shearing the test surface protuberance of metal with the resulting formation of a wear particle. Thus, for polycrystalline copper in contact with a single crystal (grain) of copper, the interface develops bonds which offer greater resistance to fracture than cohesive bonds along slip planes in the copper single crystal (grain).

ORIENTATION

Polycrystalline materials are used in most mechanical applications where adhesion, friction, and wear might be involved. This does not, however, necessarily preclude the use of materials in single-crystal form. It is certainly recognized that grain boundaries influence the behavior of materials, single-crystal observations cannot be extrapolated directly to polycrystalline materials. Grain boundaries influence deformation in a number of ways: they act as barriers to the motion of slip dislocations, they have higher surface energies than crystallite faces, and they are sites on the surface for accelerated reaction and diffusion rates as has been already discussed. The effect of boundaries can be more fully understood if the building block of polycrystalline structures - namely, the single crystal - is better understood. One of the first matters of consideration with single crystals is that of orientation. What effect, for example, does changing the crystallographic orientation at the surface have on adhesion and friction behavior? Single-crystal experiments were conducted to gain an insight into orientation effects on adhesion and friction behavior.

The term matched planes and directions is used herein to describe the relative orientations of crystal faces in adhesion and friction

experiments. It represents, in essence, the matching of the direction on one surface with that on another crystal face of the same orientation. All sliding friction experiments were conducted in the preferred crystallographic slip direction for the particular plane under consideration. Furthermore, where dissimilar metals were in contact, the greatest atomic density plane was used, even where differences in crystal structure existed.

In the initial adhesion experiments, a load was applied normal to the planar surfaces in contact. The adhesion coefficient is, then, the force required to separate the specimens divided by the applied force or load. The friction coefficients reported are all dynamic values obtained during sliding. After sliding was stopped, the force to separate the two crystal surfaces in contact was measured. This force divided by the applied load during contact sliding is termed adhesion* coefficient. The asterisk is used to differentiate this value from those obtained in standard adhesion measurements.

There are a number of terms that have been used in the literature, particularly in regard to friction, to describe solid solubility of metal couples. Therefore, to avoid confusion, the following terms are used herein: (1) complete solubility, (2) partial solubility, and (3) insolubility. Complete solubility characterizes those systems where the Hume-Rothery rules of electronegativity, valence, atomic size factor, and crystal structure are obeyed (100-percent solubility). An example of such a system is the copper-nickel of this investigation. Partial solubility refers to those systems where solubility may not cover the entire phase diagram (less than 100 percent). In these systems one or more of the Hume-Rothery rules may not be obeyed. The copper-cobalt system of this study is such a system. These metals differ in crystal structure below 400° C. Insoluble couples are those where no phase diagram exists and whose solubility, if any, is considered normally to be insignificant. In this investigation, the copper-tungsten couple represents such a system.

The cohesion of polycrystalline copper has been examined (refs. 101 to 103). The data reported in references 101 and 103 were

obtained in vacuum. Single-crystal-copper cohesion has been examined in a hydrogen atmosphere (refs. 104 and 105). The results obtained in hydrogen indicated that the friction coefficient for the (100) planes of copper in sliding contact exhibited markedly higher coefficients of friction than the (111) planes of copper in sliding contact.

Adhesion and friction coefficients were measured in vacuum at 10^{-11} torr for copper contacting copper. Three single-crystal orientations of copper were examined: The (100) plane contacting the (100) plane, the (110) plane contacting the (110) plane, and the (111) plane contacting the (111) plane. In all experiments the planes and directions were matched. In these experiments a load of 50 grams was used. This particular load was selected because earlier experiments showed that recrystallization of copper occurred in sliding contact at higher loads (ref. 106). For reference purposes, adhesion data were also obtained for polycrystalline copper. Examination of the data in column 3 of table VIII indicates that adhesion coefficients (breakaway load/applied load) of copper are dependent on crystal orientation. The highest atomic density (111) plane exhibits the lowest coefficient of adhesion.

It is of interest to note that adhesion coefficients decrease as the modulus of elasticity and the surface energies on these planes increase. The decrease in coefficient of adhesion with increase in elastic modulus might be related in part to differences in true contact area for the crystals at the interface. Since plastic deformation is also occurring at the interface, the deformation behavior of the different crystal orientations must be considered. An examination of stress-strain curves for single crystals of copper indicate that, for a given stress, the amount of strain for the (111) plane is less than that for the (110) and (100) orientations of copper. These effects would indicate that, for a given load, the true area of contact for the (111) orientation might be less than that for the (110) and (100) orientations.

The resulting contact area is the sum of elasticity and plasticity at the interface (ref. 13). The influence of elasticity and plasticity varies with orientation (ref. 107). Since the yield

point also varies with orientation, the amount of plastic shown for a given stress is greater for the (100) plane. The amount of elastic recovery for the (111) plane is greater; that is, the percent of elastic deformation to total deformation is greater for the denser (111) plane. It has been shown in reference 36 that, for metals such as gold and silver, a temperature 0.4 of that of the melting point must be reached before elastic recovery does not exert a noted influence on adhesion and the materials are plastic enough to insure strong adhesion.

Since two crystals of the same orientation are brought in contact under load, if atomic bonding occurs across the interface, then the interface may be considered to represent an interface that is analogous to a grain boundary. In these experiments all possible attempts were made to match planes and directions. In any such attempts it is assumed that some mismatch of orientations exists and that perfect matching occurs only accidently. Any bonding that occurs across the interface involves some elastic displacement of atoms near the surface. The interface then represents atomically displaced atoms connecting the individual crystals; that is, they represent a transitional region serving to link the two specimens much as in a grain boundary. The greater the mismatch, the further into the parent crystals elastic stress may be expected to occur.

An examination of the surface energies in table VIII, which are calculated values taken from reference 107, indicates that the surface energies are greatest on the (111) plane and least on the (100) plane. The adhesion data obtained would then appear to be in conflict with the surface energy theory of adhesion and friction (ref. 39). It should be indicated, however, that when two surfaces are brought into contact the interface formed has its own interfacial energy. This energy is analogous to the energies associated with grain boundaries. Each crystal surface has its own characteristic energy, and when two crystal surfaces are brought together an interfacial energy is developed. The energy of this interface depends to a large extent on the degree of mismatch of the two crystallites. The greater the mismatch, the greater the energy. For two crystals in contact, the

TABLE VIII. - VARIOUS PROPERTIES OF SINGLE-CRYSTAL AND POLYCRYSTALLINE COPPER (99.999 PERCENT)

Copper form and orientation	Young's modulus,[2] (10^{11} dynes/cm)	Surface energy, $\gamma_{hkl} = \frac{E_{hkl}}{\gamma_{hkl}}\left(\frac{a_o}{\pi}\right)^3$ [3]	Adhesion coefficient before sliding[a]	Coefficient of friction[b] during sliding	Adhesion coefficient after sliding[c]
Single-crystal (100) matched planes and directions	6.67	590	1.02	>40.0	>130
Single-crystal (110) matched planes and directions	13.1	820	.61	>40.0	50.0
Single-crystal (111) matched planes and directions	19.4	2980	.30	21.0	10.5
Polycrystal	12.0	1100 to 1350	1.00	>40.0	100

[a]Load, 50 g; 10^{-11} torr.
[b]Load, 50 g; sliding velocity, 0.001 cm/sec; 10^{-11} torr.
[c]Load, 50 g; distance slid in preferred slip directions, 0.735 cm; 10^{-11} torr.

boundary energy must be considered, since with adhesion a new interfacial surface is created.

Each adhesion coefficient value reported in column 3 of table VIII represents a 10-second contact time under load. At room temperature, diffusion effects may not be expected to greatly influence measured adhesion coefficients. At larger periods of time, with plastic materials such as metal, creep may be expected to influence this true contact area under a given load. The effect of contact time on the adhesion coefficient is shown in figure 70 for the three single-crystal orientations of copper. A marked increase in the coefficient of adhesion occurred with time. Thus, with single crystals of copper, creep at the interface (with a corresponding relaxation of elastic strains) appears to influence the measured adhesion coefficients.

The adhesion coefficient of table VIII (column 3) for polycrystalline copper is interesting. The adhesion value obtained was 1.00, or very near that of the (100) plane of copper. Since the modulus of elasticity is nearly twice that of the (100) plane and the data of reference 108 indicate that a polycrystalline material is more resistant to plastic deformation than single crystals, the real area of contact on load removal might be anticipated to be markedly less for polycrystalline material. However, while the area of contact under a given load may be less than that of the (100) plane, the tensile strength of junctions formed is greater. With deformation of polycrystals, grain boundaries act as barriers to the motion of slip plane dislocations, and a high degree of strain hardening of junctions formed must occur. This is even greater than that observed with single crystals oriented such that a high concentration of Lomer-Cottrell locks may be generated. Thus, while a smaller, true contact area may be anticipated for polycrystals for a given load, the tensile strength of junctions formed is greater than observed with single crystals. This may account for the similarity in the two adhesion coefficients.

After completing adhesion measurements, the crystals of table VIII were slid a distance of 0.735 centimeter and the friction

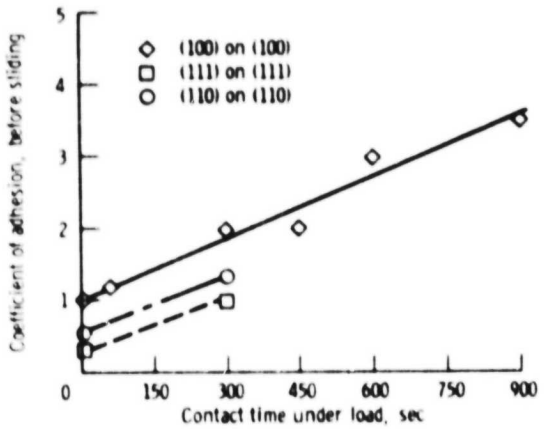

Figure 70. - Coefficient of adhesion before sliding for copper on copper with matched planes and directions in vacuum (10^{-11} torr). Simple touch contact under a 50-gram load.

coefficients observed during sliding are reported in table VIII (column 4). All the copper specimens exhibited friction coefficients in excess of 40.0 with the noted exception of the (111) plane, which had a friction coefficient of 21.0. Those specimens having friction coefficients in excess of 40.0 (the limit of the indicator) exceeded it in the first few tenths of a centimeter of sliding.

The coefficients of adhesion were again measured immediately after sliding. The measured coefficients of adhesion are also presented in table VIII (column 5). In all cases a drastic increase in the adhesion coefficient was observed after sliding. This increase may be attributed to two factors associated with the sliding of clean metals in contact. First, a marked increase in the true contact area occurs with sliding, and secondly, the area in contact represents metal that has work hardened in the process of sliding. Thus, not only has the area of contact increased with sliding but also the tensile strength of the junctions has increased.

The adhesion and friction coefficients observed in table VIII for polycrystalline copper are markedly greater than those observed in reference 109. Some explanation is, therefore, in order. In reference 119, the load employed was 1000 grams and the speed was 198 centimeters per second. At this high load and speed, recrystallization of copper at the interface is known to occur (ref. 106). Thus, the type and nature of the surface under the two sets of experimental conditions were markedly different at the higher loads and speeds. At the higher loads and speeds of the study reported herein, however, such effects were not noted. It is quite natural, therefore, to expect differences in the friction and adhesion results when the interface is different.

The results of table VIII indicate that differences in the adhesion coefficients exist for different crystallographic planes of copper. Furthermore, the results show that sliding markedly increases the adhesion of two surfaces in contact. The only friction coefficient that could be measured was that for the (111) plane, the orientation exhibiting the lowest adhesion coefficient. If the others could have been measured, a correlation of friction with orientation

might have been observed as was the correlation of adhesion with orientation.

Adhesion and friction measurements were made with the (100), (110), and (111) planes contacting a (100) plane. In all three experiments, sliding was in the [110] direction. The results obtained are presented in table IX. The data indicate, as might be anticipated, that pairs of matched planes exhibit higher adhesion coefficients before sliding than do pairs of unmatched planes across the interface or boundary differ. In all three experiments, the friction coefficient during sliding was in excess of 40.0.

A subject of much interest, related to adhesion and orientation, is that of the relative importance of solid solubility (refs. 103, 110, and 111) and crystal structure (ref. 103) on the adhesion of metal couples. Four experiments were selected to determine the influence of solubility and crystal structure on adhesion and friction. In all of these experiments the (111) plane of copper was the rider surface. The results of the cohesion experiments for (111) copper on (111) copper represent the first set of results as they were presented in table VIII. The second set of experiments represent the (111) of copper on the (111) of nickel with sliding in the preferred slip direction. Both nickel and copper have a face-centered-cubic structure and are completely soluble (100 percent).

The data of table X indicate that the adhesive forces of copper to nickel are less than the cohesive forces of copper to copper. The sliding friction coefficient was also less. These results might be anticipated since a difference (2 percent) in lattice parameters for the two crystal faces exists. Therefore, bonding across the interface could be expected to involve considerably more lattice strain than for matched copper poles.

The third set of experiments involved the contact of the (111) plane of copper on the (0001) basal plane of cobalt. Sliding was in the [1120] direction on cobalt. It is interesting to note that while cobalt is next to nickel in the periodic table and many of its properties are similar, they differ in crystal structure. Cobalt and copper are partially soluble. An examination of the data in table X

TABLE IX. - COEFFICIENTS OF ADHESION AND FRICTION FOR VARIOUS SINGLE-CRYSTAL ORIENTATIONS OF COPPER

(10^{-11} torr; 20° C; 50 g)

Matched planes	Adhesion coefficient before sliding	Coefficient of friction[a] during sliding	Adhesion coefficient after sliding
(100)/(100)	1.02	>40.0	>130
(110)/(100)	.25	↓	32.5
(111)/(100)	.20		40.0

[a]Sliding velocity, 0.001 cm/sec; [110] direction, sliding distance, 0.735 cm.

TABLE X. - COEFFICIENT OF ADHESION AND FRICTION FOR VARIOUS SINGLE-CRYSTAL METAL COUPLES IN VACUUM (10^{-11} torr; 50 g)

Metal couples and orientations	Adhesion before sliding	Friction coefficient[a] during sliding	Adhesion coefficient after sliding	Soluable	Crystal structures
$\frac{Cu(111)}{Cu(111)}$	0.30	21.0	10.5	S	$\frac{F.C.C.}{F.C.C.}$
$\frac{Cu(111)[110]}{Ni(111)[110]}$	.25	4.0	2.0	S	$\frac{F.C.C.}{F.C.C.}$
$\frac{Cu(111)[110]}{Co(0001)[1120]}$	.10	2.00	.5	S	$\frac{F.C.C.}{Hex}$
$\frac{Cu(111)[110]}{W(110)[111]}$	<0.05	1.40	.5	INS	$\frac{F.C.C.}{F.C.C.}$

[a]Sliding velocity, 0.001 cm/sec; sliding distance, 0.735 cm.

indicates that, while both cobalt and nickel are soluble in copper, significantly lower friction and adhesion were obtained with copper contacting cobalt that has only partial solubility. This difference may be related in part to crystal structure. Copper and tungsten are insoluble and therefore adhesion of copper to tungsten should not occur. Experiments were conducted to determine if adhesion would occur and what effect sliding has on adhesion. The results are presented in table X.

In table X the initial coefficient of adhesion for copper to tungsten was less than 0.05 - that is, less than that which could be detected with the system. With sliding, the friction coefficient was 1.40 and was relatively constant over the entire sliding period.

With copper contacting tungsten, a continuous decrease in adhesion coefficient was observed with subsequent breaks. This decrease reflects the nature of the interfacial bond. The work of reference 112 indicates a possible surface interaction in vacuum with copper contacting the (110) face of tungsten.

TEXTURING

The mechanical processing of metal surfaces results most frequently in the development of texturing (preferred orientation of grains) in the superficial layer. The preferred orientations or surface textures that develop depend greatly on the method of mechanical finishing. For example, with a particular metal or alloy, rolling may give a different texture than forging. Even if a surface does not exhibit texturing on components prior to their use in lubrication systems, the sliding, rubbing, or rolling process involved in these systems can cause the development of surface textures.

A limited amount of research has been conducted to determine the influence of texturing on friction and wear and the role played in the dynamic contact of lubrication system components in the development of textures. Wilman and coworkers (refs. 113 and 114) examined the development of textures during abrasion. More recently, the texturing of cobalt and cobalt alloys has been examined during the rubbing

process (ref. 115). A systematic study is, however, still lacking. A study was therefore conducted to determine the influence of sliding on the development of surface textures in elemental metals. Three metals were selected for study as representatives of each of the major crystal systems in which alloys used in lubrication systems are generally found. Iron was selected as representative of body-centered-cubic metal behavior, copper and nickel as representative of the face-centered-cubic system, and cobalt as the close-packed-hexagonal representative. Friction experiments in dry sliding were conducted with each metal sliding on itself. Wear surfaces were then examined by X-ray analysis to determine the degree and type of texturing.

The copper disk and rider specimens used were 99.998-percent copper. The iron specimens were prepared from 99.95-percent iron. Cobalt disks and riders were prepared from 99.9+-percent cobalt. The nickel was 99.99 percent pure.

The disk specimens were prepared by lapping, diamond polishing, and finishing with 0.3 micrometer of alumina. The riders were given a 0.475-centimeter radius and then finished with 240, 320, 400 and 600 grit metallurgical papers. They were finally polished with 3.0 micrometers of alumina.

The friction experiments were conducted in a typical pin on disk friction apparatus such as that shown in figure 71. The basic components of the apparatus are a 6.25-centimeter disk specimen (1.2 cm thick) and a rider specimen with a 0.475-centimeter radius. The disk specimen is rotated by a variable speed electric motor. Speed can be varied from 300 to 5250 centimeters per minute. The rider specimen is contained in an arm which has incorporated in it a strain-gage assembly for recording friction force. The rider is dead-weight loaded against the disk. The disk and rider were of the same materials in each experiment.

The apparatus is covered with a clear plastic box in which a positive argon pressure can be maintained. While the argon purge was not intended to exclude oxygen and water vapor totally, it was

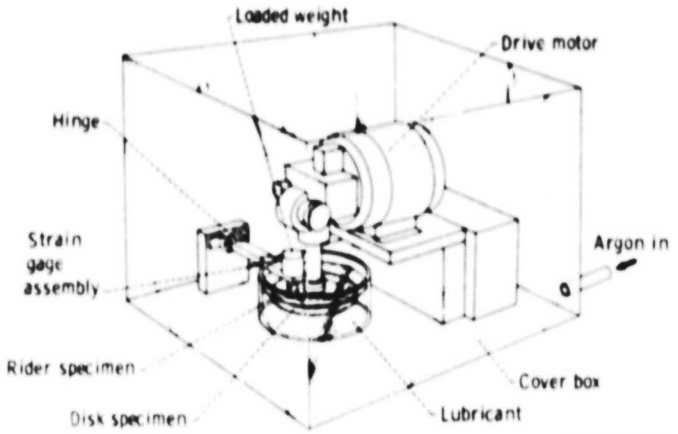

Figure 71. - Friction apparatus.

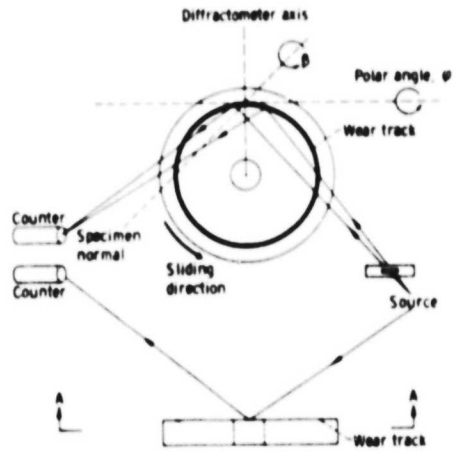

Figure 72. - X-ray examination of disk specimen after sliding.

intended to minimize the concentration of these gases and to maintain a relatively constant environment from experiment to experiment.

The X-ray instrument contained a chromium targeted tube. Radiation was filtered with a vanadium oxide film. Samples (disk specimens) were mounted in a special jig on a standard goniometer base in an orienter goniostat. The sample could be manually rotated about its own axis while counts were taken so that the intensities are averages over a number of equally spaced points around the disk.

A pin hole collimator was used because the wear track was normally only a few millimeters wide. The medium resolution (MR) soller slits were used at the detector, but no vertical slit was used; the entire filter mounting fixture was removed to give the widest possible angle of acceptance at the detector.

The schematic arrangement of the X-ray beam relative to the disk is shown in figure 72. The primary beam (source) is directed into the wear track. The reflected beam is collected with a counter. The wear track can be tilted in two directions (ϕ and β) as indicated in figure 72. The texture of the wear surface can be determined by rotating in the ϕ- and β-directions.

With the sample properly aligned, a randomly oriented, lapped copper disk specimen gave a (111) intensity that decreased by less than 10 percent as the disk was tilted 60° from the normal (vertical) position. This was done to show that the specimens prior to sliding were truly randomly oriented.

Sliding friction experiments were conducted in argon with copper sliding on copper at three different loads of the rider against the disk. The sliding velocity was 5.18 centimeters per second, and sliding continued until the rider had achieved 1000 passes against the disk surface. The resulting wear tracks generated on the copper disk surface were then examined with X-ray analysis. The (111) plane intensity is plotted as a function of polar angle (its position relative to the sliding direction) in figure 73.

An examination of figure 73 indicates that the maximum (111) intensity is achieved when the polar angle ϕ is nearly normal. This

indicates that, as a result of sliding, texturing of the initially random oriented surface layers has occurred. Figure 73 in combination with the pole figure (polar plot) of figure 74 established that the (111) planes or preferred slip planes in the face-centered-cubic metal copper are oriented nearly parallel (within 10°) to the sliding direction with the tilt of the planes in the direction of sliding. The elongation of the contours perpendicular to the sliding direction is a consequence of curvature across the width of the wear trace and scoring of one wear trace. Such irregularities produce a rotation of the (111) about an axis parallel to the sliding direction.

In figure 74 the small circle in the upper half of the pole figure indicates maximum (111) intensities. The fact that the small circle is not in the center of the pole figure indicates that the (111) orientation is tilted out of normal to the sliding direction. Its position in the upper half of the pole figure is 10°. The dashed line indicates the area scanned.

The data of figure 73 obtained at three different loads indicate that the kind and degree of texturing is the same at all three loads investigated. The data points for all three load conditions can be plotted on a single curve. A curve obtained in an experiment conducted at a 50-gram load showed significantly less texture, but the wear track was very narrow. This indicates that the X-ray beam may have sampled regions on either side of the wear track, and this could have affected the results.

The (111) planes in copper, being the highest atomic density planes, have the lowest surface energy. Also, since the distance between these planes is great, easy slip and shear result. It would, therefore, be anticipated that the orientation of these planes near parallel to the sliding direction would result in a minimum in friction. Friction experiments substantiate this (refs. 116 and 16).

To determine if surface films (oxides and adsorbed layers) exert an influence on the texturing behavior of copper, sliding experiments were conducted in air. The results of these experiments were compared to those obtained in argon. In figure 75, the data point obtained in air at 1000 passes coincides with the one obtained in argon, which

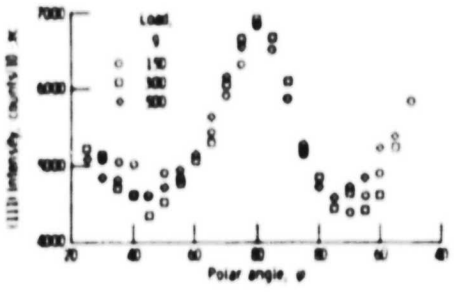

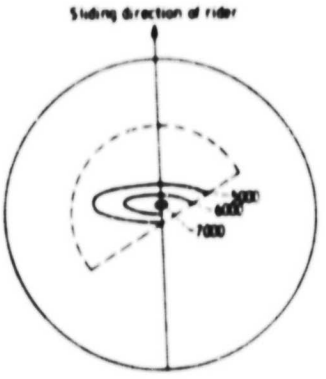

Figure 73. - X-ray analysis of copper wear track (111) intensity as function of polar angle ϕ. Copper sliding on copper in argon at three loads; total of 1000 passes at sliding speed of 5.18 centimeters per second and ambient temperature of 23° C; specimen rotated relative to sliding direction.

Figure 74. - X-ray (111) pole figure for surface texture developed on copper disk surface as result of sliding. Sliding continued for total of 1000 passes at sliding velocity of 5.18 centimeters per second; load, 200 grams; ambient temperature, 23° C. Solid lines are texture contours; numbers are counts per 19 seconds; dashed lines represent boundary of projected area which was scanned.

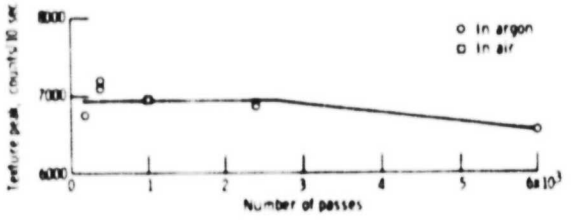

Figure 75. - Texture peak intensity in copper wear track as function of number of passes across surface in both air and argon. Sliding velocity, 5.18 centimeters per second; load, 300 grams; ambient temperature, 23° C.

indicates that the absence of oxygen to replenish worn away surface oxides does not affect the texturing of copper. This result may be due to the relatively weak nature of the copper oxide.

The effect of repeated passes over the same surface on the texturing of copper in argon is also demonstrated by the data in figure 75. At repeated passes to 2400, there appears to be very little influence of the number of passes on texturing. At 6000 passes, a slight decrease in the degree of surface texture appears to have occurred. This slight decrease may be due to surface recrystallization resulting from frictional heating.

To determine if, in fact, recrystallization were occurring, some copper disk specimens were annealed after sliding. Annealing at 400° C for 1 1/2 hours is sufficient for recrystallization of copper (ref. 117).

One disk was annealed after sliding for 400 passes. The before annealing curve was virtually the same as the curves of figure 73, indicating that the texture is fully developed. After annealing, the height of the texture peak relative to its minima decreased in a way identical to the decrease that occurred after 6000 passes.

Another disk was annealed after sliding for 6000 passes. In this case, annealing produced no change in the height of the texture peak relative to its minima.

The results of this study show that the fully developed texture in copper is reduced by sliding in the same way that it is reduced by recrystallization and that once it has been reduced by sliding no further decrease occurs on annealing. This is consistent with the hypothesis that extended sliding results in recrystallization.

With iron, a body-centered-cubic metal, not only the preferred plane but the slip direction can be identified. The triangular symbols in figure 76 indicate where peaks would occur if the sample were a single crystal with its (110) face parallel to the surface and its (111) direction in the sliding direction. Except for the 10° tilt in the direction of sliding, the wear surface has this texture.

Experimental results with copper indicated that the environment exerted essentially no influence on texture results up to 1000

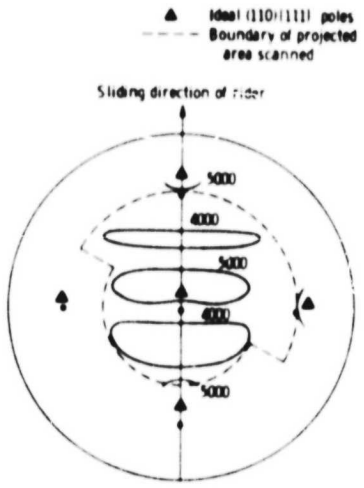

Figure 76. - X-ray pole figure for iron wear track after 1200 passes of iron rider over iron disk surface. Sliding velocity, 5.18 centimeters per second; load, 500 grams; in air at 23° C.

passes. Similar environmental determinations were made for iron as were made for copper. Friction experimental results obtained in an argon environment are compared with experimental results obtained in air in figure 77.

Figure 77 shows a plot of the (110) texture peak intensities as a function of the number of passes. In air the degree of texturing developed with sliding is greater than that observed in argon. The reduction of oxygen and water vapor results in less texturing in all probability because of a lack of replenishment of residual surface oxide. As the residual surface oxide is worn away in argon, it is not replaced, and the amount of adhesion and adhesive transfer increases. With adhesive transfer, large particles are removed from the disk surface. Subsurface fracture must occur to give rise to the generation of these particles. Thus, if orientation subsurface is random, this random orientation is exposed to the X-ray beam decreasing the total amount of texture observed. The net effect is a decrease in peak intensity.

It would appear that the aforementioned hypothesis is supported by the data in figure 77. In this figure the texture (110) peak intensity decreases with an increase in the number of passes in argon. In air this decrease is not observed.

Goddard et al. (ref. 114) observed the development of a basal texture (0001) on the surface of cobalt, a close-packed-hexagonal metal, in sliding friction studies. This is the texture which might be anticipated. In the present investigation, texturing was not observed in cobalt in repeated sliding experiments. It must be indicated that the loads employed in this study were considerably less than those obtained by Goddard et al. (ref. 114). Since there are notably fewer slip systems in the hexagonal metals (such as cobalt) than in the cubic metals, texturing could be expected to be very sensitive to load and more likely to occur at higher loads.

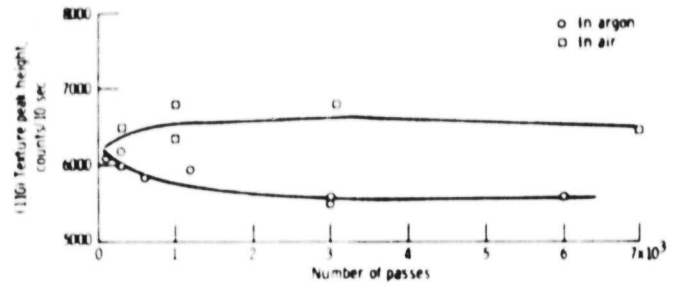

Figure 77. - X-ray (110) texture peak height as function of number of passes of rider across disk in air and argon. Sliding velocity, 5.18 centimeters per second; load, 500 grams; temperature, 23° C.

RECRYSTALLIZATION

Polycrystalline materials are aggregates of individual crystallites. The grain boundaries serve as atomic bridges to link the lattice of one crystallite with that of an adjacent crystallite. The greater the mismatch in adjacent orientations, the greater the number of atoms serving to link the two orientations. Grain boundaries in addition to having Read-Shockley dislocations of their own serve as a barrier to the motion of dislocations of the crystallites. Such a structure could be expected to offer greater resistance to shear and higher friction coefficients than single crystals.

Data obtained for single and polycrystalline iron at various loads in sliding contact with polycrystalline aluminum oxide are presented in figure 78. Aluminum oxide was selected as a mating surface because adhesion of the iron to aluminum oxide occurs with shear subsequently taking place in the iron. The results indicate marked differences in friction for the two forms of iron. As load is increased, the interface temperature increases and recrystallization occurs on the iron surface. This condition represents an increase in friction for the single crystal. Although the surface at the interface is textured, it contains grain boundaries which act as barriers to dislocation motion. It represents a decrease in friction for the polycrystalline metal because recrystallization is followed by texturing, which reduces shear stress. At higher loads the friction coefficients should be the same because the interfacial surface films are the same.

Similar results to those obtained with iron were obtained with the body-centered-cubic, face-centered-cubic, and close-packed-hexagonal metals. In general, recrystallization in the process of sliding occurs at relatively modest conditions of load and speed. The sliding velocity in figure 79 was only 0.001 centimeter per second. The only means used to provide changes in interface frictional energy was that of changing load. At a load of 3500 grams, recrystallization of a metal such as tungsten could be achieved with relative ease,

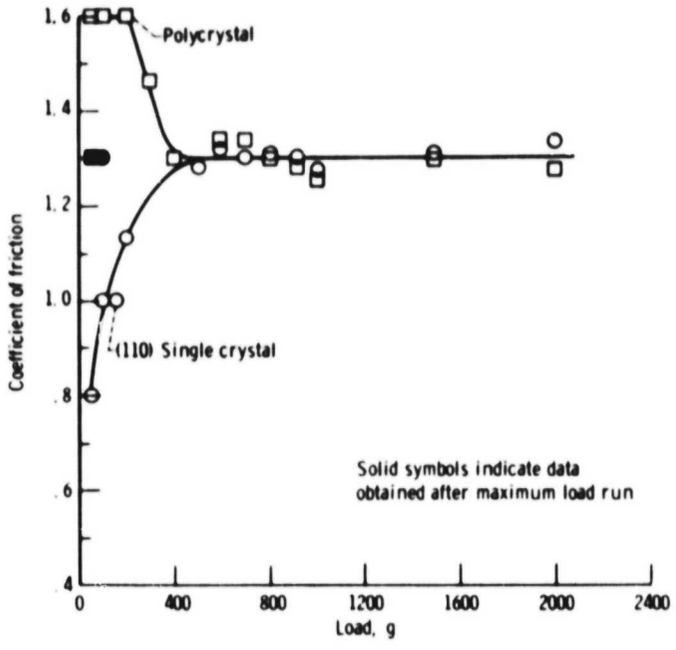

Figure 78. - Effect of load on friction for iron sliding on polycrystalline aluminum oxide in vacuum (10^{-11} torr; 1.33×10^{-9} N/m^2). Sliding velocity, 0.001 centimeter per second; no external specimen heating.

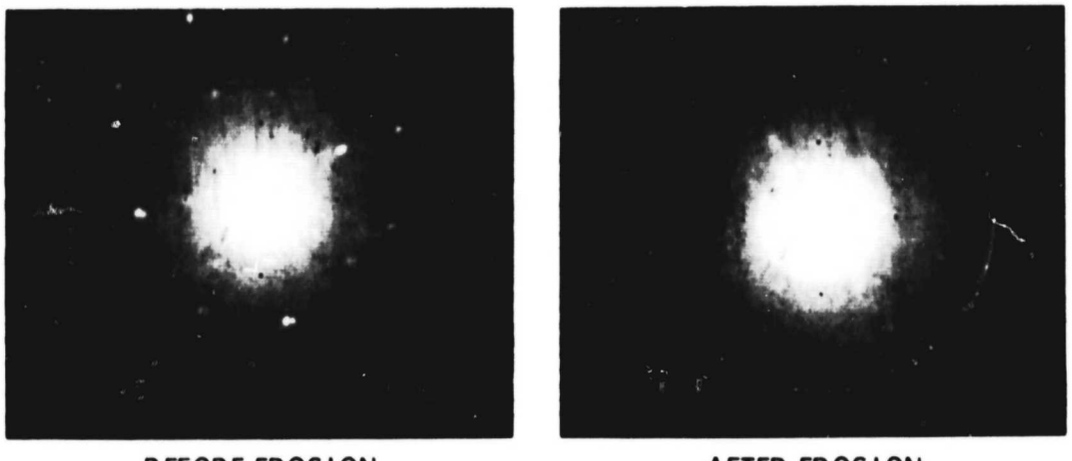

BEFORE EROSION AFTER EROSION

CS-81-1625

Figure 79. - X-ray diffraction pattern obtained from (110) aluminum single crystal before and after erosion.

indicating the extreme amount of energy involved in the sliding friction process.

The recrystallization temperatures of metals are markedly dependent on the amount of prior deformation that occurred for the metals. Severe deformation of metals can readily reduce the recrystallization temperatures by 60 percent. To gain some insight into a possible correlation between recrystallization temperatures for metals and their sliding friction behavior, the recrystallization temperature obtained for various metals from the literature together with friction coefficients obtained in the sliding friction studies are presented in table XI.

Table XI gives approximate recrystallization temperatures for the various metals examined in this investigation as well as those of titanium (examined in ref. 118). The approximate load at which the friction was equivalent for the single-crystal and the polycrystalline metallic forms of each of the various metals correlates with the recrystallization temperatures for these metals; that is, the higher the recrystallization temperature, the greater the load necessary to achieve surface recrystallization and to produce a marked change in friction properties. These results are extemely interesting in light of the fact that marked differences exist in the thermal conductivity characteristics of the various metals and in their abilities to deform.

It is well known that heat dissipation at the sliding interface is extremely important in the removal of frictional heat generated in the process of sliding. It might be anticipated that good thermal conductivity metals, such as copper, would exhibit a greater tendency to carry away frictional heat from the sliding interface. This then results in a higher load required for recrystallization than for a metal, such as nickel, which does not have the good thermal conduction characteristics of copper. An examination of table XI indicates that, while a 250° C temperature difference exists in the recrystallization temperatures for these two metals, a difference of only 100 grams in load necessary for recrystallization exists. This difference indicates that the loads for recrystallization are closer than might

TABLE XI. - RECRYSTALLIZATION TEMPERATURES AND LOADS AT WHICH EQUIVALENT FRICTION COEFFICIENTS WERE OBTAINED FOR SINGLE-CRYSTAL AND POLYCRYSTALLINE METALS

Metal	Experimental load at which friction is approximately equivalent for single-crystal and polycrystalline metal, g	Approximate[a] recrystallization temperature, °C
Copper	200	100
Nickel	300	350
Iron	400	450
Titanium	500	700
Beryllium	3500	900
Tungsten	3500	1200

[a]These temperatures from references 118, 119, and 120 are only approximate because amount of deformation influences these values.

be anticipated from the marked difference in recrystallization temperatures. Tungsten has a recrystallization temperature of approximately 1200° C. At 3500 grams recrystallization was the same for the three forms of tungsten. Beryllium has a recrystallization temperature of 900° C. The sameness in friction and load for producing recrystallization in sliding friction and the difference in recrystallization temperature between beryllium and tungsten may be accounted for by the differences in crystal structure for beryllium and tungsten. Single-crystal beryllium has a markedly lower tendency to work harden than tungsten (ref. 119). A lesser tendency to work harden influences recrystallization in metals (ref. 120). Furthermore, differences in friction coefficients for the two metals are accompanied by differences in the heat generated at the interface.

From the results obtained in many sliding friction experiments, recrystallization and texturing must be considered in interpretation of friction data. The recrystallization and texturing process markedly influences the friction properties for metals in sliding contact.

Marked differences exist in the friction characteristics for single-crystal and polycrystalline forms of metals, with the single-crystal forms exhibiting lower friction coefficients in every case. These results seem to indicate that large-grained structures might exhibit lower friction than fine-grained metallic structures. With recrystallization and texturing, the friction coefficients become essentially the same for polycrystalline and single-crystal forms of the same metal.

This recrystallization of metal surfaces was also demonstrated by the erosion behavior of aluminum single crystals. With erosion, there is not the rubbing of surfaces under load, but there is the transmission of energy by solid particles impinging a surface. Three aluminum single-crystal samples with three different orientations, (100), (110) and (111), were prepared from the same stock and then erosion tested for 2 minutes. It might have been expected that the different atomic planes with different atomic densities and cohesive forces would cause different erosion resistances. However, the

results listed in table XII clearly show that the erosion rate is the same, within experimental error, for all three orientations. This is due to the formation of a deformed recrystallized surface layer with which the erodant particles interact and which is identical for all the three crystals. The existence of such a deformed recrystallized layer is demonstrated by the X-ray back-reflection photographs obtained from the (110) sample before and after erosion (fig. 79). The impact of the eroding particles resulted in the destruction of the surface microstructure and the transformation to a polycrystalline surface as a result of recrystallization. The energy of the impacting particles is sufficient to cause recrystallization. Thus, all crystal surfaces are essentially polycrystalline and therefore give the same erosion resistance.

CRYSTAL STRUCTURE

The effect of crystal structure on the frictional behavior of metals can be seen by comparing two metals that are quite similar in physical and chemical properties because of their relative positions in the periodic table of elements. Two such elements are rhodium and ruthenium, atomic numbers 45 and 44, respectively. Their basic properties are similar, but they differ in crystal structure: rhodium has a face-centered-cubic structure, and ruthenium a close-packed-hexagonal structure. The difference in their friction properties is shown in figure 80. Polycrystalline rhodium, when sliding on itself in vacuum, has a very high friction coefficient and pronounced stick-slip motion as indicated by the cross-hatched area of figure 80 (representing the extremes in values obtained). In contrast to rhodium, ruthenium exhibits a markedly lower friction coefficient which remains relatively unchanged at temperatures to 500° C (fig. 80).

Similar differences in friction behavior have been noted with the Group VIII elements iridium (atomic number 77) and osmium (atomic number 76). Osmium, a close-packed-hexagonal metal, exhibits lower friction than iridium, a face-centered-cubic element.

TABLE XII. - EROSION OF ALUMINUM

SINGLE CRYSTALS

Orientation	Weight loss on a 2-min erosion test, g
(100)	0.0120
(110)	.0115
(111)	.0118

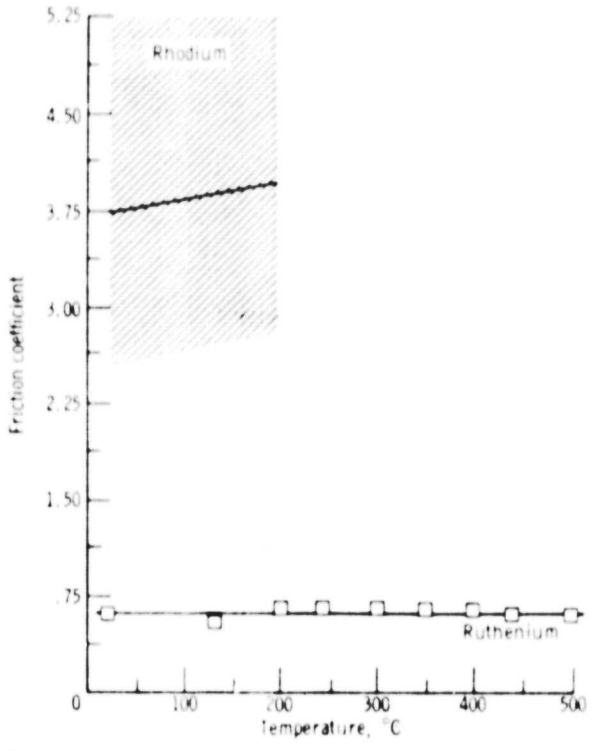

Figure 80. - Coefficient of friction for rhodium and ruthenium sliding on themselves in vacuum (10^{-11} torr). Sliding velocity, 0.001 centimeter per second; load, 100 grams.

Since the crystal structure of a material appears to influence friction behavior, then a metal which is allotropic should reflect in friction results the effect of crystal transformation. Friction studies with cobalt show that it does. The data in figure 81 are for polycrystalline cobalt sliding on itself in vacuum at various temperatures. The crystal structure of cobalt at room temperature is close packed hexagonal. It transforms a face-centered-cubic structure at 417° C. The data in figure 81 indicate that the friction coefficient is low (0.36) at temperatures up to 320° C at which point the friction begins to increase markedly until, at 550° C, complete welding of the specimens has occurred. If the weld at the interface is broken and the specimens cooled to room temperature, the friction returns to near the original value (fig. 81).

Wear is also influenced markedly by the crystal structure of cobalt. In the hexagonal form below 320° C (fig. 80) the wear is 100 times less than that at 400° C when crystal transformation to the face-centered-cubic form has occurred. The wear is adhesive in nature.

Tin is used in the field of lubrication to reduce friction and wear in mechanical components. It is employed as a thin surface film because of its low shear strength (ref. 121). It also has been used in alloys for bearings for over 50 years (refs. 122 to 124). For example, babbitt-metal bearing linings are frequently tin-base alloys. These materials must frequently operate over a broad temperature range. Depsite the extensive use of tin in lubrication, very little fundamental research has been conducted relative to the influence of various physical properties on the friction and wear of tin.

Tin is polymorphic. It exists as the so-called gray tin at temperatures below 13° C and as white tin above this temperature (ref. 125). Gray tin has a diamond type of crystal structure with each tin atom tetrahedrally coordinated by four other tin atoms. White tin has a body-centered-tetragonal structure and appears as a distorted diamond structure. The bonding of a tin atom is to four of its neighbors at the corners of a flattened tetrahedron. Gray tin has a more symmetrical structure than white tin. This difference is

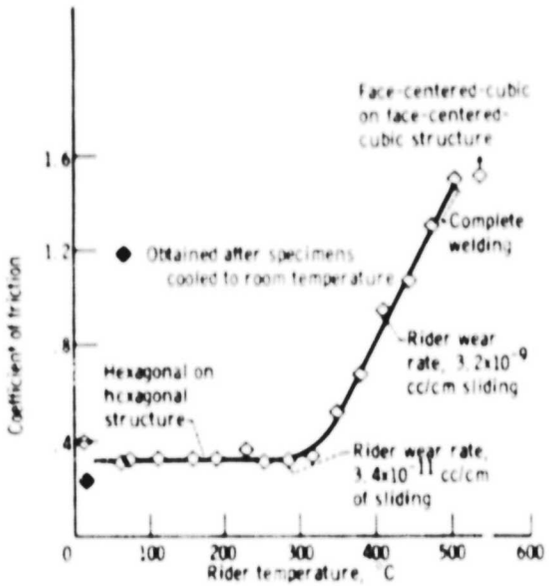

Figure 81. - Coefficient of friction at various ambient temperatures for cobalt sliding on cobalt in vacuum (10^{-9} to 10^{-7} torr). Sliding velocity, 197 centimeters per second; load, 400 grams.

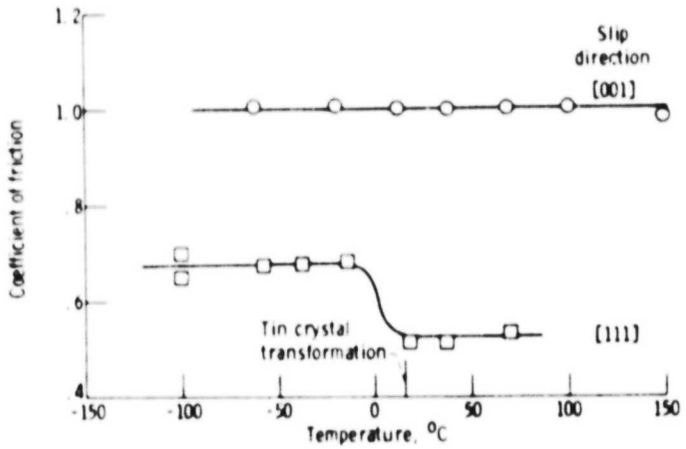

Figure 82. - Coefficient of friction for iron (110) sliding on tin (110) single-crystal surface. Sliding velocity, 0.7 millimeter per minute; load, 10 grams; pressure, 10^{-8} newton per square meter (10^{-10} torr).

thought to be due to an electron-zone overlap present in white tin which does not exist in the more symmetrical gray tin (ref. 126).

Gray tin atoms can be pictured as stacking sheets composed of continuously linked, "puckered" hexagonal rings of tin atoms parallel to the (111) planes of the crystal. Shear takes place along these planes.

White tin, with its tetragonal structure, slips on (110) planes in the [001] direction at low temperatures. At higher temperatures, slip takes place on the (110) planes, but the direction [111] is the preferred slip direction (ref. 127). The critical resolved shear stress necessary for slip in white tin (110) [001] is less than that for nickel. It is, however, greater than that necessary to initiate slip in the noble metals copper, silver, and gold (ref. 128).

With respect to strain hardening (below the recrystallization temperature), tin behaves more like the hexagonal metals (such as cadmium) than like the face-centered-cubic metals, which strain harden very readily. For both the (100) and (110) orientations of tin, crystals can be strained as much as 500 percent with only about a factor of 2 increase in shear stress. Face-centered-cubic metals (such as copper) experience a factor of 500 increase in shear stress with as little as a 50-percent increase in strain (ref. 127).

The friction coefficient as a function of temperature was measured with sliding in two crystallographic directions on the tin (110) crystal surface. Experiments were started at the higher temperatures because of the possibility that recrystallization would occur with the cooling of the crystals below the crystal transformation at 13° C. The results obtained are presented in figure 82.

An examination of figure 82 indicates that when sliding was in the [001], or low-temperature-preferred, slip direction essentially no change in friction coefficient was detected over the temperature range of 150° to -100° C. Thus, the transformation had no effect on the friction coefficient when sliding was in the [001] direction.

When sliding was initiated in the [111], or high-temperature-preferred, slip direction, the friction coefficient was markedly less

than was observed in the [001] slip direction at all temperatures. An increase in friction coefficient was observed when reducing the temperature beyond the crystal transformation at 13° C. Thus, friction was sensitive to the transformation when sliding was in the [111] direction.

A recrystallization of the tin crystals was anticipated with passage through the crystal transformation at 13° C. With repeated experiments, no evidence of recrystallization with transformation was observed.

It is of interest to note in figure 82 that the friction coefficient for the body-centered-tetragonal structure of tin was lower than that observed for the diamond structure. The opposite result was anticipated. Adhesive bonding of tin to iron occurred for both crystalline forms. With sliding, however, shear was more effectively accomplished with the body-centered-tetragonal structure. Thus, shear strength and resistance to shear were less for the tetragonal structure. Furthermore, the (110) plane of tin is the preferred slip plane with [001] and [111] being the preferred slip directions. Thus, shear resistance is at a minimum for these orientations (ref. 128).

The width of the wear track generated on the tin crystal surface varied with load and temperature. The variation of wear track width with load at -100° C is presented in figure 83. As the load was increased, the track widened. For a 50-gram load the wear track width was more than twice as wide as it was for a 10-gram load.

The variation of track width with changes in temperature is presented in figure 84. At a fixed load of 10 grams, there was no marked change in track width with temperature from -100° to 15° C. Above 15° C, which was above the crystal transformation temperature, the track width increased linearly with temperature. Below the transformation temperature, tin is a semiconductor and relative brittle. Thus, changes in temperature are not expected to exert much influence on surface deformation. Above the transformation temperature, however, tin is a metal and ductile and deforms with load

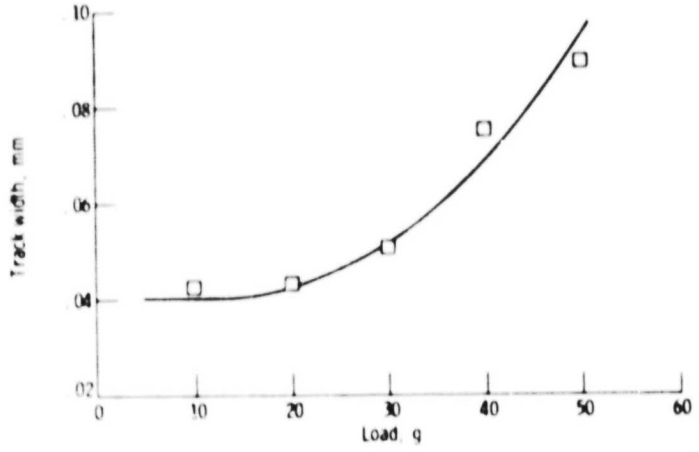

Figure 83. - Track width on tin single-crystal surface as function of load. Sliding velocity, 0.7 millimeter per minute; pressure, 10^{-8} newton per square meter (10^{-10} torr); temperature, -100° C; rider, iron (110); single pass.

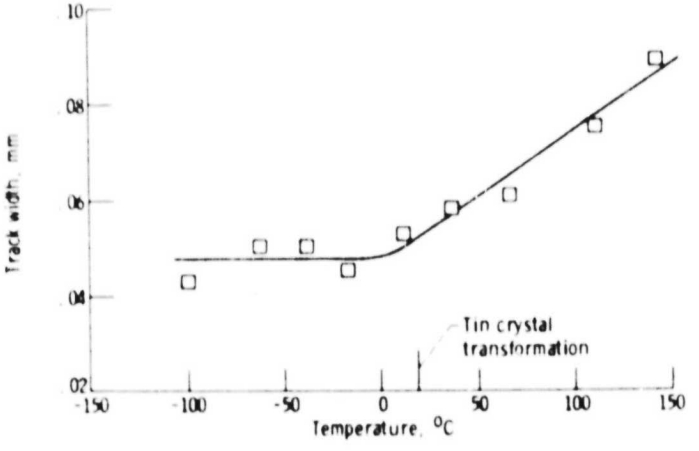

Figure 84. - Track width on tin single-crystal surface as function of temperature. Sliding velocity, 0.7 millimeter per minute, load, 10 grams; pressure, 10^{-8} newton per square meter (10^{-10} torr); rider, iron (110); single pass.

in a plastic manner. Thus, track width increases with an increase in temperature.

Sliding on the tin single-crystal surface at 23° C resulted in recrystallization in the wear track. Grain boundaries were present in the wear track. Tin recrystallizes at -4° C. [illegible] sliding and associated strain supply the necessary energy for recrystallization. The recrystallization was confined to the wear track.

Friction experiments were conducted with polycrystalline tin and alloys of tin. Binary tin alloys containing 1-atomic-percent bismuth, copper, or aluminum were examined. Coefficients of friction were measured over the temperature range of -100° to 150° C. The results obtained in these experiments are presented in figure 85.

An examination of figure 85 indicates that there was a change in the friction coefficient of polycrystalline tin at the transformation temperature. Just as shown by the single-crystal results in figure 82 for the (110) [111] orientation, friction increased with transformation from the body-centered-tetragonal to the diamond structure. The friction coefficient of polycrystalline tin was, at all temperatures, higher than those observed for the single-crystal orientations in figure 82. This observation is consistent with the friction results for hexagonal metals in their single-crystal and polycrystalline forms.

Bismuth added to tin completely eliminated the crystal transformation in tin (fig. 85). No change in the friction coefficient was observed as the alloy passed through the crystal transformation region.

Aluminum and copper both increased the kinetics of the otherwise sluggish transformation from the body-centered-tetragonal form to the diamond form of tin. With both copper and aluminum a marked change in friction coefficient was observed as these alloys passed through the crystal transformation. The presence of aluminum in tin produced a nearly twofold decrease in the friction coefficient with the transformation from the diamond form of tin to the body-centered-tetragonal form. Thus, the data in figure 85 indicate that the

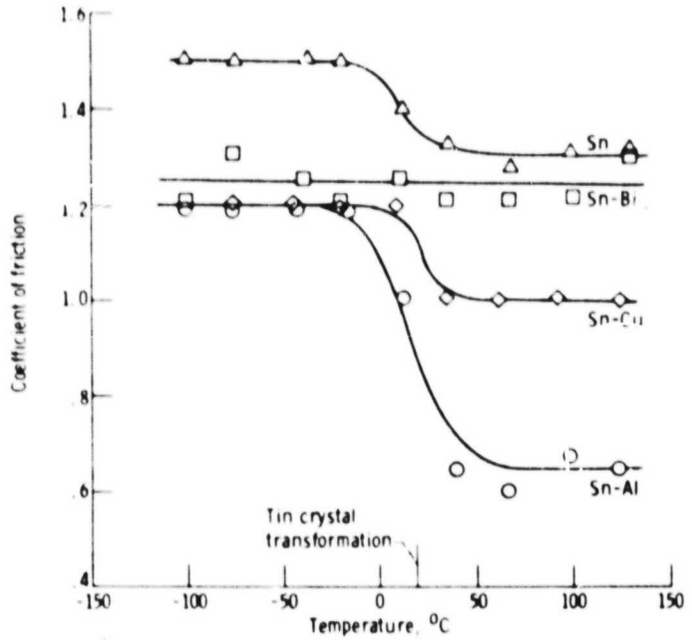

Figure 85. - Coefficient of friction for polycrystalline tin and tin alloys at various temperatures. Sliding velocity, 0.7 millimeter per minute; load, 10 grams; pressure, 1.33×10^{-8} newton per square meter (10^{-10} torr).

effects of the crystal transformation in tin on the friction coefficient can be controlled by proper alloying.

ORDER-DISORDER

The arrangement of atoms is not only important to pure metals, as discussed earlier, but it is also important to the friction behavior of alloys. It has been found that certain intermetallic compounds exhibit different distributions of atoms A in a lattice of B atoms. When A atoms take up regular sites such that they are uniformly distributed throughout the lattice, as shown in figure 86 for Cu_3Au, the structure is said to be ordered. The effect of this orderly arrangement of atoms on friction and elasticity and hardness related to friction is shown in figure 87. Friction is lowest when the alloy is in the ordered state. Transformation to the disordered atomic state results in a decrease in hardness and elasticity and an increase in the friction coefficient.

The copper-gold alloy CuAu also undergoes a transformation from the ordered to the disordered state. The transformation occurs at 410° C. Friction experiments were conducted with the CuAu alloy sliding on 440-C stainless steel in vacuum. With the alloy in the ordered state, a friction coefficient of 0.32 was obtained. An increase in sliding velocity (and hence interface temperature) showed a change in friction properties. At about 350 centimeters per second a marked increase was observed. At higher sliding velocities, the friction again began to decrease. This decrease may reflect a general decrease in mechanical properties with increasing temperature. A similar effect was noted with Cu_3Au at these higher velocities. The sharp increase in friction coefficient is believed to reflect the transformation from the ordered to the disordered state for CuAu.

In order to substantiate further the influence of ordering on CuAu, a specimen was deliberately disordered before a friction experiment was performed. With CuAu in the disordered state and sliding on 440-C stainless steel, a friction coefficient of about 1.2 was obtained over the entire range of sliding velocities

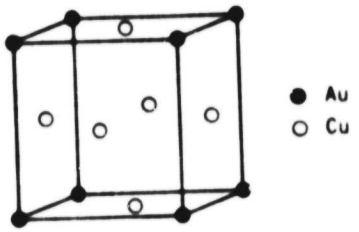

Figure 86. - Cu_3Au superlattice structure.

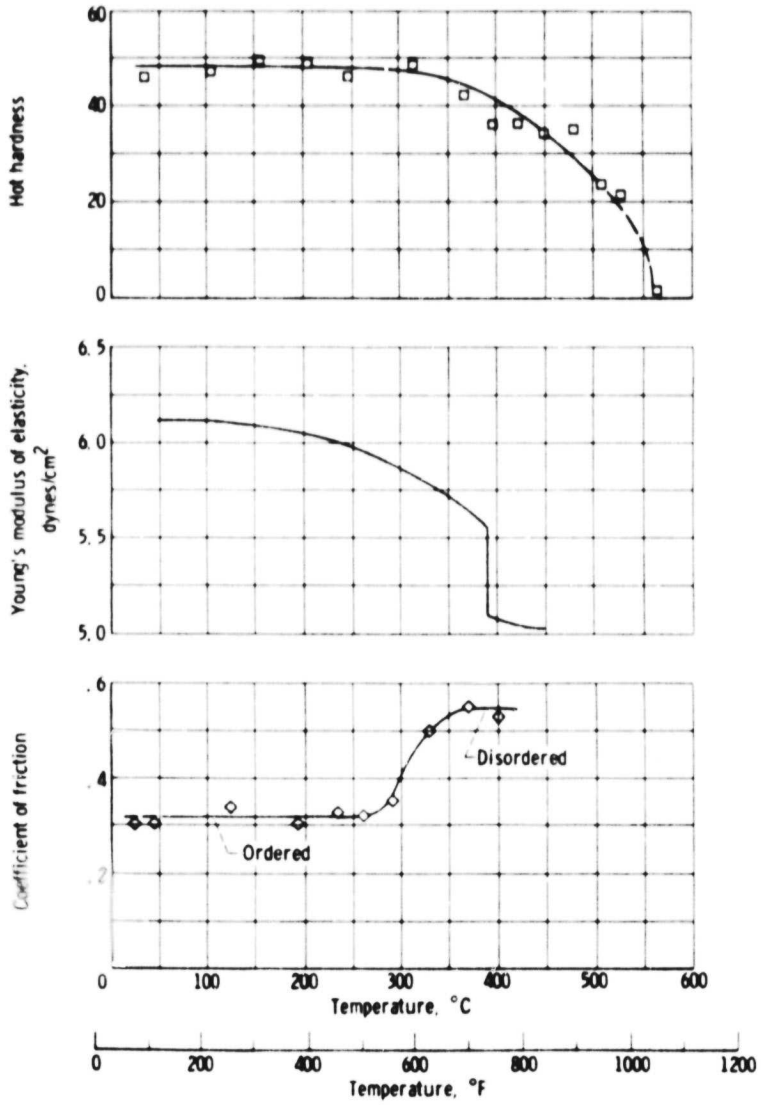

Figure 87. - Hardness, Young's modulus, and coefficient of friction for Cu_3Au (75 at. % copper - 25 at. % gold) sliding on 440-C stainless steel at various temperatures. Load, 1000 grams; ambient pressure, 10^{-9} torr.

investigated. There were no changes such as reflected when ordering was present.

Examination of friction coefficients from the ordered to the disordered state in the transformation region did not reflect an increase in friction to 1.2, the value observed when the structure was deliberately disordered before the experiment. This may be due to incomplete transformation from the ordered to the disordered state. When CuAu transforms from the ordered to the disordered state, long-range order is destroyed, but short-range order still persists above the transformation temperature. This may not be observed for Cu_3Au because of an abrupt change in properties with transformation.

A friction experiment was also conducted with CuAu sliding on 440-C stainless steel in vacuum at various ambient temperatures; the results are presented in figure 88. At a constant velocity of 198 centimeters per second the friction at 20° C was the same as that obtained in figure 87 for Cu_3Au. A slight decrease in friction was observed, then a marked increase at 280° C to 1.27. This change in friction is again believed to reflect the transformation from the ordered to the disordered state.

Hardness data at various temperatures were also obtained for CuAu, and these results are also presented in figure 88. In the temperature region for transformation a decrease in hardness was observed. These results are similar to those obtained with Cu_3Au and indicate the influence of the order-disorder transformation on properties other than friction.

DEGREE OF METALLIC NATURE

Pauling in 1948 formulated a resonating-valence-bond theory of metals and intermetallic compounds in which numerical values could be placed on the bonding character of the various transition elements (ref. 76). While there have been critics of this theory, it appears to be the most plausible in explaining the interfacial interactions of transition metals in contact with themselves and other metals.

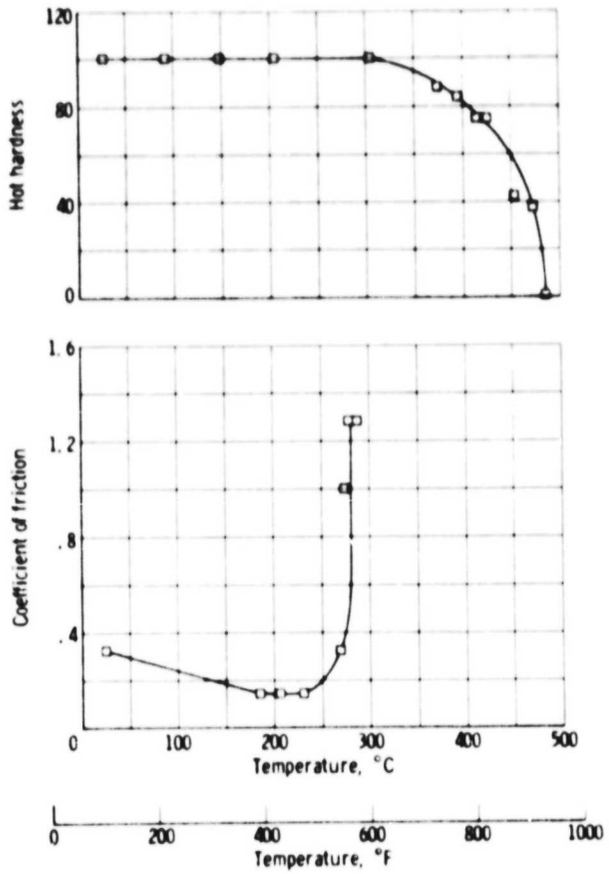

Figure 88. - Hardness and friction coefficient for CuAu (50 at. % copper - 50 at. % gold) sliding on 440-C stainless steel at various temperatures. Load, 1000 grams; sliding velocity, 198 centimeters per second; ambient pressure, 10^{-7} to 10^{-9} torr.

When two metal surfaces are placed in contact in the atomically clean state, the intermetallic bonds that form are going to depend heavily on the character of the bonding in each of the metals. One might predict from Pauling's theory that those metals with strong d character would be less likely to interact, forming strong interfacial bonds with other metals, than those metals which do not have this strong character.

Adhesion and friction experiments have been conducted with transition metals both in bulk and thin-film form. Results for bulk metal friction measurements are presented in figure 89. The surface in contact with each of the transition metals in figure 89 was a gold (111) surface. The data in figure 89 indicate a decrease in friction with an increase in the d character of the metallic bond. Similar results were obtained in adhesion experiments.

When thin films (2000 Å) of some of the transition metals examined in figure 89 were placed on a quartz substrate by sputter deposition and examined in adhesion and friction experiments, adhesion and friction to iron decreased with increasing d-bond character. With iron and those metals having stronger d-bond character (e.g., platinum), the interface between the transition metal and the quartz substrate was weaker than that between the gold and the transition metal, and with tangential motion the metal film separated from the quartz substrate. With iron an abrupt decrease occurred in friction, and with all the metals which separated from the quartz the friction was essentially the same as that for gold in contact with quartz.

Metals are not always in contact with other metals; frequently, they are in solid-state contact with nonmetals. Does the d-valence bond character concept as developed by Pauling still hold when the transition metals slide on various nonmetals?

Sliding friction experiments were conducted with ferrite in contact with a number of transition metals. The friction traces with metal-ferrite couples are generally characterized by smoothly fluctuating behavior with no evidence of stick-slip, but the traces under high loads are characterized by stick-slip behavior. With the more chemically active metal titanium marked stick-slip behavior

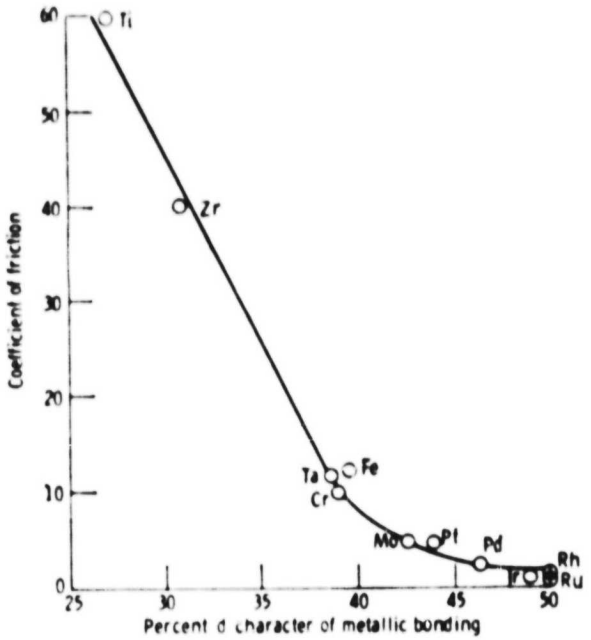

Figure 89. - Coefficient of friction as function of percent d-bond character for various metals. Sliding velocity, 0.7 millimeter per minute; load, 1 gram; temperature, 23° C; and pressure, 10^{-8} torr.

appears at a load of 0.2 newton, whereas with the less chemically active metal rhodium stick-slip behavior appears under higher loads of 0.35 newton or more. The coefficients of friction for various metals sliding on ferrite were unaffected by load in the range of 0.05 to 0.5 newton.

The coefficients of friction for various metals with ferrite are presented in figure 90 as a function of the d-bond character of the transition metal. There appears to be good agreement between the coefficient of friction and the chemical activity of the transition metals. Titanium, which has a strong chemical affinity for the iron and oxygen in ferrite, exhibits a considerably higher coefficient of friction in contact with ferrite than does rhodium, which has a lesser affinity for these two elements.

The d-valence bond character of the transition metals influences the coefficient of friction for metals in contact with silicon carbide just as it does for metals in contact with themselves and ferrite (ref. 129). Only the slope of the curve is observed to change.

The data in figure 91 indicate the coefficients of friction for some of the transition metals in contact with a single-crystal diamond (111) surface as a function of the d-bond character of the metal. The data indicate a decrease in friction with an increase in d-bond character. Titanium and zirconium, which are chemically very active when in contact with diamond, exhibit very strong interfacial adhesive bonding to diamond. In contrast, rhodium and rhenium, which have a very high percentage of d-bond character, have relatively low coefficients of friction. Figure 91 also presents the friction data for a diamond surface in sliding contact with a yttrium surface. Yttrium gives a higher coefficient of friction than that estimated from the data of other metals. This may be due to the effect of oxygen. An argon-sputter-cleaned yttrium surface seems to be covered by an oxide surface layer. It is very difficult to remove the oxide surface layer from yttrium by argon-sputter cleaning for 30 to 60 minutes. The effects of oxygen in increasing the friction is related to the relative chemical thermodynamic properties and bonding of carbon to oxygen. The greater the degree of bonding across the

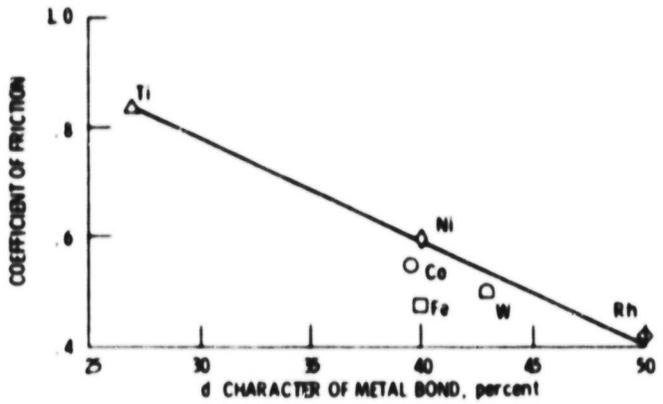

Figure 90. - Coefficient of friction as function of percent d-bond character of various metals in sliding contact with single-crystal manganese - zinc ferrite {110} surface in vacuum (10^{-8} torr). Single-pass sliding; sliding velocity, 3 millimeters per minute; load, 0.3 newton; temperature, 25° C.

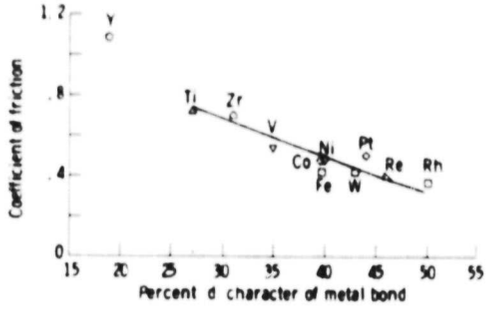

Figure 91. - Coefficient of friction as function of percent of metal d-bond character for single-crystal diamond {111} surface in sliding contact with transition metals in vacuum. Sliding direction, $\langle 1\bar{1}0 \rangle$; sliding velocity, 3×10^{-3} meter per minute; load, 0.05 to 0.3 newton; room temperature; vacuum pressure, 10^{-8} pascal.

interface, the higher the coefficient of friction. In the case of yttrium, oxygen on the surface tends to strongly chemically bond the yttrium to the diamond surface.

SHEAR STRENGTHS AND FRICTION PROPERTIES

A clean metal in sliding contact with a clean nonmetal or the metal itself fails either in tension or in shear because the interfacial bonds are generally stronger than the cohesive bonds in the cohesively weaker metal. The failed metal subsequently transfers to nonmetallic material or the other contacting metal. In adhesion, tensile fracture is usually involved; in sliding friction, the metal shear strength is extremely important. The relationship between the ideal and actual shear strengths and the friction properties of metals in contact with metals and nonmetals is now discussed. The ideal shear strength τ_{max} of a solid subjected to a simple shear mode of deformation is estimated (ref. 130). The actual shear strengths for the metals are taken from the data of Bridgman (ref. 131). The nonmetals examined included single-crystal diamond, pyrolytic boron nitride, single-crystal silicon carbide, and single-crystal manganese - zinc ferrite.

With regard to the adhesion and friction of metals in contact with nonmetals or themselves, pure metals, high purity nonmetals, and a good experimental vacuum system (10^{-8} Pa) were used to ensure a high degree of purity and cleaniness, well-defined mechanical, physical, and chemical behavior, and environment, and to facilitate the determination of the effect of material behavior. The metals, nonmetals, apparatus, and experimental procedures related to the results reported herein have already been described in reference 129.

The generally accepted thinking with respect to fracture of solids is that of the ideal elastic solid or one which exhibits elastic response to a load until such time as atomic separation takes place on a plane by overcoming the interatomic forces. At the atomistic level fracture occurs when bonds between atoms are broken

across a fracture plane and a new surface is created. This can occur by breaking bonds perpendicular to the fracture plane (fig. 92(a)) or by shearing bonds across the fracture plane (fig. 92(b)). Such behavior is expected in the case of an ideal crystalline solid which contains no defects of any kind. At this level the fracture criteria are simple; fracture occurs when the local stress builds up either to the theoretical cohesive strength or to the theoretical shear strength. The theoretical cohesive strength is discussed in reference 132.

The calculation of the theoretical cohesive strength of an ideal elastic solid is based on the proposition that all the energy of separation is available for the creation of two new surfaces; the only expenditure in creating these two surfaces is assumed to be the surface energy. If atoms A and A' in figure 92(a) are pulled apart, the stress required to separate the plane is the theoretical strength σ_{max}, and when that is reached, the bonds are broken. The theoretical strength (the ideal uniaxial tensile strength) is then given by the well-known equation

$$\sigma_{max} = \sqrt{\frac{E\gamma}{d}} \tag{1}$$

where E is the appropriate Young's modulus, γ the surface energy per unit area, and d the interplanar spacing of the planes perpendicular to the tensile axis (refs. 133 to 136). In this equation the ideal strength of the solid is directly related to other macroscopic physical properties. The foregoing approach is equally applicable to any solid. Frenkel used a similar method to estimate the ideal shear strength σ_{max} of a solid subjected to a simple shear mode of deformation (refs. 7 or 13). It is assumed that, for any solid, the shear stress to shear any plane a distance x over its neighbor was given by

$$\tau = K \sin \frac{2\pi x}{b} \tag{2}$$

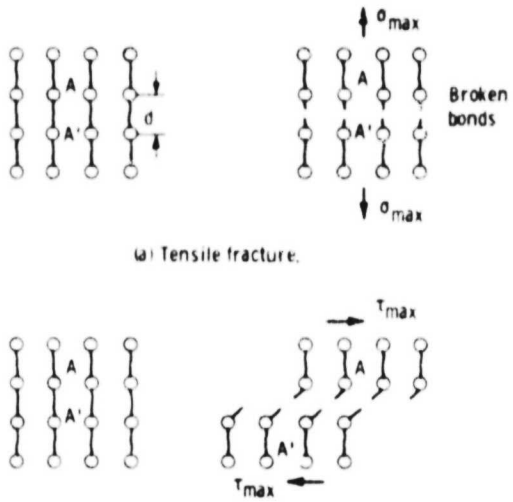

Figure 92. - Fracture viewed at atomistic level in terms of breaking of atomic bonds.

where b is the appropriate repeat distance in the direction of shear. The planes are assumed to be undistorted by the shear. K is chosen to give the correct shear modulus G. It can then be shown that

$$\tau_{max} = \frac{Gb}{2\pi d} \tag{3}$$

where d is the interplanar spacing of the shearing planes.

The values for the ideal shear strength were obtained from equation (3). It is assumed that the slip occurred on the slip plane in the slip direction.

This type of analysis of the ideal shear strength generally produces a correlation with friction properties of metals in contact with nonmetals and themselves (fig. 93). The coefficient of friction data used for various clean metals in contact with clean diamond, pyrolytic boron nitride, silicon carbide, manganese - zinc ferrite, and metals themselves were from references 129 and 137 to 139.

Figures 93 to 96 present the coefficients of friction as functions of the ideal shear strength for metals in contact with various nonmetals. The data of these figures indicate a decrease in friction with an increase in the ideal shear strength of the metal bond.

The shear strength values for the body-centered-cubic metals are average values calculated from the values of the shear strength for three dominant slip systems. Those for the hexagonal metals are average values calculated from the values of the shear strength for two dominant slip systems - that is, $\{1010\}\langle 11\bar{2}0\rangle$ and $\{0001\}\langle 11\bar{2}0\rangle$. There appears to be particularly good agreement between the friction of metals in contact with silicon carbide and the ideal shear strength (fig. 93).

Thus, the physical properties and the crystallographic system play important roles in adhesion and friction of metals contacting nonmetals or metals contacting themselves. These simple calculations of the ideal strength and the correlation between the friction and the strength can be criticized on a variety of grounds. The extent of

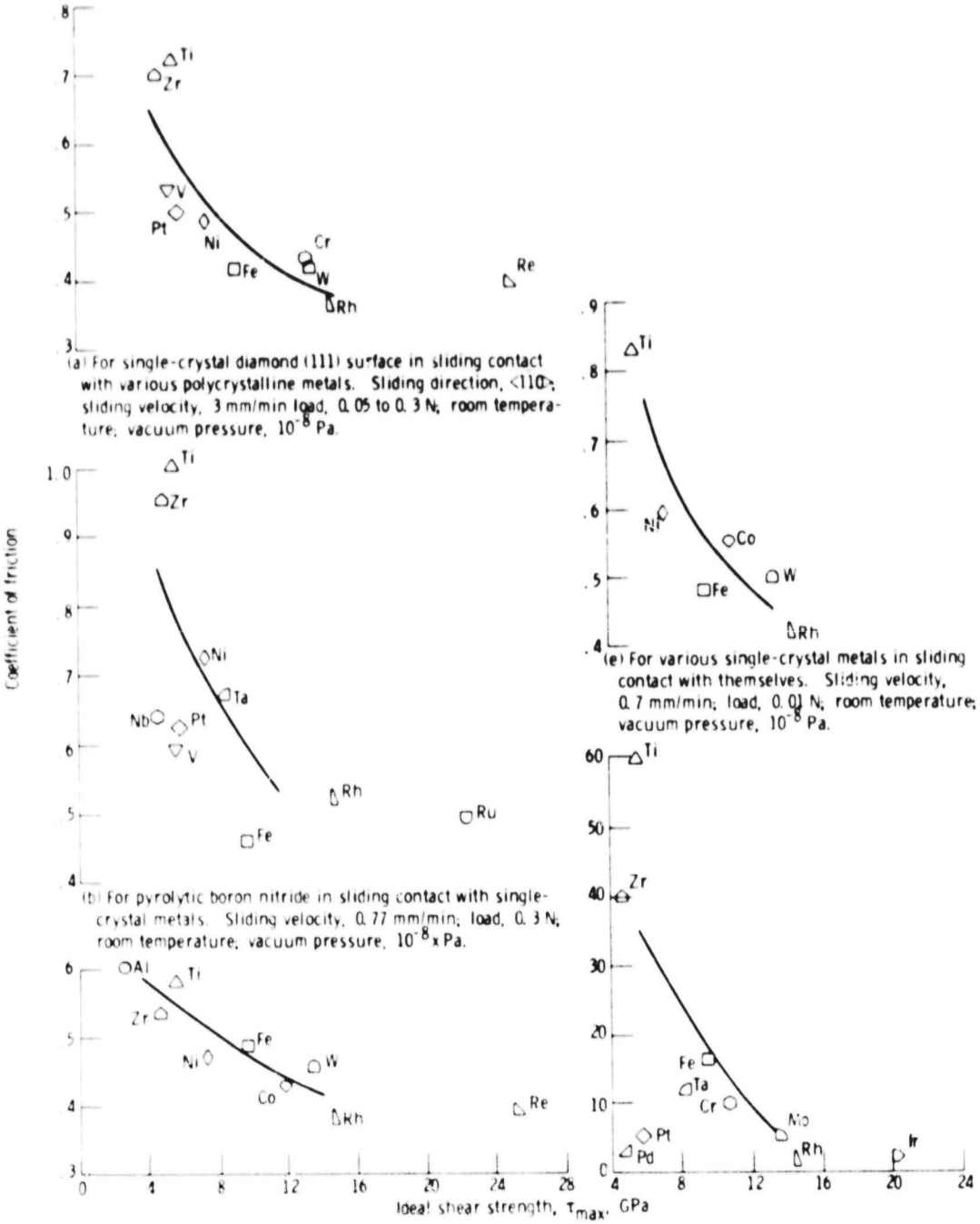

(a) For single-crystal diamond (111) surface in sliding contact with various polycrystalline metals. Sliding direction, <110>; sliding velocity, 3 mm/min load, 0.05 to 0.3 N; room temperature; vacuum pressure, 10^{-8} Pa.

(b) For pyrolytic boron nitride in sliding contact with single-crystal metals. Sliding velocity, 0.77 mm/min; load, 0.3 N; room temperature, vacuum pressure, 10^{-8} x Pa.

(c) For single-crystal silicon carbide (0001) surface in sliding contact with various polycrystalline metals. Sliding direction, <1010>, sliding velocity, 3 mm/min; load, 0.05 to 0.5 N; room temperature; vacuum pressure, 10^{-8} Pa.

(e) For various single-crystal metals in sliding contact with themselves. Sliding velocity, 0.7 mm/min; load, 0.01 N; room temperature; vacuum pressure, 10^{-8} Pa.

(d) For single-crystal manganese-zinc ferrite (110) surface in sliding contact with various polycrystalline metals. Sliding direction, <110>; sliding velocity, 3 mm/min load, 0.3 N; room temperature; vacuumpressure 10^{-8} Pa.

Figure 83. - Coefficients of friction as function of the ideal shear strength of metals.

slip in a crystal depends on the magnitude of the shearing stresses produced by the applied forces and the orientation of the crystal with respect to these applied forces. This variation can be rationalized by the concept of the crystal's resolved shear stress for slip. Depsite the foregoing, the results of the relationship between the coefficient of friction and the ideal strength may lead to an appreciation for the role of the physical properties of materials in determining the tribological properties and the mechanical behavior of metals.

A good correlation between the coefficient of friction and the shear modulus was also found with metals contacting nonmetals and metals. The correlations are very similar to those between the coefficient of friction and the shear strength (fig. 93).

SURFACE SEGREGATION

Many friction, wear, and lubrication studies are performed on materials that are either alloys or have relatively high bulk concentrations of contaminants such as carbon. The assumption is often made that bulk properties reflect surface effects. In the past 15 years, the ability to characterize surfaces has advanced greatly. LEED (low-energy electron diffraction) (ref. 140) has been used to examine changes in the surface structure of single crystals. AES (Auger emission spectroscopy) (refs. 141 and 68) has been used to determine surface composition both qualitatively and quantitatively. The ability now exists to examine to what degree bulk composition reflects surface structure and composition.

Results are presented herein on some alloys systems - single crystals of Cu - 1-atomic-percent Al, Cu - 5-atomic-percent Al, Cu - 10-atomic-percent Al, and Cu - 1-atomic-percent Sn and polycrystalline Fe - 10-atomic-percent Al. AES, LEED, adhesion, and friction experiments were performed on samples of the alloys indicated in addition to performing sputtering studies. The results of the studies demonstrate that bulk conditions do not reflect surface conditions in that in each case the minor constituent segregated at

the surface. In addition, friction and adhesion data indicate effects that are much larger than would be expected from bulk concentrations. A model for the surface segregation mechanism is also discussed in references 108 and 142 to 145.

The copper-aluminum crystals studied were cylinders varying from 0.6 to 0.8 centimeter (both in radius and height). The copper-tin crystals were rectangular prisms 1.2 by 0.85 by 0.5 centimeter. Both crystals were oriented in the (111) direction. The copper-aluminum crystals were substitutional solid solutions having 1-, 5-, and 10-atomic-percent aluminum in copper. The copper-tin crystal was a solid solution with 1 atomic percent tin in copper. The crystals, triple-zone refined, contained no more than 10 ppm impurities. Pure aluminum and copper crystals were used as standards for the AES studies. The crystals were polished to 600 grit on metallurgical papers and then electropolished in orthophosphoric acid.

The iron-aluminum alloys studied were polycrystalline solid solutions made by vacuum melting from 99.99 percent iron and 99.99 percent aluminum. The iron alloys were machined into disks and pins used in the friction experiments. These samples were given a final polish with alumina in water.

A disk of iron - 10-atomic-percent aluminum was used for the AES studies. This sample was electropolished in orthophosphoric acid before mounting in the vacuum system. High-purity research grade argon was used for sputtering the crystals.

The apparatus used for the AES-LEED and adhesion studies is described in references 156 to 158. The specimen studied could be rotated 360° to allow AES, LEED, and adhesive contact analyses as well as ion-bombardment cleaning. The vacuum system consisted of sorption pumps, an ion pump, and a sublimation pump, which enabled obtaining system pressures of 2×10^{-10} torr when data were taken.

Friction experiments on the iron-aluminum alloys were performed in the rider-disk apparatus described in reference 143. Riders and disks were formed from the same material. A plexiglass box containing the friction apparatus was continuously purged at a positive pressure with dry argo

The surfaces of all samples used in the AES-LEED studies were cleaned by first outgassing at 500° C until the system pressure reached the 10^{-10} torr range and then by alternately sputtering and heating until the principal impurity peaks - carbon, sulfur, and oxygen - were removed from the AES spectrum.

To demonstrate surface segregation, the same procedure was used for all the alloys. The alloys were first sputtered for long times to remove many layers. An AES trace was taken after sputtering. The crystals were then heated at temperatures from 100° to 700° C, and after heating the crystals were allowed to cool to room temperature. AES traces were then taken in regions which displayed the peaks of interest.

The adhesion experiments were performed by making contacts between the crystal of interest and a gold crystal oriented in the (111) direction. For the copper-aluminum alloys, the crystals were cleaned, and then the amount of force necessary to break the bond resulting from a 20-milligram load was determined. With the copper - 1-atomic-percent tin alloy the amount of force necessary to break the bond formed was determined after sputtering and after heating.

Friction coefficients were determined for the iron - 10-atomic-percent aluminum alloy and pure iron with the rider-disk apparatus. The experiments were performed with varying percentages of stearic acid in hexadacane as a lubricant. The load used was 250 grams, and the sliding velocity was 3.8 centimeters per second.

The results of the surface segregation studies are shown in table XIII for all the alloy systems studied. The alloys all show surface concentrations much higher than bulk concentration. Surface segregation occurred readily at 200° C in the copper systems. The iron system was checked only at 500° C, but it should behave similarly at 200° C. In interpreting these results, several assumptions were made. First, after sputtering and removing many layers (>1350) the peak to peak amplitude of the minor constituent Auger peak is assumed to reflect bulk concentration. Wehner (ref. 146) points out that this is a reasonable assumption. The peak to peak amplitude of the minor constituent Auger peak after heating is assumed to be linearly related

TABLE XIII. - MAXIMUM COVERAGE OF MINOR CONSTITUENT ON ALLOY SURFACES

Alloy	Ratio of surface concentration to bulk concentration	Atomic size from lattice nearest neighbor distance
Cu-1 at. % Al	6.5	Cu - 2.556 Å (f.c.c.)
Cu-5 at. % Al	4.5	Al - 2.862 Å (f.c.c.)
Cu-10 at. % Al	3.1	Sn - 3.022 Å (tetragonal)
Cu-1 at. % Sn	15.0±2	Fe - 2.481 Å (b.c.c.)
Fe-10 at. % Al	8.0	

Note: Atomic size gives a rough measure of the amount that the alloy atom strains the parent lattice.

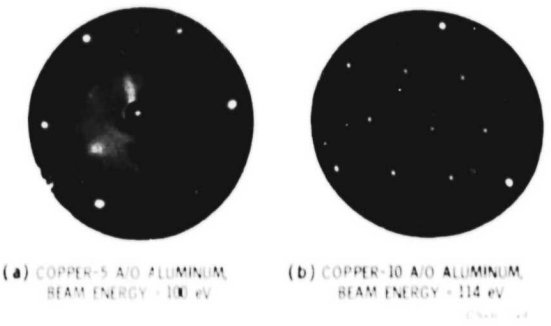

(a) COPPER-5 A/O ALUMINUM, BEAM ENERGY - 100 eV (b) COPPER-10 A/O ALUMINUM, BEAM ENERGY - 114 eV

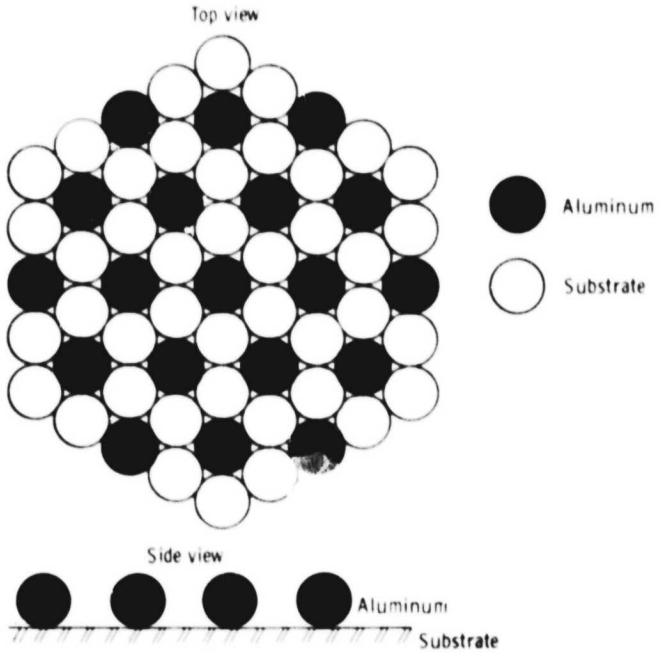

(c) Possible lattice structure observed for LEED pattern R30° (2x2) structure showing one-third monolayer coverage.

Figure 94. - LEED patterns and interpretations for copper-aluminum alloys.

to the post-sputtering amplitude. This gave a way of calibrating the concentration in the surface region. A discussion of the use of Auger spectroscopy for quantitative analysis can be found in the literature (refs. 141 and 68).

LEED gave an independent means for checking surface changes. Figure 94 gives LEED patterns and their interpretation for the copper-aluminum (Cu-Al) system. The Cu - 1-atomic-percent Al crystal (not shown) had no additional spots in its pattern. The Cu - 5-atomic-percent Al crystal had faint extra spots indicating a partially formed layer (ref. 147). The copper - 1-percent tin crystal gave the same LEED pattern as the higher concentration copper-aluminum crystals. LEED patterns give the correct symmetrics for a surface, but distances appear as reciprocals.

Interpretation of the LEED patterns (fig. 94(c)) in terms of the real crystal structure suggests that the minor constituent pops out onto the surface and diffuses to preferred locations. The LEED results agree with the AES results for surface coverage with the Cu - 10-atomic-percent Al sample. Assuming only two layers are being sampled by AES following segregation and only one layer before LEED observations would predict a concentration of 0.33 for the top layer and 0.1 for the next layer giving a total of 4.3 times, which agrees well with the maximum coverage observed by AES. The Cu - 1-atomic-percent Sn crystal had the same LEED pattern with well-defined spots. Since the iron sample was polycrystalline, no well-defined LEED pattern could be discerned. The results of controlled sputtering studies on the Cu - 10-atomic-percent Al crystals also set two layers as an upper bound on the region of increased concentration.

Figure 95 shows the results of sputtering, heating to the indicated temperature for 30 minutes, and then cooling to room temperature before taking an Auger trace on the copper-aluminum alloys. Two features can be observed in these curves: first, the surface concentration depends on bulk concentration, and second, the concentration saturates with temperature.

These and the previous observations lead to an interpretation of the results as being segregated at the surface. An analogy between

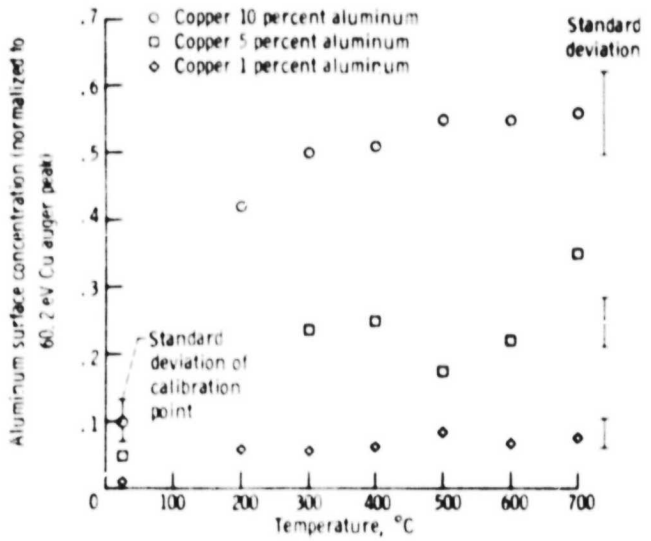

Figure 95. - Increase of aluminum surface concentration for copper - 1-, 5-, and 10-atomic-percent aluminum alloys. For each point the crystal was sputtered, heated for 30 minutes, and then allowed to cool to room temperature.

surface segregation and grain boundary segregation can be readily made. As McClean (ref. 108) describes for the grain boundary case, when the solute atom is large compared to the space available in the solvent, lattice strain results. This strain can be relieved by having the solvent occupy a less strained position in the grain boundary or on the surface in this case. In addition, there is another contribution to reducing the energy from valence interactions with the excess electronic charge in the grain boundary or on the surface. It should be pointed out that segregation of the minor component is the equilibrium condition (i.e., the condition of lowest free energy) and should be expected as the normal state of the surface. Sputtering in the experiments creates a nonequilibrium condition. However, at room temperature, diffusion is slow and, consequently, the approach to equilibrium is slow. Heating allows the surface to approach equilibrium rapidly. Heating and stresses experienced in friction experiments could also act as mechanisms promoting the rapid approach to equilibrium.

McClean has an expression based on a statistical thermodynamic argument that describes the equilibrium grain boundary or surface concentration as a function of bulk concentration, temperature, and retrieval energy:

$$C_d = \frac{C_o e^{Q/RT}}{1 - C_o + C_o e^{Q/RT}} \qquad (1)$$

where

C_d	fractional grain boundary or surface concentration of the solute
C_o	fractional bulk concentration of the solute
Q	retrieval energy gained by segregation
R	gas constant
T	temperature

The data in figure 94 are interpreted as representing the room temperature equilibrium concentrations. The saturation at high

temperature reflects the fact that for $T > 300^{\circ}$ C, $C_d \approx C_o$ and, consequently, no change is observed in what is precipitated onto the surface in the cooling process by heating or higher temperatures. The Q calculated for the three copper-aluminum samples ($1150 \begin{smallmatrix}+300\\-560\end{smallmatrix}$ cal/mole for Cu - 1-atomic-percent Al, $1020 \begin{smallmatrix}+290\\-410\end{smallmatrix}$ cal/mole for 5-atomic-percent Al, and $1190 \begin{smallmatrix}+450\\-490\end{smallmatrix}$ cal/mole for 10-atomic-percent Al) are in resonable agreement with each other. These values are smaller than the strain energy in the bulk, but this is to be expected. The aluminum in iron and the copper-tin samples show much higher surface concentrations than copper-aluminum. This result might be expected on the basis of this model since the copper-tin and the iron-aluminum misfits are larger and bulk elastic properties are different from copper-aluminum; consequently, a higher strain energy and hence higher surface concentration for a given temperature might be expected.

An important point to be made from the results of these studies is that in performing adhesion and friction experiments the surface conditions may vary radically from bulk concentration, since most materials used are either alloys or have bulk contaminants such as carbon or sulfur. In addition, surface chemistry may be radically affected by these surface conditions and surface reaction may not be at all what would be expected if bulk concentrations are assumed.

Figure 96 summarizes the results of adhesion experiments on a set of copper-aluminum alloys and a copper-tin alloy with a gold (111) single crystal. In the case of copper-aluminum, small percentages of aluminum in these alloys radically affect the adhesive properties as compared with pure copper; in fact, the bonding force rapidly approaches that observed with pure aluminum-gold.

For the copper-tin specimen (fig. 96), a somewhat different experiment was performed. The adhesive behavior following sputtering and heating was observed. As can be seen, after heating the adhesive bonding force is reduced. This behavior can readily be explained by using the results of the surface segregation experiments. As shown there, the solute is popping out onto the surface and presenting a substantially different surface to the gold crystal. One would a

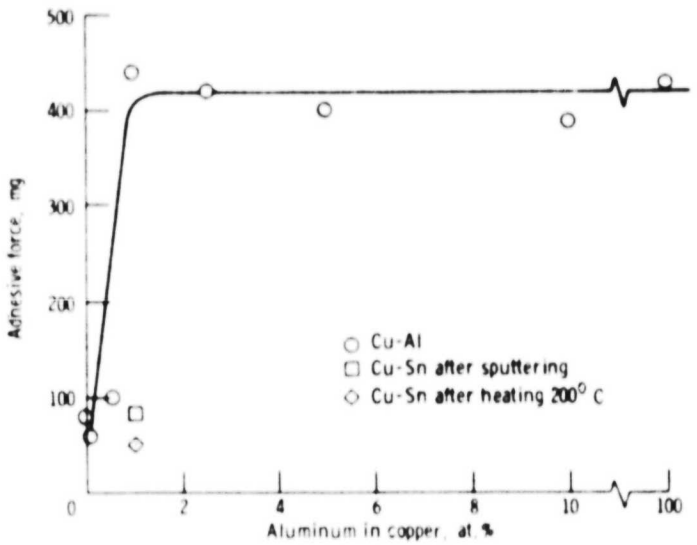

Figure 96. - Adhesive force of (111) gold to (111) surface of copper alloys as function of bulk concentration.

priori expect that the affects on adhesion would only reflect bulk concentration if surface segregation did not occur. Large changes in surface properties with adsorption are well known. For example, the work function of tungsten changes radically with cesium adsorption (ref. 148). At 0.7 monolayer the work function drops from 5 to 1.47 electron volts. At 1 monolayer it is 2.18 electron volts, approximately the work function of pure cesium. Therefore, it is not surprising that if indeed the solute atom were popping out onto the surface, large changes in adhesive behavior would be expected.

Friction experiments showed that surface segregation has practical relevance. Friction experiments were performed on a number of polycrystalline iron-aluminum (Fe-Al) alloys. The results on Fe - 10-atomic-percent Al upon which AES surface segregation experiments were performed are presented as typical examples of the results. Figure 97 shows the variation of friction coefficient for a surface lubricated with hexadecane containing varying percentages of stearic acid. The dry friction coefficients are much higher than for pure iron as would be expected from both the AES results on iron-aluminum and the adhesive behavior. The lubricated friction behavior with stearic acid present also varied greatly from pure iron; this indicates that changes in surface chemistry occurred with the Fe - 10-atomic-percent Al alloy.

Therefore, even in the friction process where the surface layer could be worn away, surface segregation can be occurring to replenish the worn layer and can be producing marked changes. As stated earlier, lattice stress along with thermal effects could be sufficient to promote surface segregation.

Alteration in both adhesive and friction properties of alloys or materials containing contaminants may occur much in excess of what would be expected on the basis of bulk concentration. This effect has been seen with copper-aluminum, copper-tin, and iron-aluminum alloys. AES and LEED can be used to supplement experimental observation in practical friction studies and aid in the interpretation of results. AES and LEED have shown that conclusions based only on bulk

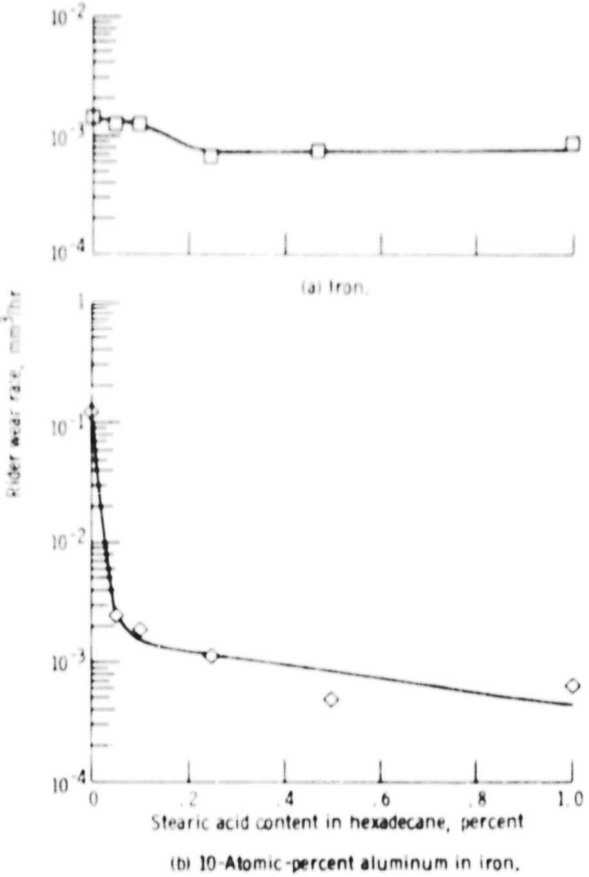

Figure 97. - Effect of stearic acid concentration in hexadecane for for iron and iron - 10-atomic-percent aluminum. Sliding velocity, 3.8 centimeters per second; load, 250 grams.

composition of materials can lead to a misinterpretation of experimental results.

METAL ALLOY EFFECTS

In practical lubrication systems the mechanical components in solid-state contact are most frequently alloys rather than elemental metals. The composition of these alloy surfaces are important in considering the chemical interactions of such solids with other solids, with gases, and with lubricants. Even where elemental metals are used, the surfaces of these metals may have compositions entirely different from the bulk which results from impurity segregation.

The field of tribology contains a number of excellent texts. Many of these books do not, however, discuss the real nature of the surface to be lubricated (see, e.g., refs. 36 and 149 to 151). Much attention is given to the chemistry of the lubricant but little to the chemistry of the alloy surface to be lubricated. In fairness to the authors of these texts the identification of these surfaces with surface tools just began to emerge at the time these texts were written. Future texts on the subject should, however, not neglect the importance of the metal or alloy surface chemistry and the interaction of the lubricant with that surface chemistry.

With elemental metals, the effect of small concentrations of impurities such as parts per million carbon in iron have been shown to affect surface chemistry. This was discussed earlier in this thesis. Similar effects have been observed with other impurity elements in a number of different metals.

The presence of small concentrations of alloying elements can alter environmental surface interactions. Certain alloying elements may react more readily with the oxygen present in the environment than would other elements. These differences in reactivity of various elements with oxygen can alter friction and wear behavior.

In figure 98 the friction coefficient is plotted as a function of oxygen exposure for iron and for an Fe - 3.5-percent Si alloy. Prior to the admission of oxygen, the friction coefficient is extremely high

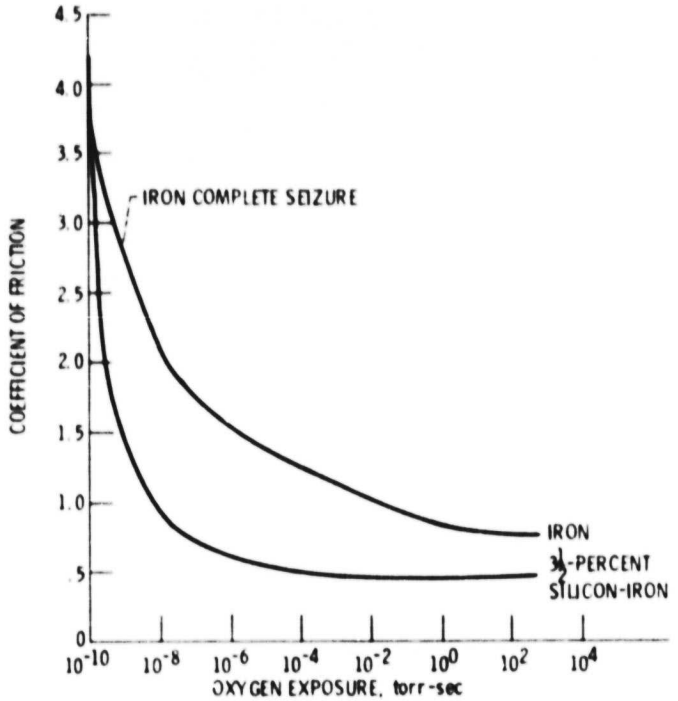

Figure 98. - Coefficient of friction for iron and 3 1/2-percent silicon-iron as function of oxygen exposure. Sliding velocity, 0.001 centimeter per second; ambient temperature, 20° C; ambient pressure, 10^{-10} torr.

for the alloy, and the pure iron seizes completely. As the surfaces are exposed to oxygen, the friction for both the alloy and the elemental iron decrease. This decrease occurs, however, much more rapidly for the alloy than for the iron. The difference is due to the segregated silicon and its interaction with oxygen at the surface. The sliding process is capable of generating sufficient frictional heating to cause the silicon to segregate at the alloy surface. Auger analysis confirmed its presence. The alloying element silicon has markedly changed surface chemistry.

Cast irons, because of their good resistance to wear, have been used in a wide variety of mechanical systems for many years. They have been used in piston rings, bearings, brakes, seals, and so forth.

The wear resitance of cast irons depends very heavily on the elements and structures present. The influence of alloying elements on wear behavior of cast irons was recognized very early (ref. 152). Disagreement, however, has existed as to the specific role of certain elements in affording wear resistance (ref. 125, p. 222).

In general, it is thought that wear decreases with increased pearlite and graphite content (ref. 35, p. 318). Furthermore, those elements which tend to increase hardness of the cast iron increase resistance to wear (ref. 153).

Friction and wear experiments were conducted in argon with the gray cast irons. The results obtained are presented in figure 99. Both friction and wear were reduced with increasing carbon content of the gray cast iron. A 2-percent increase in carbon content resulted in a fourfold decrease in the friction coefficient. Furthermore, a linear reduction in wear track width occurred with increasing carbon content. Surface profilometer examinations of the wear tracks indicated that wear occurred to the cast iron. The wear profile depth was not hemispherical as might be observed when the flat undergoes plastic deformation but was generally equidistant in depth from the surface along with width of the track.

The load applied to the steel ball to obtain the results of figure 99 was 50 grams. To determine the effect of load on friction

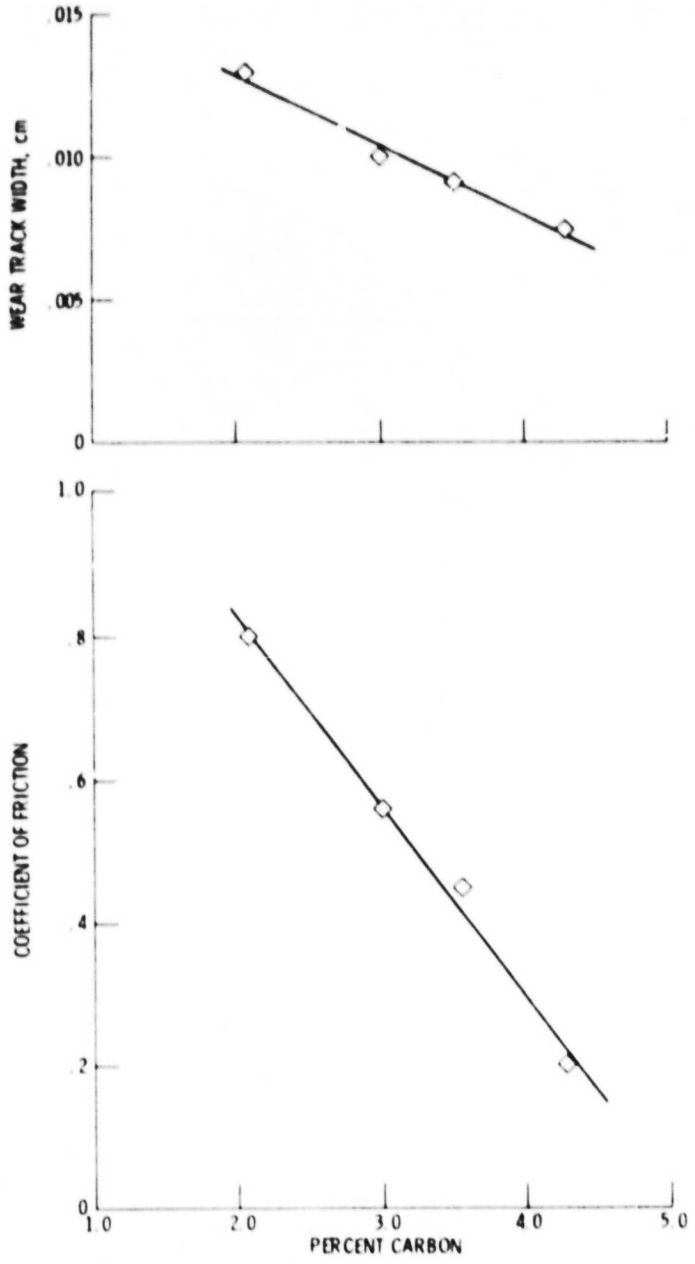

Figure 99. - Coefficient of friction and wear of gray cast iron as functions of carbon content. Mating surface steel ball, 2.5 millimeter diameter; sliding velocity, 5 centimeters per minute; load, 50 grams; argon atmosphere; temperature, 23° C, duration, 1 hour.

and wear, experiments were conducted at various loads from 50 to 250 grams for a gray cast iron having 4.32-percent carbon. The friction coefficient decreased with increasing load to 150 grams and then remained unchanged with further increases in load. Considering that sliding was conducted under dry, unlubricated conditions, the friction is extremely low at the higher loads, 0.15.

The wear of the gray cast iron is a direct linear function of the track width. The greater the load, the greater is the wear.

Figure 100 is a photomicrograph of the wear scar on the 3.02-percent gray cast iron structure. The graphite flakes have been smeared out over the surface as a result of the rubbing process. In reference 154 the observation was made that wear to cast iron was affected by the size and distribution of graphite flakes. Wear was found to be related to total carbon content, and the greater the carbon content, the greater the fraction of contact surface area covered by smeared graphite. This would seem to indicate that a relationship exists between graphite content and wear for cast iron.

In an ordinary air environment, the surface layers on the surface of cast iron have been found to be a mixture of graphite and iron oxide (Fe_3O_4) (ref. 155). With the argon environment used herein, the surface present in the wear track shown in figure 100 must be considered to be essentially graphite with a minimal amount of normal residual surface oxide.

The results obtained in figures 99 and 100 were for flake graphite in gray cast iron. Studies have been conducted on spheroidal graphite in cast iron (ref. 156). While the author of reference 174 did not specifically examine the effect of carbon content on friction and wear, he did conclude that the wear characteristics of spheroidal graphite and flake graphite cast irons were similar. It might, therefore, be reasonable to assume that carbon content in spheroidal graphite in cast iron may have a similar effect on friction and wear as that observed for a gray cast iron.

The conclusion that graphite in gray cast iron is lubricating can be strengthened if the surface of the gray cast iron can be shown to be sensitive to moisture. Since the graphite in gray cast iron is

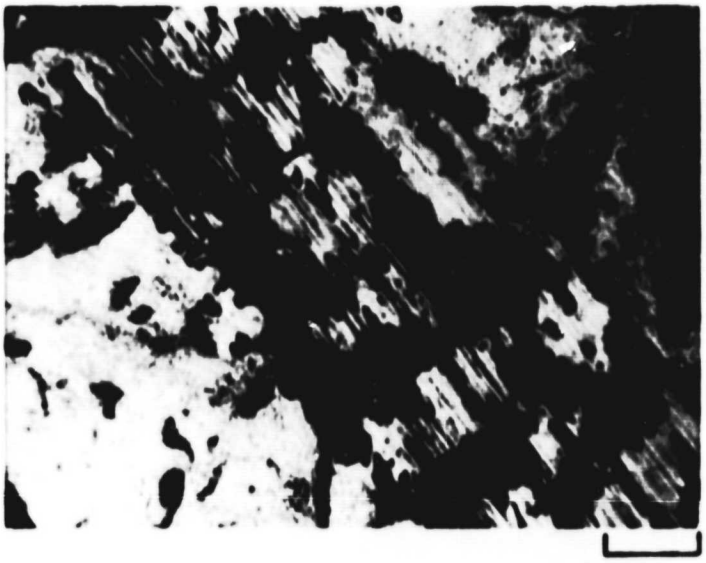

Figure 100. - Wear track on 3.02-percent carbon in gray cast iron having been in sliding contact with a 52100 steel ball for 1 hour. Sliding velocity, 5 centimeters per minute; load, 50 grams; argon atmosphere; temperature, 23° C.

lubricating the surface, the friction behavior of that surface should be sensitive to moisture. This must be so because the friction behavior of graphite, as is well known, is very sensitive to moisture.

Friction and wear experiments were conducted with 4.32-percent carbon in gray cast iron in an argon environment containing various percentages of relative humidity from zero to operating under water.

Friction data indicated that the friction coefficient of gray cast iron is sensitive to moisture. The friction coefficient decreased with increasing relative humidity to 50 percent and then increased thereafter. This decrease with an increase in relative humidity to 50 percent is consistent with the friction behavior of graphite.

At 80-percent relative humidity and under water, the wear surface contained in addition to graphite iron oxide (Fe_3O_3); it was identified from its characteristic color. The presence of this oxide was not observed in the wear track at 50-percent relative humidity and less. Iron oxide (Fe_2O_3) is abrasive, and this fact may account for the increase in friction observed at the higher amounts of humidity. It can also explain the increase in wear observed in water.

The graphite flakes present in the gray cast iron take some time to become smeared out over the surface when sliding or rubbing is initiated on a virgin surface. As a consequence, friction is initially high and decreases with time. After some time, an equilibrium condition is reached where the surface is fairly uniformly covered with graphite and friction reaches a constant value of 0.2.

If the decrease in friction coefficient with an increase in relative humidity is related to a sensitivity of the graphite rather than the iron surface to moisture, then a decrease in friction with sliding time should be observed similar to that seen in dry sliding. Iron does not exhibit this time-dependent sensitivity. The results obtained for 50-percent relative humidity indicate that there is a time-dependent sensitivity. Thus, it is the graphite sensitivity to moisture which affects the friction behavior of gray cast iron.

Oils will readily chemisorb to metal surfaces while the bonding of graphite to metal is poor. It is possible, therefore, that the

graphite films on the surface of gray cast iron might be readily displaced by a lubricating oil. Friction and wear experiments were therefore conducted with gray cast iron in the presence of oil. The results of these experiments showed that, even when gray cast iron is lubricated with a mineral oil, graphite smears out in the wear contact zone. The amount of graphite is less and the film is thinner but is nonetheless present.

The atomic size and concentration of the alloying elements are extremely important for the abrasive-wear and friction behavior of iron-base binary alloys in contact with silicon carbide. The coefficient of friction and abrasive wear volume generally decrease with increasing solute concentration (ref. 157). There is a correlation between the solute to iron atomic radius ratio and the coefficient of friction. There is also a good relation between wear and the change in solute concentration. Friction and wear decrease as the solute to iron atomic radius ratio either increases or decreases from unity. Of further interest are the effects of atomic size and concentration of alloying element on the adhesive wear and friction of alloys.

Friction experiments were conducted with silicon carbide in sliding contact with simple binary alloys of iron. Friction was measured for a 4-atomic-percent concentration of alloying element in iron and for an alloy composition representing the maximum solubility of the alloying element in iron.

Figure 101 presents the average coefficients of friction for the various alloys of iron as functions of solute to iron atomic radius ratio. In figure 101(a) the solute concentrations are all about 4 atomic percent. In figure 101(b) the coefficients of friction are plotted for the maximum solute concentration of each alloy. The maximum solute concentrations are up to approximately 16 atomic percent.

There appears to be good agreement between the adhesion and friction and the solute to iron atomic radius ratio. The correlation of the coefficient of friction and solute to iron atomic radius ratio is separated into two cases: first, the case for alloying with

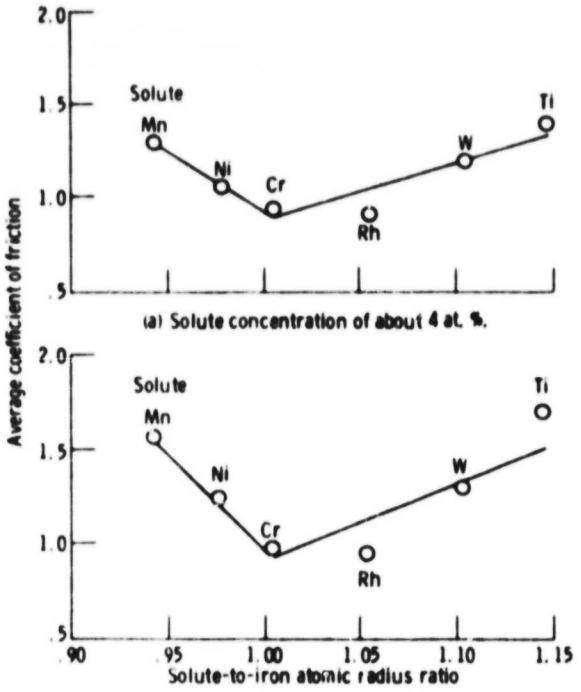

Figure 101. - Coefficients of friction for iron-based binary alloys as function of solute-to-iron atomic radius ratio. Single-pass sliding on single-crystal silicon carbide (0001) surface; sliding direction, $\langle 10\bar{1}0 \rangle$; sliding velocity, 3 millimeters per minute; load, 0.2 newton; room temperature; vacuum pressure, 10^{-8} pascal.

manganese and nickel, which have smaller atomic radii than iron, and, second, the case for alloying with chromium, rhodium, tungsten, and titanium, which have larger atomic radii than iron. The coefficients of friction increase generally as the solute to iron atomic radius ratio increases or decreases from unity. The increasing rate of the coefficients of friction for alloying elements that have smaller atomic radii than iron are much greater than that for alloying elements that have larger atomic radii than iron. The atomic size ratio values reported here are from reference 158. The correlation indicates that the atomic size of the solute is an important factor in controlling the adhesion and friction in iron-base binary alloys as well as the abrasive wear and friction reported by the present authors (ref. 175) and the alloy hardening reported by Stephens and Witzke (ref. 176).

A more detailed examination of figures 101(a) and (b) indicates that the correlations for manganese and nickel are better than those for titanium, tungsten, rhodium, and chromium. The coefficient of friction for rhodium is relatively low, while that for titanium is relatively high. The relative chemical activity of the transition metals (metals with partially filled d shell) as a group can be ascertained from their percent d-bond character, after Pauling. It has already been determined that the coefficient of friction for silicon carbide in contact with various transition metals was related to the d-bond character - that is, chemical activity of the metal (ref. 159). The more active the metal, the higher the coefficient of friction. The greater the recirprocal percent d-bond character, the more active the metal and the higher the coefficient of friction (ref. 159).

Rhodium-iron alloys in contact with silicon carbide showed relatively low friction. On the other hand, titanium-iron alloys showed relatively high friction. The results seem to be related to the chemical activity of alloying elements; that is, rhodium is less active, and titanium is more active. The good correlation for manganese, nickel, and chromium is due to the reciprocal percent d-bond character for those being the almost same value for each.

CONCLUDING REMARKS

The results presented herein indicate that real tribological surfaces are markedly different than previously thought. Surface analyses indicate that more than simply surface topography is significant in solid to solid contact. Surface chemistry, physics, and metallurgy are extremely important. It has been indicated herein that, for example, small concentrations of contaminants in metals and alloys of the order of parts per million can segregate to the surface of a solid and markedly alter its adhesion, friction, and wear behavior.

The electronic nature of a metallic surface and the physics of the surface influence the adhesive interactions of metals. In a consideration of both the Fermi surface and valency bond character, tribological relationships are observed.

A host of metallurgical effects are observed to effect adhesion, friction, and wear. These are presented in greater detail shortly.

The advent of the space age and the use of vacuum systems to study material behavior in the absence of normal environmental constituents has clearly established that the environment is an integral part of every lubrication system and must be considered in any fundamental study of tribological behavior. Fractions of a monolayer are sufficient to affect adhesion and friction forces. Both oxygen and water vapor of the environment alter the friction and wear behavior of surfaces in sliding. Dissolved gases in oils come from the environment and alter tribological performance. Furthermore, even solid-film lubricants are affected in their performed by environmental components. Molybdenum disulfide lubricates more effectively in the absence of moisture than in its pressure, just contrary to that observed with graphite.

Returning to the subject of metallurgical properties and their effect on tribological characteristics, crystal structure and orientation exert a strong influence on friction and wear behavior. Hexagonal metals have superior friction and wear properties to cubic metals, both body centered and face centered cubic. High atomic

density, low surface energy planes in metal systems exhibit lower friction, wear, and adhesive behavior than do planes of lesser density and higher energy. Likewise, the adhesive and friction forces are lower in the high atomic density or preferred slip directions of crystal faces.

Texturing a metal surface generally results in changes in friction and wear behavior of metals with the resulting texture in sliding to be that of the high atomic density plane orienting itself nearly parallel to the sliding surface. Friction also changes with recrystallization.

Ordering simple binary alloy systems has an effect on friction. Friction is lower for the alloy systems in the ordered than in the disordered state.

Crystallinity itself has an effect on tribological response. Experiments with amorphous metal alloys (metallic glasses) reveal that friction and wear are lower in the amorphous state than in the crystalline state. This observation is consistent with lower energy surfaces exhibiting better tribological properties (i.e., lower friction and wear).

Friction characteristics can be related to fundamental physical and chemical properties of elemental metals. Both ideal tensile and shear strength of metals correlate with observed friction behavior. The d valence bond character of elemental metals relates to observed adhesion and friction. The greater the degree of bond saturation, the lower the adhesion and friction.

With metal alloys, abrasive wear resistance and friction can be related directly to the lattice ratios of the alloying element to the solvent element. When the lattice radius ratio of the solvent to the solute element is unity, friction and wear are minimal. Deviation of the ratio in either direction from unity results in higher friction and wear.

Surface segregation of alloy constituents to the surface results in changes in adhesion, friction, and wear behavior. Some alloying elements increase these properties while others reduce them. Very small amounts of alloying element profoundly influence tribological characteristics.

REFERENCES

1. Williamson, J. B. P.: In Interdisciplinary Approach to Friction and Wear. NASA SP-181, 1968, p. 85.
2. Westwood, A. R. C.; and Stoloff, N. S.; eds: Environment-Sensitive Mechanical Behavior. Gordon and Breach Science Publishers, Inc., 1966.
3. Rideal, E. K.: SCI (London) Monogr., vol. 3, no. 28, 1968.
4. Clark, D. T.; and Feast, W. J.: J. Macromol. Sci., Rev. Marcomol. Chem., vol. 12, 1975, p. 191.
5. McLean, D.: Grain Boundaries in Metals. Clarendon Press, 1957.
6. Roscoe, R.: The Plastic Deformation of Cadmium Single Crystals. Philos. Mag., vol. 21, 1936, p. 399.
7. Westbrook, J. H., ed.: Mechanical Properties of Intermetallic Compounds. John Wiley & Sons, 1960.
8. Likhtman, V. I.; Rebinder, P. A.; and Karpenko, G. V.: Effect of Surface-Active Media on the Deformation of Metals. Chemical Publishing Company, Inc., 1960.
9. Müller, E. W.; and Tsong, T. T.: Field Ion Microscopy: Principles and Applications. American Elsevier Publishing Co., Inc., 1969.
10. Kane, P. F.; and Larrabee, G. B.; eds.: Characterization of Solid Surfaces. Plenum Press, 1974.
11. Wheeler, D. R.: Improved Adhesion of Sputtered Reflecting Carbides to Metal Substrates. Wear, vol. 58, 1980, pp. 341-358.
12. Buckley, D. H.; and Johnson, R. L.: Friction and Wear of Hexagonal Metals and Alloys as Related to Crystal Structure and Lattice Parameters in Vacuum. ASLE Trans., vol. 9, no. 2, Apr. 1966, pp. 121-135.
13. Tabor, D.: Junction Growth in Metallic Friction: The Role of Combined Stresses and Surface Contamination. Proc. Roy. Soc. London, Ser. A., vol. 251, 1959.
14. Buckley, D. H.: Definition and Effect of Chemical Properties of Surfaces in Friction, Wear, and Lubrication. NASA TM-73806, 1978.
15. Wheeler, D. R.: Effect of Adsorbed Chlorine and Oxygen on the Shear Strength of Iron and Copper Junctions. J. Appl. Phys., vol. 47, no. 3, 1976, pp. 1123-1130.

16. Buckley, D. H.: Friction, Wear, and Lubrication in Vacuum. NASA SP-277, 1971.
17. Buckley, D. H.: Adsorption of Ethylene Oxide and Vinyl Chloride on an Iron (011) Surface and Effect of These Films on Adhesion. NASA TN D-5999, 1970.
18. Wheeler, D. R.: X-ray Photoelectron Spectroscopic Study of Surface Chemistry of Dibenzyl Disulfide on Steel Under Mild and Severe Wear Conditions. Wear, vol. 47, no. 2, 1978, pp. 243-254.
19. Gilman, J. J.: The Mechanism of Surface Effects in Crystal Plasticity. Philos. Mag., vol. 6, 1961, pp. 159-161.
20. Hansen, M.: Constitution of Binary Alloys. McGraw-Hill Book Co. Inc., 1958.
21. Gschneidner, K. A., Jr.: Physical Properties and Interrelationships of Metallic and Semimetallic Elements. Solid State Physics, vol. 16, F. Seitz and D. Turnbull, eds., Academic Press, 1964, pp. 275-426.
22. Pauling, L. C.: The Nature of the Chemical Bond and the Structure of Molecules and Crystals: An Introduction to Modern Structural Chemistry, Cornell Univ. Press, 3rd ed., 1960.
23. Hampel, C. A.: Rare Metals Handbook. 2nd ed., Reinhold Publishing Corp., 1961.
24. Holm, R.: Electric Contacts. Almquist and Wiksell, Uppsala, 1946.
25. May, J. W.: Electron Diffraction and Surface Chemistry. Ind. Eng. Chem., vol. 47, no. 7, July 1965, pp. 18-39.
26. Somorjai, G. A.: Low Energy Electron Diffraction and Auger Electron Spectroscopy: Studies of the Structure of Adsorbed Gases on Solid Surfaces. Sur. Sci., vol. 34, 1973, pp. 156-176.
27. Johnson, O. W.; and Gibbs, P.: Brittle Fracture of Germanium. Vol. 20 of Fracture of Solids. D. C. Drucker and J. J. Gilman, eds., Interscience Publishers, 1962, pp. 315-338.
28. Alexander, H.: Electronenmikroskobie eingefrorener Versetzungen. Phys. Stat. Sol., vol. 26, 1968, pp. 725-741.
29. Kabler, M. N.: Dislocation Mobility in Germanium. Phys. Rev., vol. 131, no. 1, July 1963, pp. 54-58.

30. Malov, Y. V.; and Rozhanskii, V. N.: Investigation of the Dislocation Structure of Silicon Deformed During the Easy Slip Stage. Sov. Phys. State, vol. 9, no. 4, Oct. 1967, pp. 805-812.

31. Hahn, G. T.; Kanninen, M. F.; and Rosenfield, A. R.: Fracture Toughness of Materials. Annu. Rev. Mater. Sci., vol. 2, 1972, pp. 381-404.

32. Bocker, E. R.: Crystallographic Imperfections in Silicon, Dislocations in Solids. Discuss. Faraday Soc., no. 38, 1964, pp. 298-308.

33. Bowden, F. P.; and Tabor, D.: The Friction and Lubrication of Solids. Oxford Press, 1954.

34. Bowden, F. P.; and Hanwell, A. E.: The Friction of Clean Crystal Surfaces. Proc. Roy. Soc. London, Ser. A., vol. 295, no. 1442, p. 233.

35. Kragelskii, I. V.: Friction and Wear. Leo Ransom and J. K. Landraster, transl. Butterworth and Co., Ltd., 1965.

36. Rabinowicz, E.: Friction and Wear of Materials. John Wiley & Sons, Inc, 1965.

37. Wiederhorn, S. M.: Environment-Sensitive Mechanical Behavior of Materials. Gordon and Breach Science Publishers, Inc., 1966, p. 293.

38. Buckley, D. H.; and Pepper, S. V.: NASA TN D-6[illegible], 1971.

39. Lee, L-H, ed.: Advances in Polymer Friction and Wear. Vols. 5A and 5B of Polymer Science and Technology Series, Plenum Publishing Corp., 1974.

40. Tabor, D.; and Willis, R. F.: The Formation of Silicone Polymer Films on Metal Surfaces at High Temperatures and Their Boundary Lubricating Properties. Wear, vol. 13, 1969, pp. 413-442.

41. Cohen, S. C.; and Tabor, D.: The Friction and Lubrication of Polymers. Proc. Roy. Soc. London, Ser. A, vol. 291, no. 1425, April 5, 1966, pp. 186-207.

42. Tanaka, K.: The Friction and Deformation of Polymers. J. Phys. Soc. Japan, vol. 16, no. 10, Oct. 1961, pp. 2003-2016.

43. Bueche, A. M.; and Flom, D. G.: Surface Friction and Dynamic Mechanical Properties of Polymers. Wear, vol. 2, 1958-1959, pp. 168-182.

44. Pooley, C. M.; and Tabor, D.: Friction and Molecular Structure: The Behavior of Some Thermoplastics. Proc. Roy. Soc. London, Ser. A, vol. 329, no. 1578, 1972, pp. 251-274.

45. Sviridyonok, A. I., et al.: A Study of Transfer in Frictional Interaction of Polymers. Wear, vol. 25, 1973, pp. 301-308.

46. Tanaka, K.; and Miyata, T.: Studies on the Friction and Transfer of Semicrystalline Polymers. Wear, vol. 41, 1977, pp. 383-398.

47. Bisson, E. E.; and Anderson, W. J.: NASA SP-38, 1964.

48. Braithwaite, E. R.: Solid Lubricants and Surfaces. The Macmillan Co., 1964.

49. Clauss, F. J.: Solid Lubricants and Self-Lubricating Solids. Academic Press, 1972.

50. Lanzan, W. R.; Shelton, B. R.; and Waldheger, R. A.: Lubr. Eng., vol. 19, 1963, p. 201.

51. Campbell, W. E.; and Kozak, R.: ASME Trans, vol. 70, 1948, p. 491.

52. Bisson, E. E.; Johnson, R. L.; and Anderson, W. J.: Friction and Lubrication with Solid Lubricant at Temperatures to 1000° F with Particular Reference to Graphite. Paper 23, Inst. Mech. Eng. Conf. on Lubrication and Wear, Oct. 1957.

53. Bowden, F. P.: Experimental Studies of Solid Friction: Friction and Wear. Proc. Symp. Friction and Wear, 1959, pp. 84-103.

54. Ehrlich, G.: Adsorption on Clean Surfaces. Ann. N.Y. Acad. Sci., vol. 101, 1963, pp. 583-1014.

55. Pace, E. L.: The Theoretical Calculation of the Heat of Adsorption for Gases Physically Adsorbed on Carbon Surfaces. Proceedings of the Fourth Conference on Carbon, Pergamon Press Ltd., 1960, pp. 35-45.

56. Studebaker, M. L.: Observations on the Reaction Between Carbon Black and Water at Low Temperatures. Proc. Third Conference on Carbon, Pergamon Press Ltd., 1959, pp. 289-294.

57. Trapnell, B. M. W.: Chemisorption. Academic Press, 1955.

58. DiBoci, J. H.: Advances in Catalysis, Vol. 8. Academic Press, 1956.

59. Smith, R. N.; Pierce, C.; and Joel, C. D.: The Low Temerature Reaction of Water with Carbon. J. Phys. Chem., vol. 58, 1954, pp. 298-302.

60. Snow, C. W.; Wallace, D. R.; Lyon, L. L.; and Crocker, G. R.: Reaction of Carbon Blacks with Oxygen. Proc. Third Conference on Carbon, Pergamon Press, 1959, pp. 279-287.
61. Dayton, B. B.: Outgassing Rate of Contaminated Metal Surfaces. Paper presented at Am. Vacuum Soc. Nat. Vacuum Symposium, 1961.
62. Garner, W. E., ed.: Chemisorption. Academic Press, 1957, pp. 68-75.
63. Prutton, C. F.; and Maron, S. H.: Fundamental Principles of Physical Chemistry. The Macmillan Co., 1957.
64. Bansal, R [illegible]; Vastola, F. J.; and Walker, P. L., Jr.: Carbon, vol. 8, 19[illegible]. 443.
65. Barton, S. S.; and Harrison, B. H.: Carbon, vol. 10, 1972, p. 245.
66. Thomas, J. M.; Evans, E. L.; Barber, M.; and Swift, P.: Trans. Faraday Soc., vol. 67, 1971, p. 1875.
67. Barber, M.; Evans, E. L.; and Thomas, J. M.: Chem. Phys. Letts., vol. 18, 1973, p. 423.
68. Musket, R. G.; and Ferrante, J.: Auger Electron Spectroscopy Study of Oxygen Adsorption on W(110). J. Vac. Sci. Tech., vol. 7, no. 1, 1970 p. 14-17.
69. Hart, P. J.; Vastola, F. J.; and Walker, P. L., Jr.: Carbon, vol. 5, 1967, p. 363.
70. Hennig, G. R.: Chem. Phys. Carbon, vol. 2, 1966.
71. Bowden, F. P.; and Tabor, D.: The Friction and Lubrication of Solids - Part 2. Oxford University Press, 1964.
72. Thrower, P. A.: Chem. Phys. Carbon, vol. 5, 1969, p. 217.
73. Lurie, P. G.; and Wilson, J. M.: Diamond Research, 1976, p. 26.
74. Thomas, J. M.; and Evans, L. L.: Diamond Research, 1975, p. 2.
75. Lurie, P. G.; and Wilson, J. M.: Surf. Sci., vol. 65, 1977, p. 476.
76. Pauling, L.: Proc. Roy. Soc. London, Ser. A, vol. 196, 1949, p. 343.
77. Buckley, D. H.: J. Colloid Interface Sci., vol. 58, 1977, p. 36.
78. Miyoshi, K.; and Buckley, D. H.: Friction and Wear of Single-Crystal and Polycrystalline Manganese - Zinc Ferrite in Contact with Various Metals. NASA TP-1059, 1977.
79. Miyoshi, K.; and Buckley, D. H.: Effect of Oxygen and Nitrogen Interactions on Friction of Single-Crystal Silicon Carbide. NASA TP-1265, 1978.

80. Wawra, H. H.: Temperatur-und Druckabhängegkait der freien Oberflächenenergie von festem and flüssigem KCl zwischen 0° K und 1400° K, Radex Rundsch., no. 5, Dec. 1972, pp. 351-364.

81. Tyson, W. R.: Estimation of Surface Energies from Phonon Frequencies for BCC and FCC Metals. J. Appl. Phys., vol. 47, no. 2, Feb. 1976, pp. 459-465.

82. Averbach, B. L.: Some Physical Aspects of Fracture. Fracture, An Advanced Treatise. Vol. 1 of Microscopic and Macroscopic Fundamentals, H. Liebowitz, ed., Academic Press, 1968, chap. 7.

83. Mykura, H.: The Variation of the Surface Tension of Nickel with Crystallographic Orientation. Acta Metall., vol. 9, no. 6, June 1961, pp. 570-576.

84. Sundquist, B. E.: A Direct Determination of the Anisotropy of the Surface Free Energy of Solid Gold, Silver, Copper, Nickel, and Alpha and Gamma Iron. Acta Metall., vol. 12, no. 1, 1964, pp. 67-86.

85. Kumar, R.; and Grenga, H. E.: Surface Energy Anisotropy of Iridium. Surf. Sci., vol. 50, 1975, pp. 399-406.

86. Winterbottom, W. L.; and Gjostein, N. A.: Determination of Anisotropy of Surfacea Energy of Metals - II: Experimental Y-Plot of Gold, Acta Metall., vol. 14, no. 9, 1966, pp. 1041-1052.

87. Roberts, R. W.: Reactions of Saturated Hydrocarbons with Clean Rhodium Films. Ann. N. Y. Acad. Sci., vol. 101, Art. 3, 1963, pp. 766-777.

88. Ehrlich, G.: Atomistics of Metal Surfaces. Surface Phenomena of Metals, SCI Monogr., no. 28, 1968, pp. 13-38.

89. Müller, A.; and Drechsler, M.: Eine Messung Der Anisotropie Der Oberfldchenenergie Von Reinem Wolfram Mit Dem Fildionenmikroskop. Surf. Sci., vol. 13, 1969, pp. 471-490.

90. Brenner, S. S.: The Thermal Rearrangement of Field-Evaporated Irdium Surfaces. Surf. Sci., vol. 2, 1964, pp. 496-508.

91. Jones, H.: Splat Cooling and Metastable Phases. Rep. Prog. Phys., vol. 36, 1978, pp. 1425-1497.

92. Gilman, J. J.: Metallic Glasses. Physics Today, May 1975, pp. 46-53.

93. Gilman, J. J.: Metallic Glasses - A New Technology, Chapter III.1, Crytal Growth and Materials, E. Kaldis and H. J. Schul, eds., North-Holland Publishing Co., 1977, pp. 728-741.

94. Pepper, S. V.: Effect of Interfacial Species on Shear Strength of Metal-Sapphire Contact. Appl. Phys., vol. 50, no. 12, 1979, pp. 8062-8065.

95. Steijn, R. P.: On the Wear of Sapphire. J. Appl. Phys., vol. 32, no. 10, Oct. 1961, pp. 1951-1958.

96. Eiss, N. S., Jr.; and Fabiniak, R. C.: Wear of Sapphire on Steel: Chemical and Mechanical Mechanisms. Paper No. 7-C-65, Am. Ceram. Soc., May 1965.

97. Coffin, L. F., Jr.: A Fundamental Study of Synthetic Sapphire as a Bearing Material. ASLE Trans., vol. 1, no. 1, 1958, pp. 108-114.

98. Duwell, E. J.: Friction and Wear of Single-Crystal Sapphire Sliding on Steel. J. Appl. Phys., vol. 33, no. 9, 1962, pp. 2691-2698.

99. Bartlett, R. W.; and McCamont, J. W.: The Influence of Crystal Orientation on the Oxidation of Tungsten. J. Electrochem. Soc., vol. 112, no. 2, 1965, pp. 148-152.

100. Opinsky, A.; and Smoluchowski, R.: The Crystallographic Aspect of Slip in Body-Centered-Cubic Single Crystals. Proc. Symp. on the Plastic Deformation of Crystalline Solids. No. NAVEXOS P-834, Office of Naval Research, May 20, 1950, pp. 216-223.

101. Bowden, F. P.; and Rowe, G. W.: The Adhesion of Clean Metals. Proc. Roy. Soc. London, Ser. A, vol. 233, 1956, pp. 429-442.

102. Gilbreath, W. P.; and Sumsion, H. T.: Solid-Phase Welding of Metals Under High Vacuum. Proc. AIAA 6th Structure and Materials Conf., 1965.

103. Sikorski, M. E.: The Adhesion of Metals and Factors that Influence It. Wear, vol. 7, 1964, p. 144.

104. Gwathmey, A. T.; and Dyer, L. D.: Cohesion Between Two Oriented Single Crystals of Copper. Friction and Wear, American Elsevier, 1959.

105. Bailey, J. M.; and Gwathmey, A. T.: Friction and Surface Deformation During as a Single Crystal of Copper. ASLE Trans., vol. 5, 1962, pp. 45-56.

106. Buckley, D. H.: The Influence of Recrystallization and Preferred Orientation on the Friction of Copper in Vacuum (10^{-11} torr). NASA TN D-3794, 1967.

107. Gilman, J. J.: Cleaveage, Ductility, and Tenacity in Crystals. Fracture. Massachusetts Institute of Technology Press and John Wiley & Sons, 1959, pp. 193-224.

108. McClean, D.: Grain Boundaries in Metals. Oxford University Press, 1957.

109. Buckley, D. H.: Influence of Orientation of Grains in Tungsten on its Frition Characteristics. NASA TN D-3238, 1966.

110. Roach, A. E.; Goodzeit, C. L.; and Hunnicutt, R. P.: Scoring Characteristics of Thirty-Eight Different Elemental Metals in High Speed Sliding Contact with Steel. Trans. ASME, vol. 78, no. 8, 1956, pp. 1659-1667.

111. Ernst, H.; and Merchant, M. E.: Chip Formation, Friction, and Finish. The Cincinnati Milling Machine Co., Aug. 24, 1940.

112. Taylor, N. J.: A LEED Study of the Epitaxial Growth of Copper on the (110) Surface of Tungsten. Surf. Sci., vol. 4, 1966, pp. 161-194.

113. Scott, V. D.; and Wilman, H.: Surface Reorientation Caused on Metals by Abrasion - Its Nature, Origin and Relation to Friction and Wear. Proc. Roy. Soc. London, Ser. A., vol. 247, no. 1250, 1958, pp. 353-368.

114. Goddard, J.; Harker, H. J.; and Wilman, H.: The Surface Reorientation Caused by Unidirectional Abrasion on Face-Centered Cubic Metals. Proc. Phys. Soc. London, vol. 80, no. 3, 1962, pp. 771-782.

115. Huppmann, W. J.; and Clegg, M. A.: The Tribological Behavior of Polycrystalline Cobalt as Related to Crystallographic Texture and Structure. ASLE-ASME Int. Lubric. Conf., New York, Oct. 1972.

116. Buckley, D. H.: Recrystallization and Preferred Orientation in Single-Crystal and Polycrystalline Copper in Friction Studies. NASA TN D-3794, 1967.

117. Avner, S. H.: Introduction to Physical Metallurgy. McGraw-Hill Book Co., Inc., 1964.

118. Brophy, J. H.; Rose, R. M.; and Wulff, J.: Thermodynamics of Structure. The Structure and Properties of Materials, vol. 2, John Wiley & Sons, 1964, pp. 112-131.

119. Dieter, George E.: Mechanical Metallurgy. McGraw-Hill Book Co., Inc., 1961.

120. Burke, J. E.; and Turnbull, D.: Recrystallization and Grain Growth. Progress in Metal Physics. Vol. 3, Bruce Chalmers, ed., Interscience Publishing, 1952, pp. 220-292.

121. Peterson, M. B.; Florek, J. J.; and Murray, S. F.: Consideration of Lubricants for Temperatures Above 1000° F. ASLE Trans., vol. 2, no. 2, 1960, pp. 225-234.

122. Ellis, O. W.; and Karelitz, G. B.: A Study of Tin-Base Bearing Metals - I. ASME Trans., vol. 50, 1928, pp. 10-13.

123. Karelitz, G. B.; and Ellis, O. W.: A Study of Tin-Base Bearing Metals - II. ASME Trans., vol. 52, pt. 2, 1930, pp. 87-99.

124. Freeman, J. R., Jr.; and Brandt, P. F.: The Effect of Impurities on the Compressive Strength and Brinell Hardness of Babbitt Metal at Normal and Elevated Temperatures. Proc. Am. Soc. Test. Mater., vol. 24, pt. 1, 1924, pp. 253-258.

125. ASM Metals Handbook. 1948 ed., American Society for Metals, 1948.

126. Azaroff, L. V.: Introduction to Solids. McGraw-Hill Book Co., Inc., 1960.

127. Schmid, E.; and Boas, W.: Kristallplastizität, mit Besonderer Berucksichtigung der Metalle. Julius Springer, Berlin, 1935.

128. Barrett, C. S.: Structure of Metals, Crystallographic Methods, Principles, and Data. 1st ed., McGraw-Hill Book Co., Inc., 1943.

129. Miyoshi, K.; and Buckley, D. H.: Friction and Wear Behavior of Single-Crystal Silicon Carbide in Sliding Contact with Various Metals. ASLE Trans., vol. 22, no. 3, 1979, pp. 245-256.

130. Macmillan, N. H.: Review: The Theoretical Strength of Solids. J. Mater. Sci., vol. 7, 1972, pp. 239-254.

131. Bridgman, P. W.: Shearing Phenomena at High Pressures, Particularly in Inorganic Compounds. Proc. Amer. Acad. Arts and Sci., vol. 71, 1937, pp. 387-460.

132. Miyoshi, K.; and Buckley, D. H.: The Relationship Between the Ideal Tensile Strength and Friction Properties of Metals in Contact with Nonmetals and Themselves. NASA TP-1883, 1981.

133. Polanyi, M.: Z. Phys., vol. 7, 1921, p. 323.
134. Orowan, E.: Krist., vol. A89, 1934, p. 327.
135. Orowan, E.: Reports Prog. Phys., vol. 12, 1949, p. 185.
136. Orowan, E.: Weld. J., vol. 34, 1955, p. 157.
137. Miyoshi, K.; and Buckley, D. H.: Adhesion and Friction of Single-Crystal Diamond in Contact with Transition Metals. Applications of Surface Science, vol. 6, 1980, pp. 161-172.
138. Buckley, D. H.: Friction and Transfer Behavior of Pyrolytic Boron Nitride in Contact with Various Metals. ASLE Trans., vol. 21, no. 2, 1978, pp. 118-124.
139. Miyoshi, K.; and Buckley, D. H.: Friction and Wear of Single-Crystal Manganese - Zinc Ferrite. Wear, vol. 66, 1981, pp. 157-173. (Also, Proc. Wear of Materials, 1979.)
140. Lander, J. J.: Low-Energy Electron Diffraction and Surface Structural Chemistry. Progress in Solid State Chemistry, vol. 2, H. Reiss, ed., Pergamon Press, Inc. 1965, pp. 26-116.
141. Palmberg, P. W.; and Rhodin, T. N.: Auger Electron Spectroscopy of fcc Metal Surfaces. J. Appl. Phys., vol. 39, no. 5, 1968, pp. 2425-2432.
142. Ferrante, J.: An Auger Electron Spectroscopy and LEED Study of Equilibrium Surface Segregation in Copper-Aluminum Alloys. Acta Metall. vol. 19, 1971, pp. 743-748.
143. Buckley, D. H.: Influence of Aluminum on Friction and Wear of Iron-Aluminum Alloys Dry and Lubricated. NASA TN D-6359, 1971.
144. Buckley, D. H.: Effect of Various Properties of FCC Metals on Their Adhesion as Studied with LEED. J. Adhes., vol. 1, 1969, pp. 264-281.
145. Ferrante, J.; and Buckley, D. H.: Auger Electron Spectroscopy Study of Surface Segregation in Copper-Aluminum Alloys. NASA TN D-6095, 1970.
146. Wehner, G.: Sputtering. Int. Sci. Technol., no. 81, Sept. 1968, pp. 32-39.
147. Germer, L. H.; and May, J. W.: Diffraction Study of Oxygen Adsorption on a (110) Tungsten Face. Surf. Sci., vol. 4, 1966, pp. 452-470.

148. Swanson, L. W.; and Strayer, R. W.: Field-Electron-Microscopy Studies of Cesium Layers on Various Refractory Metals: Work Function Change. J. Chem. Phys., vol. 48, no. 6, 1968, pp. 2421-2442.

149. Halling, J.: Introduction to Tribology. Wykeham Publications (London) 1976.

150. Cameron, A.: Principles of Lubrication. Longmans Green & Co., Ltd., London, 1966.

151. Akhmatov, A. S.: Molecular Physics of Boundary Friction. Translated from the Russian by N. Kaner, Israel Program for Scientific Translations (Jerusalem), 1966.

152. Boegehold, A. L.: Wear Testing of Cast Iron. Proc. Am. Soc. Test Mater., vol. 29, pt. II, 1929, p. 115.

153. Boegehold, A. L.: Wear Tests and Value of Hardness for Control of Product. Trans. Am. Foundrymen's Assoc. Q., vol. 5, no. 2, 1934, p. 575.

154. Takeuchi, E.: The Mechanism of Sliding Wear of Lubricated Flake Graphite Cast Iron. Wear, vol. 15, no. 3, 1970, pp. 201-208.

155. Montgomery, R. S.: Run-in and Glaze Formation on Gray Cast Iron Surfaces. Wear, vol. 14, no. 2, 1969, pp. 99-105.

156. Takeuchi, E.: The Mechanism of Wear of Spheroidal Graphite Cast Iron in Dry Sliding. Wear, vol. 19, no. 3, 1972, pp. 267-276.

157. Miyoshi, K.; and Buckley, D. H.: Friction and Wear with a Single-Crystal Abrasive Grit of Silicon Carbide in Contact with Iron-Base Binary Alloys in Oil: Effects of Alloying Element and Its Content. NASA TP-1394, 1979.

158. Stephens, J. R.; and Witzke, W. R.: Alloy Softening in Binary Iron Solid Solutions. J. Less-Common Met., vol. 48, 1976, pp. 285-308.

159. Miyoshi, K.; and Buckley, D. H.: Friction and Metal Transfer for Single-Crystal Silicon Carbide in Contact with Various Metals in Vacuum. NASA TP-1191, 1978.